AN ABSTRACT OF THE DISSERTATION OF

Hamid Reza Vejdani Noghreiyan for the degree of Doctor of Philosophy in Robotics and Mechanical Engineering presented on December 15, 2014.

Title: Dynamics and Control for Spring-Mass Legged Robots

Abstract approved: ______________________________

Jonathan W. Hurst

The objective of this study is to propose control strategies for legged robots to walk and run naturally like humans and animals. To achieve this goal, we use the spring-mass model for the legged robots to be able to create the same dynamics in the leg as humans and animals. In this way, understanding the natural dynamics of the system plays the central role and the strategy is to manipulate the dynamics of the system in the favor of final goals. This research elaborates to follow the template-anchor-robot notion, therefore the process starts with reduced order model (template) and then shows the validity of the control policy on the full order model (anchor) and finally implements the policy on the robot.

The study starts with analyzing the dynamics of the bipedal spring-mass model to find the workspace and the possible limit cycles in each energy level. After that, a deadbeat control strategy is proposed to pinpoint the system to the desired limit cycle. It is shown that two steps are necessary and sufficient for the deadbeat control but it turned out that the sensitivity of the system to the touch-down angle

is a challenging issue for implementing on real robots. Therefore, unlike the deadbeat control technique that pinpoints the system to the desired states, four swing leg control policies are proposed to gradually approach the desired limit cycles. The large basins of attraction of these proposed control policies show that the system can be reliably controlled to the desired gaits after large perturbations. The implementation on the full order model of the robot as well as the robot itself confirms this conclusion. Furthermore, a time-based feed-forward control strategy for the stance phase of the bipedal spring-mass model is combined with one of the proposed swing leg control policies to stabilize the model and manages the energy of the system. The simulations show that this technique can stabilize the model and manages the energy level of the system and the rate of convergence would be higher for spring-mass system with some damping in parallel to the spring. By implementing this policy on the full order model of the robot, stable walking gaits, as were predicted by the reduced order model, were obtained. Finally, a flight phase control policy is proposed for spring-mass running robots through investigating birds' running experiments. In this control policy, three objective functions were considered to fulfill safety and efficiency during running. It turned out that with a simple swing leg policy (constant leg angular acceleration), both goals of damage avoidance and energy efficiency can be fulfilled at once.

Dynamics and Control for Spring-Mass Legged Robots

by

Hamid Reza Vejdani Noghreiyan

A DISSERTATION

submitted to

Oregon State University

in partial fulfillment of
the requirements for the
degree of

Doctor of Philosophy

Presented December 15, 2014
Commencement June 2015

Doctor of Philosophy dissertation of Hamid Reza Vejdani Noghreiyan presented on December 15, 2014.

APPROVED:

Major Professor, representing Robotics and Mechanical Engineering

---

Head of the School of Mechanical Industrial and Manufacturing Engineering

---

Dean of the Graduate School

I understand that my dissertation will become part of the permanent collection of Oregon State University libraries. My signature below authorizes release of my dissertation to any reader upon request.

Hamid Reza Vejdani Noghreiyan , Author

ACKNOWLEDGMENTS

I would like to especially thank my major adviser, Jonathan W. Hurst, for all of his guidance and support. I would also like to thank my thesis committee and the professors at Oregon State University whom I had the chance to be in their classes and/or received advices and guidance, and many professors at my previous schools especially Ferdowsi University of Mashhad. As always in my life, for all I have and all I achieve, I am profoundly thankful and indebted to my family: my parents, my siblings and my spouse for everything they have been providing for me that I can not even count, especially my brother, my best and closest friend, Alireza who has supported me and encouraged me in all levels of my life.

Funding for this work was provided by the National Science Foundation (NSF) and the Human Frontier Science Program (HFSP).

TABLE OF CONTENTS

TABLE OF CONTENTS (Continued)

TABLE OF CONTENTS (Continued)

LIST OF FIGURES

LIST OF TABLES

Chapter 1 – Introduction

Despite of the recent remarkable advances in the field of legged robotics, animals can still outperform the legged robots in performance, efficiency and robustness during walking and running in natural environment. Part of this superiority is due to the difference in the actuator mechanisms, and part of it is due to the superior control policies that animals use during locomotion. The goal of this work is to elaborate to understand the principles of the dynamics of walking and running and then propose control policies based on the natural dynamics of the system to achieve stable locomotion.

We use the spring-loaded inverted pendulum (SLIP) model as the passive model for running and its bipedal extension as the reduced order model for walking [6, 7]. Recent studies showed that these models have self-stabilizing characteristic [4, 7, 8], which implies that they do not require complicated control effort to become stable and hence is aligned with the concept of passive dynamics [9].

The actuated versions of the aforementioned models are also used in this work [10]. They are mathematically similar to our robot ATRIAS (figure 1.1). In the actuated model, a motor is used in series with the leg spring to add or remove energy and change the zero force leg length of the legs. When it is desired for the system to be conservative, the leg motor is kept locked during the stance phase to provide a passive and conservative gait.

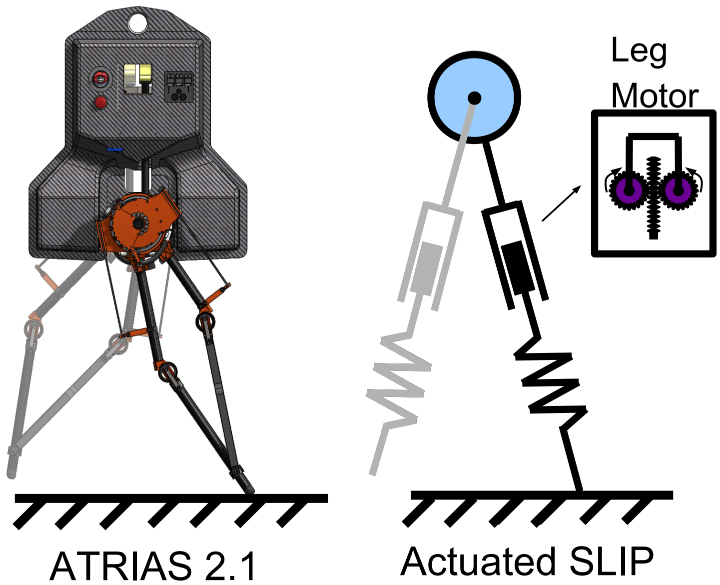

Figure 1.1: ATRIAS 2.1 vs the actuated SLIP model. The leg motor allows the model to change the zero force leg length during the flight phase. The leg is assumed massless and position controller is used for the leg angle placement.

1.1 Contributions

The contributions of this research are:

- **Analyzing the dynamics of the bipedal spring-mass model and understanding the relation of the limit cycles with respect to each other by determining the position of them in the workspace.** By finding all the states in the state-space that can be used in the process of walking, the maneuverability of the bipedal spring-mass model is realized. The location of the equilibrium points in the workspace and with respect to each other explains how the behavior of the limit cycles (like the CoM trajectory and force profile) can be changed and the fact that the equilibrium gaits are not distinct gaits and continuously evolve to each other to form different gaits.

- **Proposing deadbeat control for walking and investigating the applicability of this strategy for walking.** It is demonstrated that two steps are necessary and sufficient to pinpoint the states of the system to the desired equilibrium point. The sensitivity of the system to the touch-down angle of the swing leg makes the deadbeat control strategy challenging for real world application.

- **Four swing leg control policies are proposed that stabilize the bipedal spring-mass model with large basins of attraction. The proof of concept is validated through implementing on full order model and on real platform.** Two state-based control policies and one time-based control strategy that are proposed, exponentially stabilize the system to the desired limit cycles with large basins of attraction for most of the equilibrium points. Another state-based control technique that is proposed in this work can provide marginal stability for the system.

- **Proposing a feed-forward control strategy for the stance phase to stabilize the system and manages the energy.** A feed-forward function based on time for stance phase combined with the proposed time-based technique, stabilizes the system to the desired limit cycle and energy level. The study uses undamped spring-mass model and the spring-mass model with some damping in parallel to the spring. For the bipedal spring-mass model with physical damping in parallel to spring, the convergence rate and stability enhances significantly suggesting that adding additional damping through software in the control or actual physical damper can enhance the performance of the system.

- **Proposing a bio-inspired flight phase control policy for spring-mass running model over rough terrain.** Inspired from animals' running experiments, three objective functions to provide safety and efficiency are investigated for flight phase policy. It is shown that by a simple flight phase trajectory for the leg, the peak force in the leg can be regulated in the presence of ground level change and both safety and efficiency can be fulfilled together.

1.2 Thesis outline

Chapter 2 reviews the models that have been used for dynamic walking with the emphasis on the passive dynamics of the systems. The bipedal spring-mass model that is the focus of this study is also introduced and reviewed in this chapter. After that in chapter 3, the analysis of the bipedal spring-mass model is presented. The state space of this model for walking is investigated in more detail and the workspace for walking is introduced. Moreover, the equilibrium gaits are found in each energy level and the location and relation between the equilibrium points in the workspace are found. In chapter 4, a deadbeat control strategy based on the limitations and the control authority of the bipedal spring-mass model is proposed in one energy level and extended for different energy levels for walking on rough terrain. Four new control strategies for controlling the swing leg are proposed in chapter 5 to produce stable and robust walking. After presenting the stability analysis of the control policies, the size and shape of the basin of attraction that each control policy creates, are calculated and compared against each other. Furthermore, to manage the energy level of the system, a feed-forward control strategy is presented in chapter 6 for stance phase control of the actuated bipedal spring-mass model. The study will be with and without the presence of damping in the system. Finally in chapter 7, three control strategies are proposed for the flight phase of running. Each of these control policies targets a different objective function to regulate during running and the only control parameter that is used in this chapter is the leg angle at the moment of touch-down. The objective functions are considered for damage avoidance and energy efficiency, bio-inspired control policies that are also important technical issues for real robots. It is concluded that by implementing either of the control policies that are proposed in chapter 7, both goals will be hit at once with a very simple implementation strategy for leg retraction.

Chapter 2 – Background

There are two broad classes for the control of bipedal walking robots: static walking and dynamic walking. In static walking, the robot walks with moderately low velocity such that it is statically stable at each instant of time. On the other side, in dynamic walking control strategies, robots are not stable at each moment of time individually and instead the stability is achieved over time. Therefore, dynamic walking techniques impose less constraints to the system and hence allow more efficient and agile walking. In this study the emphasis will be solely on the dynamic walking models and control strategies.

The story of dynamic walking robots started after McGeer [9] showed that having natural looking and efficient walking robot does not require complicated actuation and sensing. Instead, it requires proper design of mechanical mechanisms and passive elements. In mathematical language he showed that dynamical systems for walking can be stable as a whole over time and not necessarily locally stable at each moment individually. There are many improvements since then to the field of passive dynamics for walking robots inspired from his work [11, 12, 13, 14, 15, 16, 17, 18]. In the following sections, the models and the dynamics that have been used for dynamic walking robots are reviewed.

2.1 Models for walking robots

In this section a review of the models that have been used for dynamic walking is presented. In each part first the mathematical model is presented and then the dynamics of that model and the robots designed and built based on them are enumerated.

2.1.1 Rimless wheel model

The rimless wheel is one of the most elementary conceptual model for passive dynamic walking [9]. Due to the geometry of this model (figure 2.1), it has always one leg on the ground [9]. The angle between the legs (and consequently the number of the legs) can be adjusted to have different types of locomotion. The first idea from passive dynamic walking came from the movement of this model on an inclined surface.

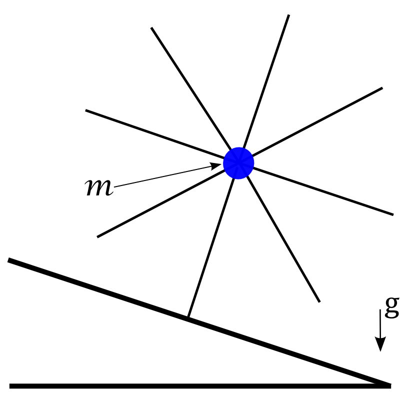

Figure 2.1: The rimless wheel model is a conceptual model for dynamic walking.

2.1.2 Compass gait model

The second basic and most inspiring model for passive dynamic walking is the compass gait model [11]. It is called compass gait because of the shape of this model that is similar to compass [15, 11, 19, 20]. Garcia et al. [11] found that there are stable gaits with respect to the surface slope and Wisse [15] showed that the stable gaits of this model have very narrow basin of attractions. To solve the geometric constraints, four-link compass gait was also investigated. The four-link model has a knee in each leg with a similar dynamics to the compass gait model [15].

The nonlinear behavior of this model was investigated by many researchers to find the bifurcation points and chaos behavior of that to understand the passive dynamics walking with this simple model [21, 22, 23, 24].

The first demonstration of purely passive walker was McGeer [9] passive walker robot. There was no actuation or sensor in his passive walker and the whole walking gaits were based on proper design of mechanical elements and passive dynamics of the system. One of the outstanding characteristics of the passive walker is its natural looking behavior during walking. Therefore, some researchers have used the passive walking control strategy even for fully actuated systems [25]. For example, Anderson et al. [25] controlled three fully actuated robots to walk like passive dynamic walker to take advantage of the natural way of walking properties of passive walkers.

Inspired by the passive dynamic walkers, powered passive dynamic walkers were proposed [14, 26]. Iida et al. [27, 28] found control strategy for powered compass gait when it is walking on rough terrain. Byl et al. [29] included a torque as a control parameter at the hip of the compass gait model and investigated the optimal control for this model. For the powered passive walkers, the controller is based on the passive dynamics of the system, but there exist some actuators mainly to just compensate for the lost of the energy due to impact and friction. The most important source of energy loss in passive walkers are the rigid impact of the striking leg with the ground. To reduce the effect of this problem, researchers used properly designed curved foot for legs that can reduce the energy loss at the time of impact [30, 31, 14, 26]. This idea is used in Cornell university's robots [14, 26].

2.1.3 Compass gait with torso (three-link bipedal robot)

In the compass gait model, the whole body mass is assumed as a concentrated mass at the hip. To consider the effect of the upper body inertia in the passive behavior of the system, a torso is added to the compass gait model [32] to be included in the dynamics of the system.

The results of the analysis for this system showed that it is more efficient and slightly more robust compared to the compass gait model [15]. Moreover, in a more complicated model, it was shown that the existence of the spring between the two legs helped for providing stable walking [15]. Recently, Chen et al. [33] investigated the concept of this model on stochastically rough terrain. They compared the effectiveness of the upper body in the model to the original compass gait model. They found that with torso, the model can handle a five times bigger perturbation than the model without a torso.

Gritfl et al. [34] investigated the chaotic behavior of this model but with a control input between the stance leg and the torso and instead they did not assume the kinematic coupling. They showed that the system can walk stable on steeper slopes and hence reach higher velocities during walking.

2.1.4 Five-link bipedal robot

Another model is five-link bipedal robot which has a torso and knee in each leg. If the legs are assumed massless, the dynamics of the system is the same as the compass gait with torso, but if upper and lower parts of the leg (shin and thigh) have separate mass, the dynamics of the swing leg would be different and consequently it affects the dynamics of the whole system [35, 36]. The existence of the knee in each leg allows the swing leg to have some clear distance from the ground during walking.

For the passive walker models (including compass gait, five-link bipedal robot and the more complicated version seven-link bipedal model), simple leg retraction during walking can enhance the disturbance rejection characteristic of the system [37, 16]. Even though the leg retraction is very simple control strategy, but it requires actuation for walking on level ground and therefore the model should be powered to provide the required swing-leg retraction [37, 16].

2.1.5 Three link walking model with hip springs

Assuming the legs are connected to the torso with passive springs is another model for passive dynamic walking. This model can potentially be able to walk with zero energy cost [17] meaning that the energy loss due to impact can be vanished. The idea is to walk such that the foot has zero velocity with respect to the ground to have zero energy cost. Walking pattern with this model to have zero impact energy lost is far from natural walking and the torso has huge oscillations during walking. Moreover, the authors [17] reported that, they did not find stable fixed point in the analysis of the system which means even though the fixed point to give zero energy cost does exist, but it may not be stable. Chyou et al. [38] have shown that adding torso connected to the legs with passive springs, improves the stability of the system in addition to efficiency.

2.1.6 Bipedal spring-mass model

The bipedal spring mass model (figure 2.2) is inspired by the dynamics and behavior of human walking gaits. The notion is that the locomotion of humans and animals are optimal in both mechanism and control. Therefore, one intelligent way of having optimal legged robots is to reproduce the dynamics of human CoM on the robots. The simplest model that can represent the same dynamics to the body is the spring-mass model [39, 7, 40]. Studies have shown that the bipedal spring-mass model can capture important features of human locomotion like the forces applied to the CoM, the movement of the CoM and the change in the energy level during the gait which are not similar with other simple models.

This model is the bipedal extension of the spring loaded inverted pendulum (SLIP) model which is one of the most accepted model for running [39, 40, 41, 4, 42, 43, 44, 45, 46, 47]. For walking, the rigid inverted pendulum model has been used by

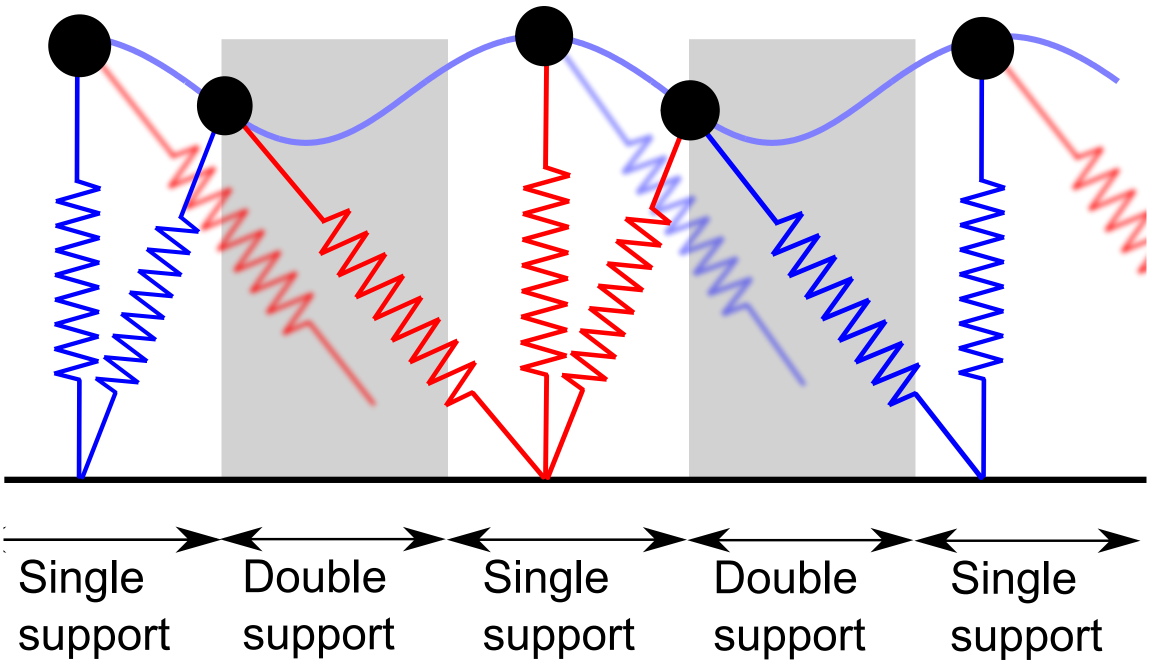

Figure 2.2: Bipedal SLIP model for walking is constituted of two massless legs and a point mass at the hip. The dynamics of the system is hybrid with two phases during walking. When both legs are on the ground, the system is in double support phase and when only one leg is on the ground the model is in single support phase.

numerous researchers [9, 19, 11, 48, 14, 15, 37, 17]. The rigid inverted pendulum can well explain many features of walking [48, 49] and also it is simple to understand the principles of walking [15, 11, 9, 48]. But the ground reaction forces (GRF) between the rigid inverted pendulum model and human data are not consistent [40, 50] which lead to different dynamics between the two system. Also the vertical movement of the human center of mass (CoM) during walking is less than the amplitude that the rigid inverted pendulum model predicts [51, 52]. To match the dynamics of the CoM between human and robots, researchers added more details to the model (like leg segment and leg damping) to generate the double hump force profile of human walking, but these systems are more difficult to understand and gain insights about the locomotion.

Geyer et al. [6, 7] introduced the bipedal spring-mass model by adding a massless leg to the conventional monopod SLIP model that had been used for running. Therefore, the new model has two massless legs and a point mass at the hip. The dynamics of the model is still hybrid for walking [53] because it allows the two legs to be on the ground at the same time as well as one leg alone. When a single leg is on the ground the equations of motion is the same as the conventional SLIP model in stance phase [54, 45, 55, 56], and when two legs are on the ground, the model follows the double support dynamics [7, 53, 57] of the bipedal spring-mass walking model which will be investigated more in detail later. The model is shown in figure 2.2 with the two phases during walking.

This model is capable of generating the shape of the human walking force profile if the transition between single support phase and double support phase is defined properly. It should be noted that to get the double hump force profile (like human walking force profile), the double support phase is crucial [7]. Comparing the simulation results from the bipedal spring-mass model and human experimental data reveals that by setting proper touch-down angles during the passive walk, similar force profile can be generated [7]. In addition to the shape of the force profile, other important dynamical features like the vertical movement of the CoM and the change in the energy during a gait are also compatible between the spring-mass walking model and human walking data [6].

Even though the bipedal spring-mass model was proposed to explain human walking data, from mechanical and physics point of view, too, the bipedal spring-mass model has a huge advantage over other passive model counterparts. This advantage is related to the energy efficiency of this system [58] that makes it theoretically energy conservative and hence provides it the possibility to walk on a flat surface in theory without any need of actuator or ground level inclination to compensate for the energy loss during impact because there is no impact at the contact due to the existence of the spring in the leg. This part along with the inherent passive dynamics of the system, allow it to walk efficiently in comparison to other models that suffer from energy loss at each gait. From the practical point of view, there is some mass between the toe and the spring that are influenced by the impact, but since the mass in this region can be very small (depends on the mechanical design of the system), the loss of energy in the presence of the spring can be negligible [7, 59]. Another mechanical advantage of having spring in the system relates to the interaction of the actuators with environment. The existence of some compliance between actuators and environment would also enable us to measure the forces more accurately, design a safer mechanism and avoid possible mechanical damages that may occur in some situations.

The spring-mass model (the monopod version and the biped version) has been the inspiration for many legged robots [60, 61, 62, 2, 63, 64, 65]. ATRIAS is one of the new robots that has been developed recently (figure 2.3) [2, 1] to have the same dynamics of this model as much as possible.

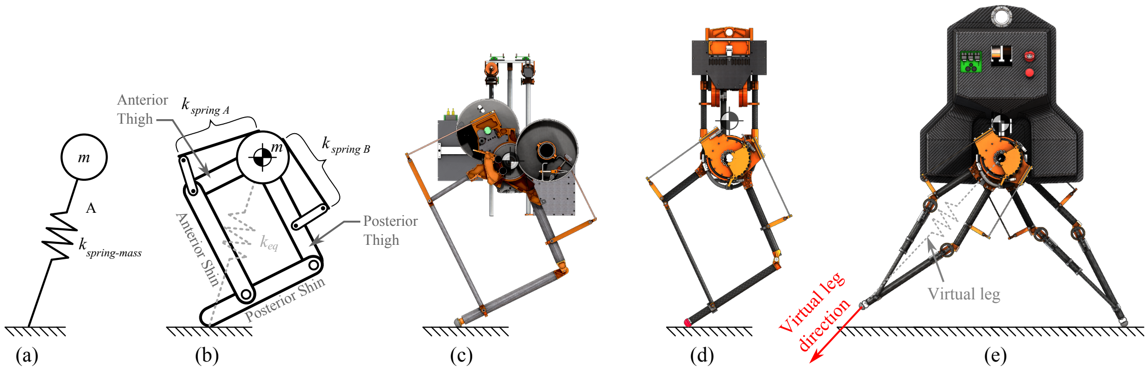

Figure 2.3: Different versions of ATRIAS [1]. a) the concept of ATRIAS, b) leg mechanism, c)ATRIAS 1.0 [2], d) ATRIAS 2.0 and e)ATRIAS 2.1 [1] .

2.1.7 Spring-mass model with torso/trunk (TSLIP)

By adding a torso to the SLIP model, a new reduced order model is obtained [66]. To keep the torso upright in this model, a torsional spring is used between the torso and the leg. One way of stabilizing the torso is to redirect the ground reaction force to a point above the CoM such that the torso behaves like a rigid pendulum [67] hanging from a point above its center of mass.

Rummel et al. [66] used passive spring in the hip and investigated the effect of that on the robustness of the system when the virtual pivot point [67] strategy is implemented. They concluded that the hip spring reveals best robustness with moderate stiffness.

2.2 Dynamics and behavior of the bipedal spring-mass model

In this section we investigate the state of the art knowledge of the behavior of the bipedal spring-mass model in more detail. As mentioned before, the bipedal spring-mass walking model is a hybrid nonlinear system with two distinct phases: single support phase and double support phase. The interval that only one leg is on the ground is called single support phase and when both legs are on the ground it is called double support phase. The dynamics of the system in each of these phases are different. The equations of motion during the single support phase is:

$$m\ddot{\boldsymbol{r}} = \boldsymbol{F_1} - m\boldsymbol{g} \tag{2.1}$$

And for double support phase, the equations of motion would be:

$$m\ddot{\boldsymbol{r}} = \boldsymbol{F_1} + \boldsymbol{F_2} - m\boldsymbol{g} \tag{2.2}$$

Where $\boldsymbol{F_1}$ and $\boldsymbol{F_2}$ in these equations are the force vector of the two legs and can be obtained as:

$$\boldsymbol{F_i} = k_{\mathrm{i}} \left(\frac{l_{0\mathrm{i}}}{|\boldsymbol{r} - \boldsymbol{r_{ti}}|} - 1 \right) (\boldsymbol{r} - \boldsymbol{r_{ti}}), \quad i = 1, 2 \tag{2.3}$$

In these equations k_{i} and $l_{0\mathrm{i}}$ are the stiffness and the zero force length of leg i and $\boldsymbol{r}$ and $\boldsymbol{r_{ti}}$ are the position vector of the CoM and the toe respectively. This is the cartesian representation of the dynamics of the system, there is also another representation of the dynamics of walking with this model that uses the polar coordinates

[53] which is very common for running [55, 45, 41, 54].

Since the spring-mass model is conservative by its nature, the states of the system are related through the constraint coming from the conservation of energy during walking. Therefore, at each instant of time during the single support phase the whole mechanical energy of the system can be obtained as:

$$E = \frac{1}{2}k_1(l_{01} - |\boldsymbol{r} - \boldsymbol{r_{t1}}|)^2 + \frac{1}{2}m(v_x^2 + v_y^2) + mgy \tag{2.4}$$

And for double support phase:

$$E = \frac{1}{2}k_1(l_{01} - |\boldsymbol{r} - \boldsymbol{r_{t1}}|)^2 + \frac{1}{2}k_2(l_{02} - |\boldsymbol{r} - \boldsymbol{r_{t2}}|)^2 + \frac{1}{2}m(v_x^2 + v_y^2) + mgy \tag{2.5}$$

In these equations v_x and v_y are the horizontal and vertical components of the velocity vector and y is the height of the CoM with respect to the ground.

We can simplify the analysis of this system by using the concept of Poincare section given the fact that walking is a periodic process [68, 69, 70]. One way of defining Poincare section for bipedal spring-mass walking to minimize the number of independent states is to define it during the single support phase and when the stance leg has vertical orientation (figure 2.4) it is also known as Vertical Leg Orientation (VLO) [8].

The behavior of the system between the Poincare sections can be studied based on the values of the independent states at the Poincare sections. The history of the states between two consecutive Poincare sections is defined as one gait or one step

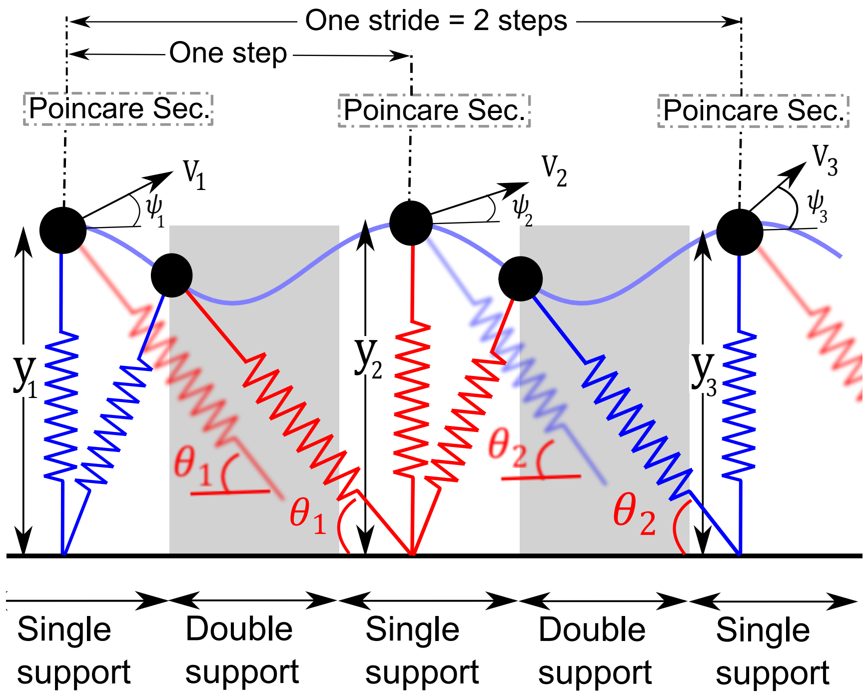

Figure 2.4: Definition of vertical leg orientation (VLO) and the Poincare section for bipedal spring-mass walking system.

[71]. Because of the conservation of energy for the whole gait, the number of the independent states shrink to two variables on the Poincare section. For example, the height of the center of mass and the orientation of the CoM velocity vector at the Poincare section are enough to find the behavior of the system given the touch-down angle of the swing leg (which is the control input). It should be noted that the magnitude of the velocity vector is obtained here from the conservation of energy. The energy equation at the defined Poincare sections can be written as follows:

$$E = \frac{1}{2}k(l_0 - y)^2 + \frac{1}{2}m(v_x^2 + v_y^2) + mgy \tag{2.6}$$

By defining the following variables, the constraint surface due to conservation of energy is obtained [53].

$$w = \sqrt{\frac{k}{m}} \tag{2.7}$$

$$\hat{v}_x = \frac{v_x}{w} \tag{2.8}$$

$$\hat{v}_y = \frac{v_y}{w} \tag{2.9}$$

$$\hat{y} = y - (l_0 - \frac{mg}{k}) \tag{2.10}$$

$$R = \sqrt{\frac{2}{k}(E - mg(l_0 - \frac{mg}{2k}))} \tag{2.11}$$

Therefore, the energy equation can be rewritten in the following form at the Poincare sections which depicts a sphere surface.

$$R^2 = \hat{v}_x^2 + \hat{v}_y^2 + \hat{y}^2 \tag{2.12}$$

In the above equation, to have the largest velocity magnitude, the deflection of the spring should be equal to the static deformation $\Delta_s = \frac{mg}{k}$ when the only force is the weight of the system.

Researchers have chosen different variables at the Poincare section as the independent states. For example, Salazar et al [53] used the height of the CoM and the vertical component of the velocity vector, but Rummel et al [8] chose height of the CoM and the angle of the velocity vector with respect to horizon. Geyer [7] assumed the Poincare section is at the time that the system goes to double support and therefore the number of the independent variables at the Poincare section would be three.

Salazar et al [53] analyzed the dynamics of this model and found the states with finite stability using the well-known and simple constant angle of attack control policy. Based on this control policy, the system keeps the angle of attack constant until it falls or walks for more than 25 steps that they considered as infinite stability (mathematical definition of stability). They analyzed the behavior of the system for three types of locomotion with bipedal spring-mass model: walking, grounded running and running. They showed that it is possible to travel between these three regions by controlling only the touch-down angle of the swing-leg. In [72], Salazar also investigated the evolution of the walking state space as the whole energy of the system changes.

One deficiency of their study about state space is that since they found the states through constant angle of attack policy (CAAP), only the states that can start a walking gait can be found and the states that can be reached at the end of walking gaits cannot be captured.

Rummel et al [8] considered the height of the CoM and the angle of the velocity vector as the independent states at the Poincare section. They compared the robustness of the bipedal spring-mass model with respect to the leg stiffness. The control policy that they used is the constant angle of attack control policy. They found five types of equilibrium gaits with different CoM trajectories and reported that within three types of these five types, local stability (in the sense of constant angle of attack policy) was found. Among the stable gaits they found that one type of asymmetric equilibrium gaits is stable and they did not find stable gaits for other asymmetric gaits. They concluded that the robustness of the bipedal spring-mass model increases with leg stiffness until a moderate value and after that the robustness decreases slightly with increasing the leg stiffness, meaning that there is an optimal leg stiffness for the robustness of the system in walking. It should be noted that the control policy that they used in their study is also the constant angle of attack policy and with different control policy, the results for the optimal leg stiffness and robustness would be different.

Merker et al. [73] showed that even for asymmetric legs, achieving stable walking is possible and in some cases, the stability of the gaits are even improved. They investigated three types of asymmetries: asymmetry in the touch-down angle, in the leg stiffness and in the leg length. They concluded that leg asymmetries does not necessarily reduce the stable region of walking, for example the touch-down angle asymmetry can even enhance the stability of the equilibrium gaits. It should be noted that when the asymmetry in legs is considered, the Poincare section is defined from VLO of each leg until the VLO of the same leg meaning two steps (or one stride) until the same leg is in vertical orientation.

Recently Maus et al [74] investigated the bipedal spring-mass model walking in circle by extending the 2D version of the model. They showed the gaits can be stable if the leg is aligned with the body (the velocity vector of the CoM for example) instead of a world reference frame.

Geyer [7] found an interesting possible behavior for walking that can happen only in the presence of spring in the leg. Because of the existence of spring, different types of oscillation may happen during the stance phase of each leg. For example, for low energy level that the velocity of the system is low, if the leg spring is stiff enough, the natural frequency of the leg is bigger than the duration of the stance phase and it lets the spring to oscillate several times while the leg is passing through its stance phase and he called this type of walking exotic walking. Depends on the leg spring stiffness and the energy of the system, different number of oscillations may happen and hence produce different walking force profiles.

2.3 Control policies for the bipedal spring-mass model

In this section the control strategies that are derived based on the dynamics of the bipedal spring-mass model are explained. These control policies are the direct result of the natural dynamics of the system to achieve the desired goal and not using control theory methods to shape the behavior of the system.

2.3.1 Constant angle of attack policy

The simplest control policy for the bipedal spring-mass model is the constant angle of attack control policy. Based on this strategy, the system keeps a constant touch-down angle each time the swing leg hits the ground [7]. One of the big advantages of this control policy is that it does not require any sensing from outside and the dynamics of the system corrects the error which is also known as self-stable characteristic of the system [7]. Later Rummel et al. [8] analyzed the constant angle of attack in more detail and investigated the robustness of this control policy with different leg parameters. Salazar et al. [53] introduced the concept of finite stability and viability for this control policy and showed for human like parameters, there are equilibrium points that are finite stable. One problem with this control policy is that the stable gaits do not exist everywhere and at each energy level. The robustness of the stable gaits is another issue for the practical purposes. Furthermore, the rate of convergence can be very low inside the basin of attraction. Therefore, after an external perturbation and before recovering from the disturbance, the robot can encounter another perturbation and the accumulating effects of consecutive disturbances may lead to falling.

2.3.2 Constant aperture angle

Inspired by quails grounded running (walking with leg force profile similar to running with no flight phase), Andrada et al. [75] showed that fixed angle between legs (which they called it aperture angle) can lead to finite stability with a large tolerance of perturbation (which means a system with high robustness). Therefore, from engineering point of view, they proposed that grounded running gaits may be useful to avoid quick locomotor changes when facing perturbations. The simplicity of the controller is a remarkable characteristic of it, but since this control policy is very new, it is not still clear if this policy can also be useful for other types of walking gaits (like double hump force profile) or it is only useful for grounded running gaits. Also, they reported that this policy does not necessarily stabilize the gait, it leads to finite stability which means continuing walking for more than 25 steps after the perturbation. This study is very recent, there would be useful to know lot more about this control policy, like the size of the basin of attraction, or if this policy really stabilizes some gaits and the effects of energy change on the behavior of a system under this policy and the sensitivity of the policy to the aperture angle.

Chapter 3 – Analysis of the dynamics of the bipedal spring-mass model

The goal of this chapter is to analyze the behavior of the bipedal spring-mass model for walking. To achieve this goal, the states that can be used as the initial conditions for walking gaits that can complete at least one step are found. After that, the states that are reachable at the end of walking gaits are sought in the state space. The intersection of these two sets contains the states that can be reached at the end of walking gaits and at the same time can start a new walking gait. This characteristic is required for transition states as well as equilibrium points since they come from walking gaits and are used as the initial conditions for the next gaits. This set is the workspace for spring-mass model since any state outside of this set either can not be reached or can not continue the walking process. Furthermore, the behavior of the equilibrium points in the workspace and the relative location of them with respect to each other are investigated.

3.1 Introduction

The bipedal spring-mass model is used as the template for control and design of walking and running robots [2, 1] and in this study the dynamics of this model is investigated. The bipedal spring-mass model represents the system as a lumped mass attached to two massless elastic legs (Figure 3.1). Inspired by human locomotion, it captures key characteristics from the dynamics of human walking [6, 7] including the shape of the ground reaction force profile and the center of mass (CoM) oscillation. This model is a natural extension of the spring loaded inverted pendulum model (SLIP) which has been widely used in literature for modeling and controlling running systems [39, 40, 4, 76].

Using the bipedal spring-mass model, researchers have identified limit cycles for walking, analyzed the stability of these gaits, and investigated the transitions between them. They have applied the resulting insights towards robot control and understanding animal locomotion. However, these existing techniques do not take full advantage of behavior that can be theoretically achieved through manipulating the landing angle.

Rummel et al [8] investigated the role of the leg parameters of the bipedal spring-mass model for robustness and efficiency. Using a constant angle of attack control policy, they found five types of equilibrium gaits with different basins of attraction and local convergence properties.

Through defining the concepts of finite stability and viability, Salazar et al [53] analyzed the model under constant angle of attack policies to demonstrate stability of certain gaits and the ability to transition between gaits across many steps.

The spring-mass model has also been used as a template for controlling full body model of robots [58], and Garofalo et al [77] applied this model to control a fully actuated robot in simulation.

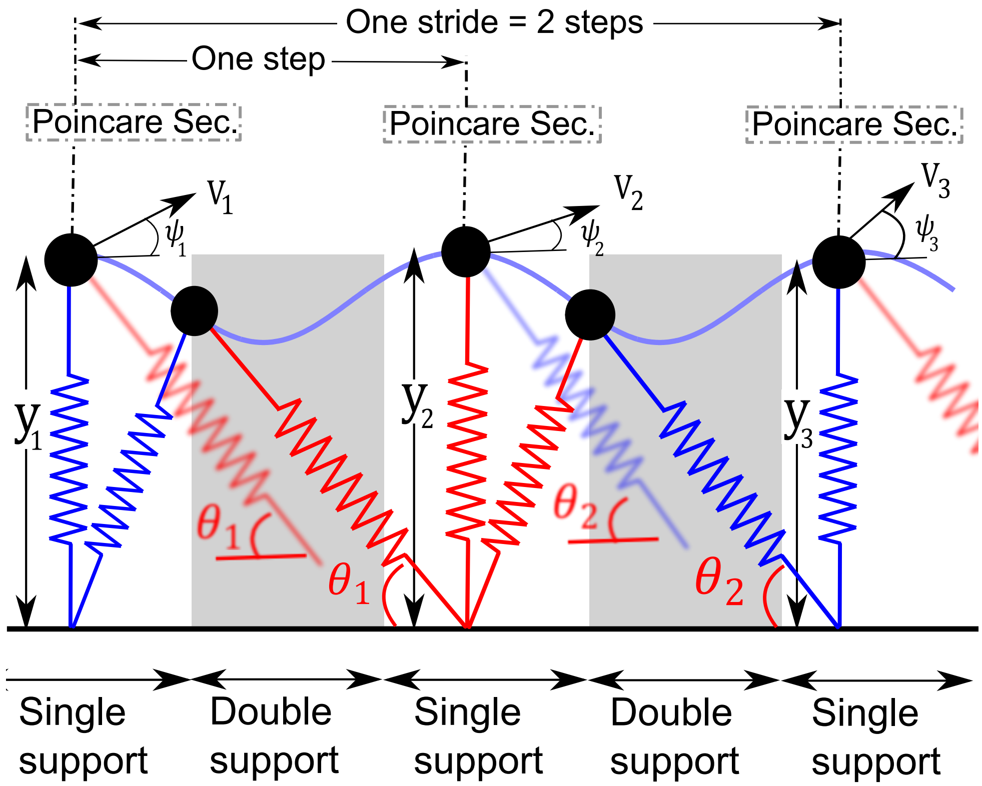

Figure 3.1: The bipedal spring-mass model with single support phase and double support phase. The Poincare section is defined during the single support phase where the stance leg has vertical orientation. The states of the system at the Poincare section are y and ψ. One step is defined from one Poincare section to the next Poincare section and two consecutive steps constitute one stride.

Andrada et al. [75] showed that keeping the angle between the two legs constant leads to robust and finite stable ground running gaits, which may explain how quails walk; while Maus et al [74] extended the model to 3D and investiagted walking in a circle to potentially explain how blindfolded or disoriented people walk.

In this chapter, first by defining Poincare sections and tabulating the transitions in an appropriate state space, we identify a workspace that captures all possible walking behaviors allowed by the model and the equilibrium gaits are found and investigated in the workspace. The outcome of this chapter will allow us to understand the control authority that the swing leg touch-down angle control can provide for the model and where the equilibrium gaits with their specific behaviors are located in the workspace and for transitioning to the desired behavior how to move in the workspace.

3.2 Dynamics of the bipedal spring-mass model

In the bipedal spring-mass model two massless elastic legs are attached to a point mass body [6, 7, 53], and when only one leg is on the ground, the system is equivalent to a spring loaded inverted pendulum (Figure 3.1). The springs store and return energy, rendering the system theoretically conservative with no energy losses. While in this model there is no impact losses like other hybrid walking models [11, 70, 78, 28, 79], this model still has hybrid dynamics due to the distinct single support and double support phases in which respectively only one or both legs are on the ground. In each phase, the dynamics are as follows:

single support:

$$\begin{Bmatrix} \ddot{x} \\ \ddot{y} \end{Bmatrix} = \begin{Bmatrix} \frac{F_1(x-x_{t1})}{m.l_1} \\ \frac{F_1(y-y_{t1})}{m.l_1} - g \end{Bmatrix} \tag{3.1}$$

double support:

$$\begin{Bmatrix} \ddot{x} \\ \ddot{y} \end{Bmatrix} = \begin{Bmatrix} \frac{F_1(x-x_{t1})}{m.l_1} + \frac{F_2(x-x_{t2})}{m.l_2} \\ \frac{F_1(y-y_{t1})}{m.l_1} + \frac{F_2(y-y_{t2})}{m.l_2} - g \end{Bmatrix} \tag{3.2}$$

where the spring compression force F_i and length l_i of each leg are given by

$$F_i = k(l_0 - l_i) \geq 0 \quad i = 1, 2 \tag{3.3}$$

$$l_i = \sqrt{(x - x_{ti})^2 + (y - y_{ti})^2} \quad i = 1, 2 \tag{3.4}$$

In these equations, $[x,\ y]$ are the coordinates of the center of mass (CoM), $[x_{ti},\ y_{ti}]$ are the coordinates of each toe, and the parameters m, k, l_0, and g are respectively the mass, spring stiffness, rest length, and gravitational acceleration.

Single support transitions to double support when the CoM has negative vertical velocity and the condition $y = l_0 \sin(\theta)$ is fulfilled where θ is the touchdown angle of the swing leg and we use this value, which parameterizes leg placement, as the single control input of the system. Double support transitions to single support when the spring deflection $l_0 - l_i$ of one leg returns to zero.

3.2.1 State space

The state space of the bipedal spring-mass model for walking is the set of all the independent states that the system can take in the process of walking. The state space of a system can be parameterized by any set of values that are sufficient to resolve the dynamics, and the representation can be further simplified by defining a Poincare section to convert the system into a series of discrete states [69, 68].

Similar to [8, 71], we define the Poincare section at the vertical leg orientation

(VLO) in single support (illustrated in Figure 5.1). At this condition, the system dynamics and subsequent states can be computed from the height y_n of the CoM and the orientation ψ_n of the velocity vector of the CoM, assuming a control input θ_n for the landing angle of the free leg (subscript $_n$ is used to denote the indexing of the now-discretized system). This holds true because the system has constant energy E, so magnitude $|v_n|$ of the velocity is known given the height y_n and are related through

$$E = \frac{k(l_0 - y_n)^2}{2} + mgy_n + \frac{mv_n^2}{2}. \tag{3.5}$$

Therefore, we define the discrete states at the Poincare sections as

$$\boldsymbol{X_n} = \begin{Bmatrix} y_n \\ \psi_n \end{Bmatrix} \tag{3.6}$$

and express the state-to-state transitions as the following discrete mapping:

$$\boldsymbol{X_{n+1}} = A(\boldsymbol{X_n}, \theta_n), \tag{3.7}$$

since $\boldsymbol{X_n}$ and θ_n provide sufficient information to integrate the equations of motion between Poincare sections.

3.3 Workspace of walking and equilibrium gaits

We start by defining the workspace as all the VLO states that the model can encounter while continuously walking. To find the workspace, we look for two different sets in the state space: the start states, which are all the initial conditions $\boldsymbol{X_n}$ from which a subsequent Poincare section ($\boldsymbol{X_{n+1}}$) can be successfully reached for at least one value of θ_n; and the reachable states, which are all the subsequent states $\boldsymbol{X_{n+1}}$. Here, we take "successfully reach" to mean entering the next Poincare section without falling or entering the flight phase. In the $[y,\ \psi]$ plane of states, these two sets are reflections of each other across the $\psi = 0$ axis, since any trajectory from $\boldsymbol{X_n}$ to $\boldsymbol{X_{n+1}}$ is also a legitimate trajectory from $\boldsymbol{X_{n+1}}$ to $\boldsymbol{X_n}$ if played in reverse (i.e, Figure 3.1 from right to left), which effectively changes the sign of ψ. By definition, the workspace is simply the intersection of the start states and the reachable states.

To find the aforementioned sets, we mesh the $[y,\ \psi]$ plane of possible VLO states (as was mentioned in [53]) into grids of size ($\delta y = 2.5mm, \delta\psi = 1°$), scan over touchdown angles with an increment of $\delta\theta = 0.1°$, and integrate the dynamics from each set of initial conditions. Equilibrium points $\boldsymbol{X_n}$, corresponding to a periodic limit cycle repeated between sequential single support phases, exist wherever

$$\boldsymbol{X^*} = A(\boldsymbol{X^*}, \theta^*) \tag{3.8}$$

for some landing angle θ^*. Similar to [8], we use Newton-Raphson iteration to interpolate equilibrium points between sampled grid points.

To accomplish the simulations, the model was implemented in Matlab (R2012a, Mathworks Inc., Natick, MA, USA) and the following properties for the robot (table 3.1) were assumed. To solve the differential equations, ode45 was used with relative and absolute tolerances equal to 1e-11.

Table 3.1: Properties of the spring-mass robot

Parameter	**Description**	**Value**
m	robot mass	$58.0kg$
k	leg spring stiffness	$12000\frac{N}{m}$
l_0	initial leg length	$0.85m$

3.3.1 Workspace in one energy level

To find the workspace of the system, first all the states that can start and complete at least one walking gait are found (start states). After that, we find the reachable states that can be reached at the end of walking gaits. The intersection of these two sets is the workspace of the system and includes all the states that come from a walking gait and can continue the process of walking.

In Figure 3.4 the aforementioned sets are shown in different colors (green for start states, blue for reachable states and gray to represent the workspace). The workspace has the elliptical shape and represents all the states that are useful for sequential walking. The equilibrium points are distinguished separately by the red color. There are both symmetric and asymmetric equilibrium points in the state space in one energy level. The force profiles for the various types of equilibrium gaits are shown along with their center of mass trajectories from grounded running type of gait to double hump human walking behavior.

Comparing the results from figures 3.2 and 3.3, shows that the states that can start walking gaits and the states that can be reached at the end of walking gaits are mirror of each other. As previously Rummel et al. [8] reported five types for equilibrium points, these states can be shown in the state space of the system.

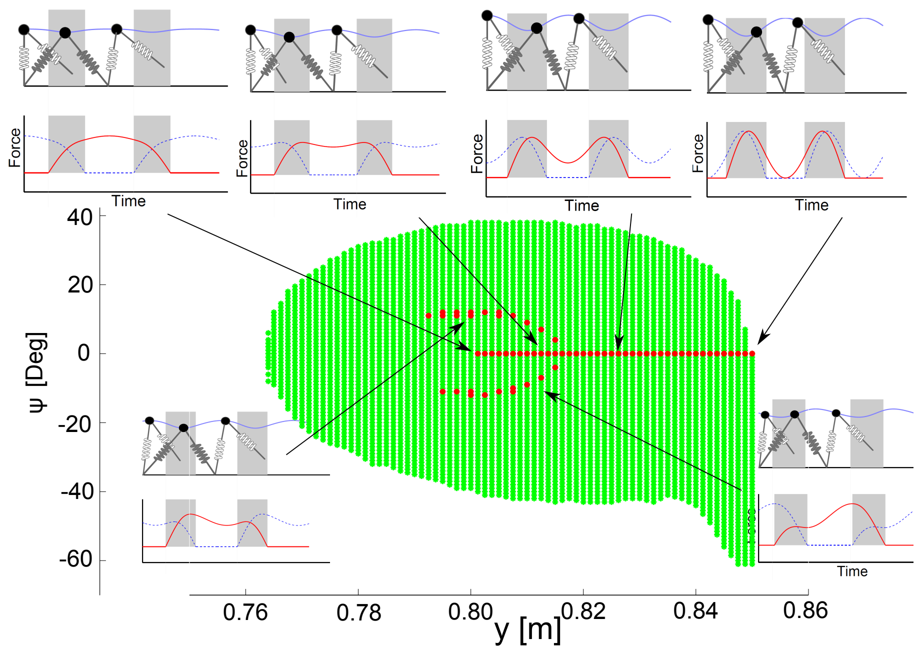

Figure 3.2: The states of the bipedal spring-mass walking model are the height of the CoM (y) and the velocity vector orientation (ψ). All the states that can start successful walking gaits are shown in green. The equilibrium points are highlighted in this region with the red color. The equilibrium points with $\psi = 0$ are symmetric and other equilibrium points (with $\psi \neq 0$) are called asymmetric. The states outside of this region can not start and finish a walking gait with any touch-down angle for the swing leg.

We can find the equilibrium gaits in the state space. Because the equilibrium points return themselves at the end of a walking gait, these states are in both start states and reachable states. The symmetric equilibrium gaits are located on the line $\psi = 0$ in the state space. The equilibrium gaits are shown in figure 3.4.

If due to some disturbances the states of the system are located outside of the workspace, the system can not continue walking. Therefore, the control authority of the bipedal spring-mass model with the touch-down angle control input is limited to the size of this region.

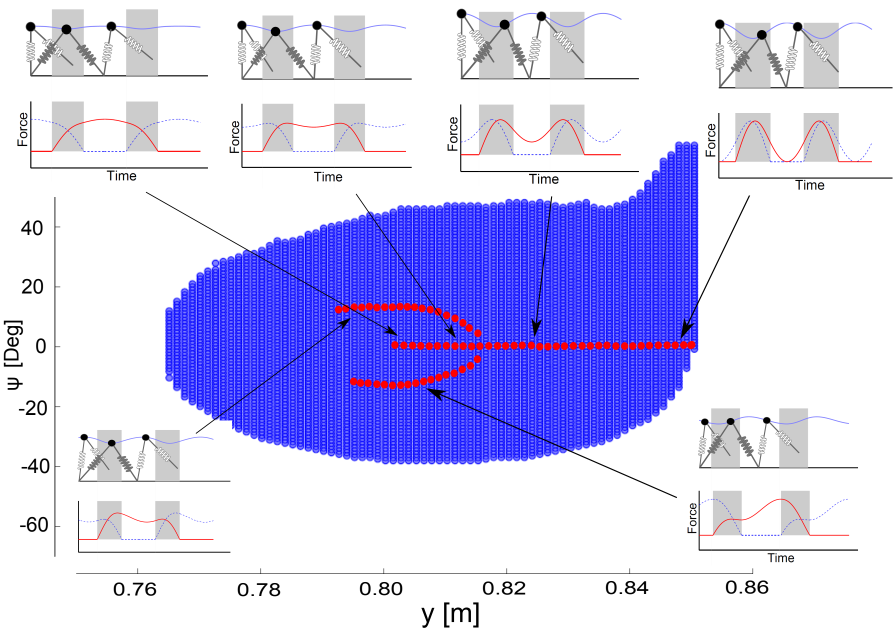

Figure 3.3: The blue region shows the states that can be reached at the end of walking gaits. The states of the bipedal spring-mass walking model are the height of the CoM (y) and the velocity vector orientation (ψ). The equilibrium points are highlighted in this region with the red color. The equilibrium points with $\psi = 0$ are symmetric and other equilibrium points (with $\psi \neq 0$) are called asymmetric.

3.3.1.1 Characterization of the equilibrium gaits

The equilibrium gaits in one energy level are shown in Figure 3.4 as a continuum changing behavior of the system. The force profiles of symmetric gaits evolve from a single hump in the middle of the workspace to a flat shape as it goes to the right and gradually to a double hump (like what we observe from typical human walking [6]) and finally at the far right side of the workspace it looks like hopping with both legs. The shapes of the force profiles for the equilibrium gaits are consistent with the results in [8]. The different behavior of equilibrium gaits provides various choices for

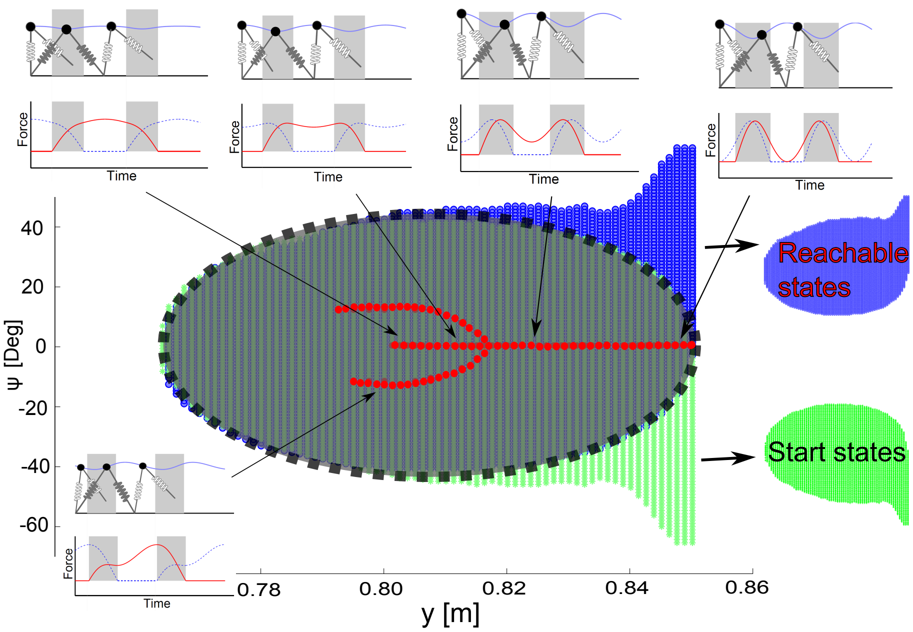

Figure 3.4: Three regions are shown in the state space. The blue region shows the states that can be reached at the end of walking gaits. Green region shows the states that can start walking gaits and gray region (the elliptical region) is the workspace of the system which is the intersection of the reachable states and start states. The equilibrium points are highlighted with the red color. The behavior of the symmetric equilibrium gaits evolve from left to right as a continuous change. For those equilibrium gaits with small CoM height, the COM trajectory is like a straight line and as the CoM height increases at the Poincare section, the behavior of the system becomes bouncier until it evolves to hopping with two legs.

limit cycle walking gaits and can also be useful to explain different locomotion gaits in nature. For example, the schematic force profile of chimpanzee walking gait and the corresponding CoM trajectory of that, is located in the middle of the elliptical [80] while the behavior of human walking gait can be explained by another gait in the right side of the workspace [6], while for grounded running birds like quail the equilibrium gaits are in the left side of the ellipse [75]. Maybe the differences between the types of walking gaits that are observed from different animals depend on the morphology and mechanism of their legs and each gait is optimized for its mechanism.

3.3.2 Workspace in different energy levels

Since the bipedal spring mass model is a conservative system, the workspace is defined assuming a constant system energy. However, on rough terrain, the changing level of the ground height changes the energy of the system, so the workspace and the equilibrium gaits within it across a range of energy levels can be identified.

3.4 Conclusions

In this chapter the dynamics of the bipedal spring-mass model was analyzed and the control authority of the system for walking was investigated. Even though the spring-mass model is energetically conservative and keeps its energy level constant, the analysis can be extended to different energy levels to simulate the cases that external disturbances like the ground level changes varies the energy level of the system.

In each energy level, three regions in the state space were investigated: 1- the states that can start walking gaits (start states), 2- the set of the states that can be reached at the end of walking gaits (reachable states), and 3- the intersection of the aforementioned sets (the states that come from walking gaits and they can start new walking gaits). The Results showed that start states and reachable states are similar in shape and size but mirrored in the shape about the y axis in the state space. The intersection of these two sets has the shape of the eclipse in the $y - \psi$ plane and it is the workspace for walking. The length of the workspace along the y axis is approximately equal to two times of the static deflection of the spring under the weight which means the onset of hopping.

If the state of the system is outside of the start state region, the touchdown angle control is not enough to finish the walking step (the system would fall or would go to flight phase). Similarly, the set of the reachable states shows the limitation of the touchdown angle to the states that it can reach. Therefore, if for any reason we are interested in reaching the states outside of the reachable set, it would not be possible by only controlling the touchdown angle of the swing leg and hence other control inputs are needed.

Results show that the equilibrium gaits with different CoM trajectories and force profiles exist in the workspace of the spring-mass model. The symmetric equilibrium gaits continuously evolve with the CoM height at the Poincare section and it is possible to move between the equilibrium points.

3.5 Future work

For the future work, we plan to study the shape of the workspace in more detail as the parameters of the model change. We also intend to find out the characteristic of the point in the workspace that the asymmetric equilibrium gaits start branching from the symmetric equilibrium gaits.

Chapter 4 – Touch-down angle control for spring-mass walking

In this chapter the fastest converging control policy (also known as deadbeat control) is proposed for walking with the bipedal spring-mass model, which serves as an abstraction of a robot on compliant legs. To fully leverage the passive dynamics of the system, the touchdown angle of the swing-leg is assigned as the only control input of the system. It is shown that two steps (or one stride) are necessary and sufficient to converge to target walking gaits. We present the two-step deadbeat control policy that guarantees stability with the fastest possible convergence rate for the system. For each equilibrium gait, the basin of attraction in which this two-step control exists is a measure of the robustness of the system. The simulation results show that human-like walking gaits (double hump ground reaction force profile) have relatively large basins of attraction. Finally, the policy is extended to various energy levels to accommodate walking on uneven ground that has height changes. It is shown in simulation that the system indeed rejects various disturbances and converges to the desired equilibrium gait in two steps. The study in this chapter was a collaboration with Dr. Hartmut Geyer and his graduate student Albert Wu in Robotics Institute in Carnegie Mellon University. The results in this chapter are benefited from conversation with them.

4.1 Introduction

We use the bipedal spring-mass model as the template for control and design of walking and running robots [2, 1] and in this paper we derive control strategy from the dynamics of the model. The bipedal spring-mass model represents the system as a lumped mass attached to two massless elastic legs (Figure 5.1). Inspired by human locomotion, it captures key characteristics from the dynamics of human walking [6, 7] including the shape of the ground reaction force profile and the center of mass (CoM) oscillation. This model is a natural extension of the spring loaded inverted pendulum model (SLIP) which has been widely used in literature for modeling and controlling running systems [39, 40, 4, 76].

Using the bipedal spring-mass model, researchers have identified limit cycles for walking, analyzed the stability of these gaits, and investigated the transitions between them. They have applied the resulting insights towards robot control and understanding animal locomotion. However, these existing techniques do not take full advantage of behavior that can be theoretically achieved through manipulating the landing angle.

In this chapter, we systematically map out the dynamics of the bipedal spring-mass model as state to state transitions using leg placement as a control input. From this mapping, we identify deadbeat control that converges to target gaits in the minimum number of steps, and the control is defined over explicit regions of attraction. First, by defining Poincare sections and tabulating the transitions in an appropriate state space, we identify a workspace that captures all possible walking behaviors allowed by the model. Within this workspace, any state has a non-zero

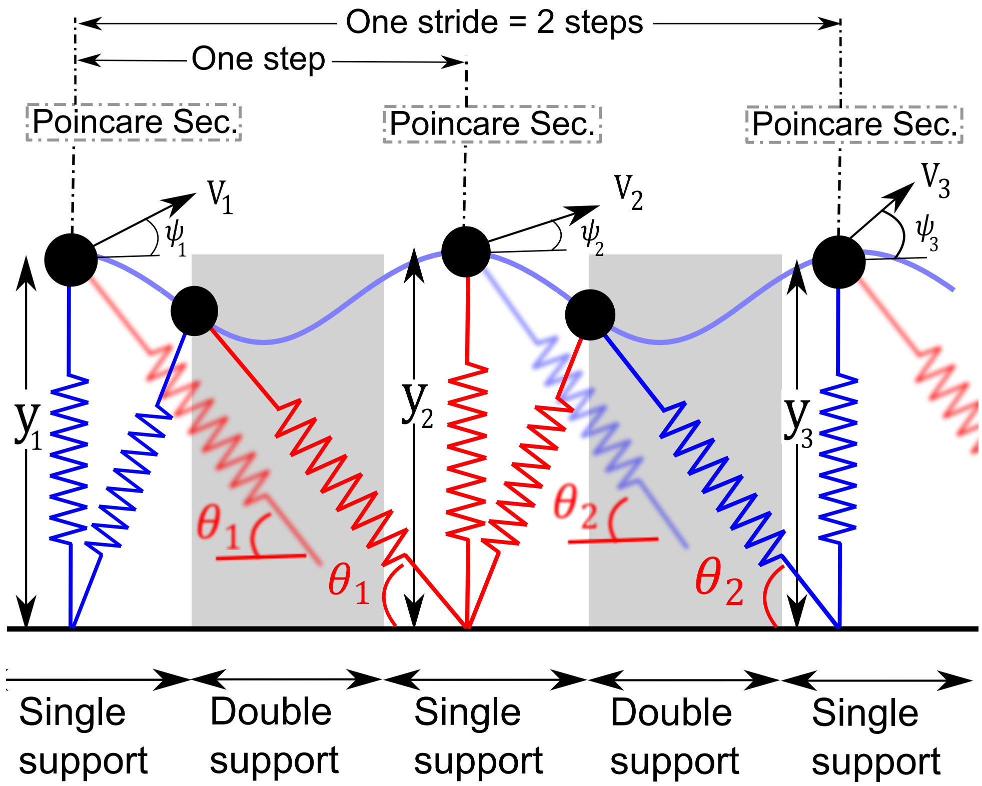

Figure 4.1: The bipedal spring-mass model with single support phase and double support phase. The Poincare section is defined during the single support phase where the stance leg has vertical orientation. The states of the system at the Poincare section are y and ψ. One step is defined from one Poincare section to the next Poincare section and the touchdown angle of the swing leg is shown by θ_1 in the first step and θ_2 in the second step.

region of attraction from which the state can be reached in two steps. Specifically, we deadbeat stabilize the equilibrium gaits with a two-step policy in their regions of attraction, thus achieving the fastest possible convergence. The size of the region of attraction and the relative location of the equilibrium state describes the robustness of each gait. Finally, while the workspace is defined for a constant system energy, we extend the control across different energy levels to demonstrate robust walking on simulated uneven ground.

4.2 Dynamics of the bipedal spring-mass model

In the bipedal spring-mass model two massless elastic legs are attached to a point mass body [6, 7, 53], and when only one leg is on the ground, the system is equivalent to a spring loaded inverted pendulum (Figure 4.1). The springs store and return energy, rendering the system theoretically conservative with no energy losses. While in this model there is no impact losses like other hybrid walking models [11, 70, 78, 28, 79], this model still has hybrid dynamics due to the distinct single support and double support phases in which respectively only one or both legs are on the ground. In each phase, the dynamics are as follows:

single support:

$$\begin{Bmatrix} \ddot{x} \\ \ddot{y} \end{Bmatrix} = \begin{Bmatrix} \frac{F_1(x-x_{t1})}{m.l_1} \\ \frac{F_1(y-y_{t1})}{m.l_1} - g \end{Bmatrix} \tag{4.1}$$

double support:

$$\begin{Bmatrix} \ddot{x} \\ \ddot{y} \end{Bmatrix} = \begin{Bmatrix} \frac{F_1(x-x_{t1})}{m.l_1} + \frac{F_2(x-x_{t2})}{m.l_2} \\ \frac{F_1(y-y_{t1})}{m.l_1} + \frac{F_2(y-y_{t2})}{m.l_2} - g \end{Bmatrix} \tag{4.2}$$

where the spring compression force F_i and length l_i of each leg are given by

$$F_i = k(l_0 - l_i) \geq 0 \quad i = 1, 2 \tag{4.3}$$

$$l_i = \sqrt{(x - x_{ti})^2 + (y - y_{ti})^2} \quad i = 1, 2 \tag{4.4}$$

In these equations, $[x,\ y]$ are the coordinates of the center of mass (CoM), $[x_{ti},\ y_{ti}]$ are the coordinates of each toe, and the parameters m, k, l_0, and g are respectively the mass, spring stiffness, rest length, and gravitational acceleration.

Single support transitions to double support when the CoM has negative vertical velocity and the condition $y = l_0 \sin(\theta)$ is fulfilled where θ is the touchdown angle of the swing leg and we use this value, which parameterizes leg placement, as the single control input of the system. Double support transitions to single support when the spring deflection $l_0 - l_i$ of one leg returns to zero.

4.2.1 State space and discrete dynamics

The state space of the bipedal spring-mass model for walking is the set of all the independent states that the system can take in the process of walking. The state space of a system can be parameterized by any set of values that are sufficient to resolve the dynamics, and the representation can be further simplified by defining a Poincare section to convert the system into a series of discrete states [69, 68].

Similar to [8, 71], we define the Poincare section at the vertical leg orientation (VLO) in single support (illustrated in Figure 4.1). At this condition, the system dynamics and subsequent states can be computed from the height y_n of the CoM and the orientation ψ_n of the velocity vector of the CoM, assuming a control input θ_n for the landing angle of the free leg (subscript $_n$ is used to denote the indexing of the now-discretized system). This holds true because the system has constant energy E, so magnitude $|v_n|$ of the velocity is known given the height y_n and are related through

$$E = \frac{k(l_0 - y_n)^2}{2} + mgy_n + \frac{mv_n^2}{2}. \tag{4.5}$$

Therefore, we define the discrete states at the Poincare sections as

$$\boldsymbol{X_n} = \begin{Bmatrix} y_n \\ \psi_n \end{Bmatrix} \tag{4.6}$$

and express the state-to-state transitions as the following discrete mapping:

$$\boldsymbol{X_{n+1}} = A(\boldsymbol{X_n}, \theta_n), \tag{4.7}$$

since $\boldsymbol{X_n}$ and θ_n provide sufficient information to integrate the equations of motion between Poincare sections.

Using a feedback controller for the control input ($\theta_n = H(\boldsymbol{X_n})$) and substituting it to the dynamics of the system, we will obtain the return map ($f : \chi \to \chi$)

$$\boldsymbol{X_{n+1}} = A(\boldsymbol{X_n}, H(\boldsymbol{X_n})) = f(\boldsymbol{X_n}), \tag{4.8}$$

where manifold χ contains all possible Poincare states $\boldsymbol{X_n}$.

4.3 Workspace of walking and equilibrium gaits

We start by defining the workspace as all the VLO states that the model can encounter while continuously walking. To find the workspace, we look for two different sets in the state space: the start states, which are all the initial conditions $\boldsymbol{X_n}$ from which a subsequent Poincare section ($\boldsymbol{X_{n+1}}$) can be successfully reached for at least one value of θ_n; and the reachable states, which are all the subsequent states $\boldsymbol{X_{n+1}}$. Here, we take "successfully reach" to mean entering the next Poincare section without falling or entering the flight phase. In the $[y,\ \psi]$ plane of states, these two sets are reflections of each other across the $\psi = 0$ axis, since any trajectory from $\boldsymbol{X_n}$ to $\boldsymbol{X_{n+1}}$ is also a legitimate trajectory from $\boldsymbol{X_{n+1}}$ to $\boldsymbol{X_n}$ if played in reverse (i.e, Figure 5.1 from right to left), which effectively changes the sign of ψ. By definition, the workspace is simply the intersection of the start states and the reachable states.

To find the aforementioned sets, we mesh the $[y,\ \psi]$ plane of possible VLO states (as was mentioned in [53]) into grids of size ($\delta y = 2.5mm, \delta\psi = 1°$), scan over touchdown angles with an increment of $\delta\theta = 0.1°$, and integrate the dynamics from each set of initial conditions. Equilibrium points $\boldsymbol{X_n}$, corresponding to a periodic limit cycle repeated between sequential single support phases, exist wherever

$$\boldsymbol{X^*} = A(\boldsymbol{X^*}, \theta^*) \tag{4.9}$$

for some landing angle θ^*. Similar to [8], we use Newton-Raphson iteration to interpolate equilibrium points between sampled grid points.

To accomplish the simulations, the model was implemented in Matlab (R2012a, Mathworks Inc., Natick, MA, USA) and the following properties for the robot (table 4.1) were assumed. To solve the differential equations, ode45 was used with relative and absolute tolerances equal to 1e-11.

Table 4.1: Properties of the spring-mass robot

Parameter	**Description**	**Value**
m	robot mass	$58.0kg$
k	leg spring stiffness	$12000\frac{N}{m}$
l_0	initial leg length	$0.85m$

4.4 Control policy

In this section, we introduce a deadbeat control policy for walking that vanishes the perturbations in the minimal number of steps.

Deadbeat control means a policy that exactly corrects the perturbation in a finite amount of time (usually minimal) [81]. Mathematically, the return map f is called deadbeat on domain χ_d for a specific target X^* if there exists a $K \in \mathbb{N}$ such that [82]:

$$\overbrace{f \circ f \circ \cdots \circ f}^{K \text{ times}}(X) = X^* \quad \forall X \in \chi_d \tag{4.10}$$

The existence of the deadbeat control for running was shown for both 2D and 3D spring-mass models [81, 46]. In this section, we construct a deadbeat control policy for walking that pinpoints the target gait in the minimal number of steps.

As discussed in [81] using the implicit function theorem, a single step would be insufficient for stabilizing an equilibrium gait $(\boldsymbol{X^*}, \theta^*)$ in the bipedal spring-mass model. By varying the single control input θ from a given initial condition $\boldsymbol{X_n}$, the system can only reach a one-dimensional set of states $\boldsymbol{X_{n+1}}$ in the two dimensional $[y,\ \psi]$ plane. Likewise, only a one-dimensional set χ_{d1} of states $\boldsymbol{X_n}$ can be mapped to $\boldsymbol{X^*}$ through the choice of θ_n (In figure 4.2, each blue curve shows the states that can reach each target equilibrium in red). For a hypothetical one-step controller, this deadbeat domain χ_{d1} has zero area; the single-step deadbeat control cannot be properly defined on a meaningful domain.

However, by increasing K to two steps, we can define a two dimensional subset χ_{d2} of the $[y,\ \psi]$ plane as the region of attraction. For any X^*, χ_{d2} is the set of states $\boldsymbol{X_n}$ such that

$$A(\boldsymbol{X_n}, \theta_n) = \boldsymbol{X_{n+1}} \in \chi_{d1} \tag{4.11}$$

where

$$A(\boldsymbol{X_{n+1}} \in \chi_{d1}, \theta_{n+1}) = \boldsymbol{X^*} \tag{4.12}$$

for some sequential pair of touchdown angles θ_n and θ_{n+1}. Therefore, χ_{d2} is the set of states that can transition to some state in χ_{d1}, from which the target $\boldsymbol{X^*}$ can then be reached. This gives us the green regions in Figure 4.2. For any $\boldsymbol{X_n} \in \chi_{d2}$, we solve for θ_n numerically, having tabulated representations of state-to-state mapping A and intermediate domain $\chi_{d1}(\boldsymbol{X^*})$. In execution, we do not explicitly use θ_{n+1}, though if no disturbances are encountered after the first step, re-solving for θ_n at the next iteration yields the previous θ_{n+1} that satisfies $A(\boldsymbol{X_{n+1}}, \theta_{n+1}) = \boldsymbol{X^*}$. Thus, our feedback controller is expressed as

$$\theta_n = H(\boldsymbol{X_n}) = A^{-1}|_{\boldsymbol{X_n}}(\boldsymbol{X_{n+1}} \in \chi_{d1}), \tag{4.13}$$

where the existence of a valid intermediate state $\boldsymbol{X_{n+1}}$ is guaranteed by construction of domain χ_{d2}. This policy yields the Poincare map $f = A(\boldsymbol{X_n}, H(\boldsymbol{X_n})) : \chi \rightarrow \chi$ deadbeat stable on the two-dimensional subset χ_{d2}.

4.4.1 Properties and limitations of two-step control

By construction, $\boldsymbol{X^*} \in \chi_{d1} \subset \chi_{d2}$. The derived control gives the fastest possible convergence for any initial condition in χ_{d2}, and this region of attraction reflects the robustness of the stabilized gait. If the system is perturbed from the red point $\boldsymbol{X^*}$ to a state within this region, the limit cycle will be restored in two steps. Otherwise, more steps are required. Dynamic programming would naturally extend the formulation to optimally solve as many steps as desired (or sequential composition [83] as an approximate method), but here we implement $N = 2$ for sake of simplicity as it is the minimum for a domain of attraction with non-zero area.

Since χ_{d2} exactly represents the region of attraction of the two-step control, the size of χ_{d2} and the proximity of $\boldsymbol{X^*}$ to its boundaries measures the disturbances that the stabilized gait can handle. As can be seen in Figure 4.2, human-like two-humped walking gaits have large regions of attraction, and the nominal behaviors lie well within the boundaries. This shows that these gaits can handle relatively large disturbances in arbitrary directions.

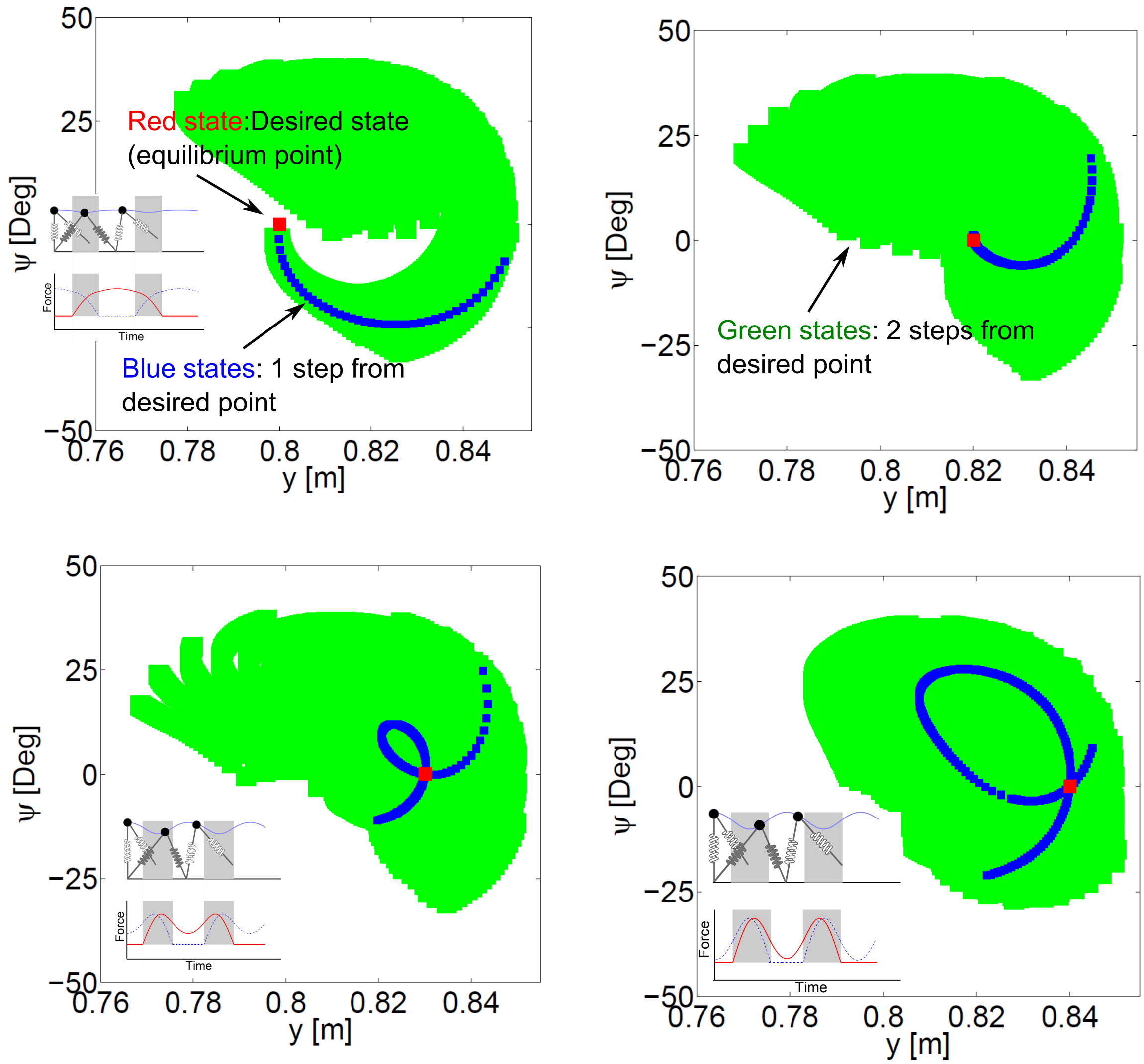

Figure 4.2: Each of the figures above show the region (green area) in the workspace that can return to its equilibrium point (red point). The blue curve is the set of the states that can go to the equilibrium point in one step. When the equilibrium points (red points) are well inside the green region, they are less prone to disturbance. The leg force profile and the CoM trajectory of the red points are shown next to each part.

4.5 Simulation results

In this section we show in simulation that the bipedal spring-mass model can accomplish the two-step deadbeat control and fully recover from random perturbations. Furthermore, we extend the policy from a constant energy level to different energy levels and show that the system can walk on rough terrain that the energy of the system changes due to the change of the ground level change.

We start by showing how to make transition from one equilibrium gait to another desired limit cycle using the two-step deadbeat control policy. In Figure 4.3, transition between the two equilibrium gaits is shown. The system starts from a limit cycle with Poincare state $A(y, \psi) = (0.81m, 0°)$ and goes to transition state $B(y, \psi) = (0.817m, 12°)$ and finally settles into $C(y, \psi) = (0.835m, 0°)$ using the deadbeat control policy.

In the presence of small noises, the final outcome is not desirable. In the figure 4.5 a small noise of magnitude about 0.5° is applied to the touch-down angle. Here, contrary to the ideal noise-free situation, the transition state is changed drastically to another location and the system can not go to the desired state from the transition state.

It should be remembered that the sensitivity of the deadbeat control policy to the touch-down angle of the swing leg is not constant everywhere. Sometimes, the sensitivity is small and therefore the system can reasonably accomplish the transition.

Figure 4.8 shows the stability of the system under different perturbations. As it can be seen in the figure, various different initial conditions all converge to the desired gait $(y, \psi) = (0.83m, 0°)$ in two steps although the horizontal position and history of the CoM are different. The initial conditions are seen from the height and slope of the CoM trajectories ($y,\ \psi$) at the beginning.

For walking on rough terrain, Figure 4.9 shows the model encountering an unexpected drop step with no prior information about the location and size of the disturbance. After the drop step, the preceding Poincare states as well as the system energy are changed. In the workspace of the new energy level, the two-step control to return to $\boldsymbol{X}^* = [y = 0.84m,\ \psi = 0°]$ is computed and applied. The drop step added energy to the system, so while $\boldsymbol{X}^*$ preserved its values of relative height y and direction of motion ψ across ground levels, the new equilibrium gait moves at a faster horizontal speed at the VLO. As can be seen, the new limit cycle is reached in exactly two steps.

4.6 Conclusions

In this chapter we analyzed the dynamics of the bipedal spring-mass model and investigated the control authority of the system for walking. We identified the periodic limit cycles and designed a deadbeat control policy to recover the system from perturbations in the fewest number of steps. We showed that at least two steps are necessary, and that two steps are sufficient to provide regions of attraction that cover significant portions of the workspace. The region of attraction of each stabilized limit cycle reflects its robustness, thus providing useful information for selecting robot walking gaits. We also observed that the gaits most similar to human-like walking have larger regions of attraction with the equilibrium point far away from the edges. Further, we extended the control to handle energy changes in the system from external disturbances like ground level changes and demonstrated its stability in simulation.

4.7 Future work

We showed in this chapter that sensitivity to the touch-down angle is a practical barrier to implementing this control policy on the robot. For the future work, we first intend to exclude the states that are very sensitive to the touch-down angle and then we intend to extend the concept of the deadbeat from a desired gait to a desired region in the workspace. With this modification small errors lead to a neighborhood of the desired gait which is also acceptable. The size of the acceptable region depends on the noises of the system.

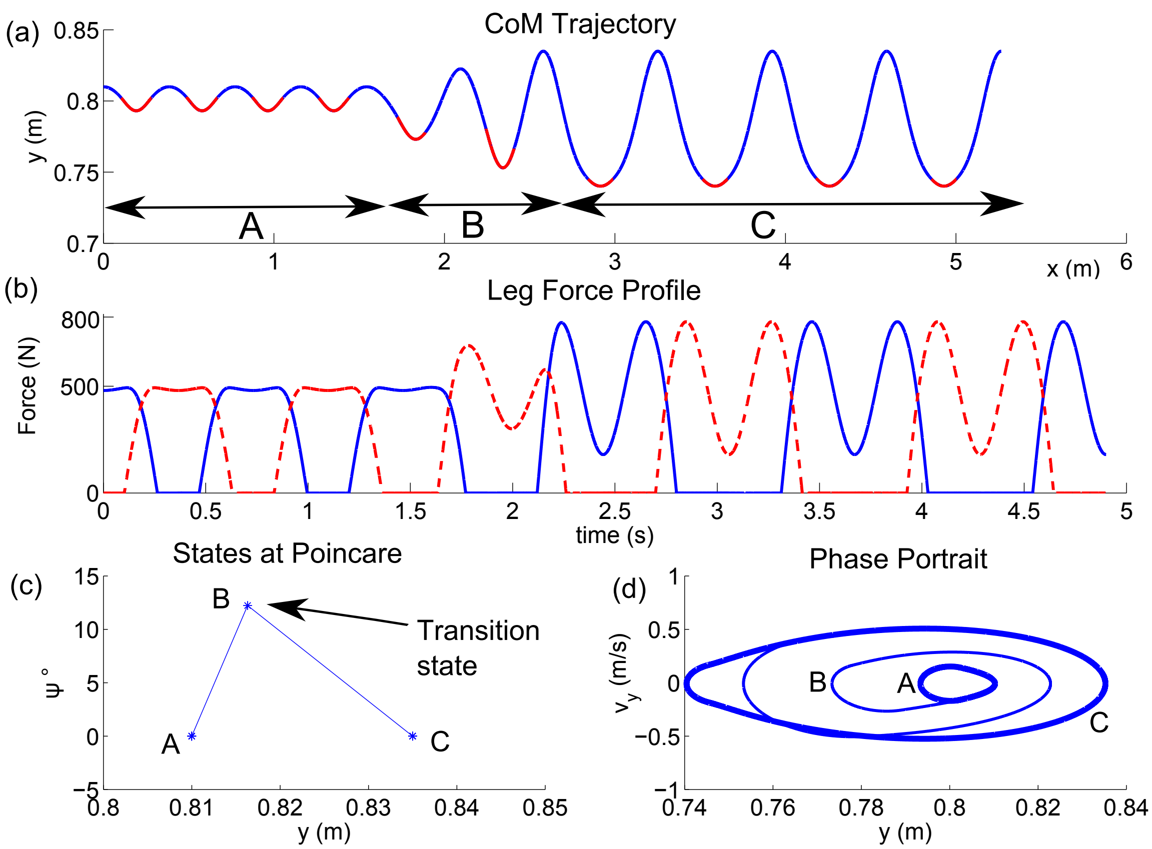

Figure 4.3: Demonstration of the two-step deadbeat control policy for transitioning from $A(y, \psi) = (0.81m, 0°)$ to $C(y, \psi) = (0.835m, 0°)$ using $B(y, \psi) = (0.817m, 12°)$ as transition state. Part (a) shows the CoM trajectory of the system and in part (b) the leg force profiles are shown. The states at the Poincare section are demonstrated in part (c) and (d) shows the phase portrait of the system.

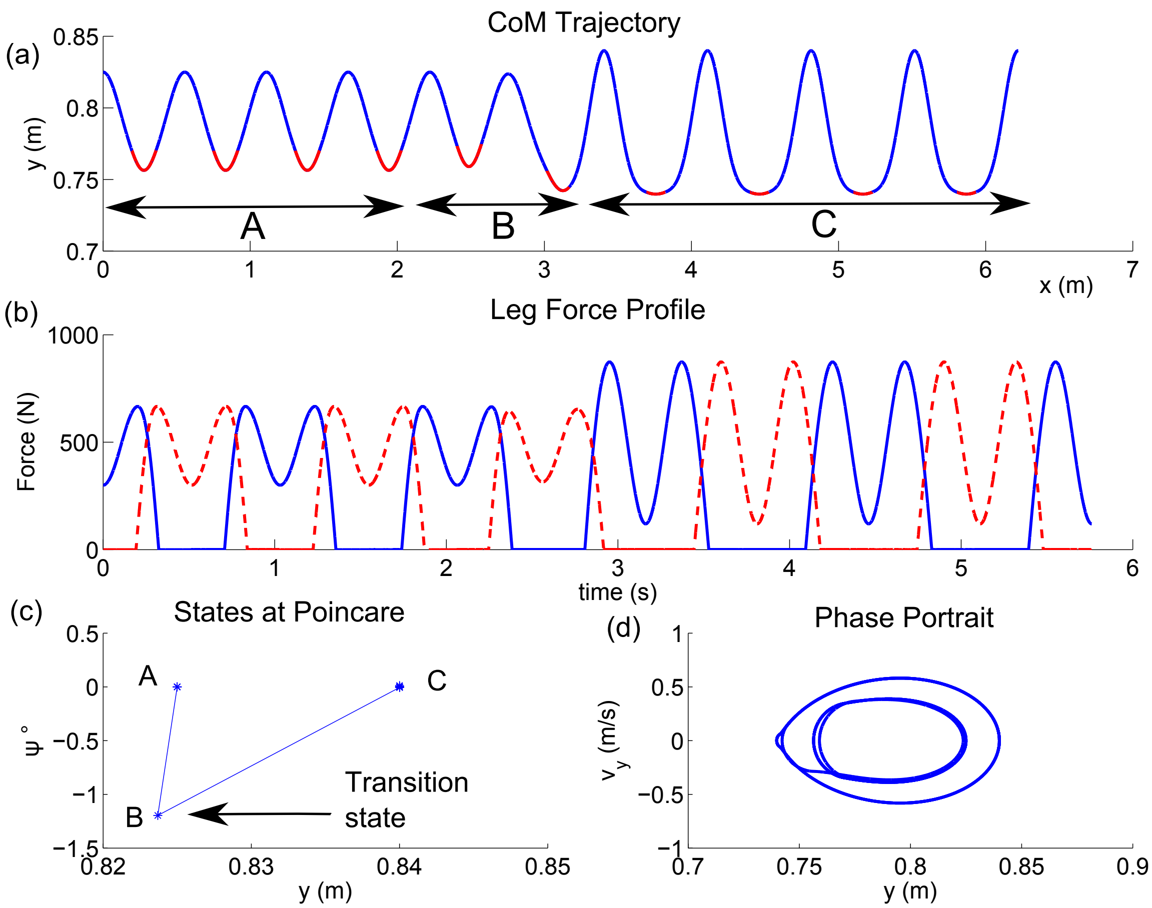

Figure 4.4: The deadbeat control policy can transition the system from $(y, \psi) = (0.825, 0)$ to $(y, \psi) = (0.84, 0)$ through the transition state. In part (a) the CoM trajectory is shown and the force profile is depicted in part (b). The states of the system at the Poincare section is shown in part (c). The phase portrait of the system from the initial limit cycle to the final limit cycle and the transition between them are shown in part (d).

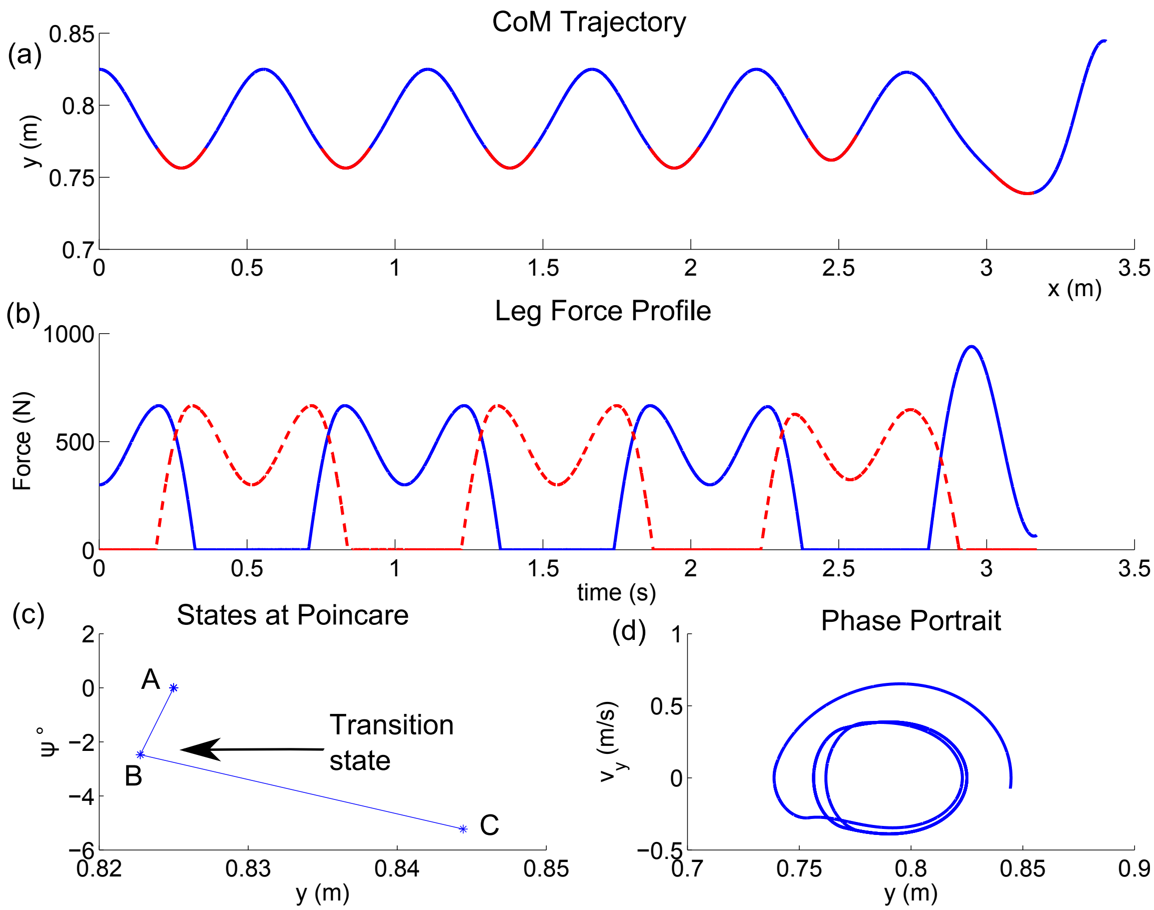

Figure 4.5: The behavior of the deadbeat control policy in the presence of noise. A small noise of magnitude about 0.5° is applied to the touch-down angle. Part (c) shows the states of the system at the Poincare section and the phase portrait of the transition is shown in part (d).

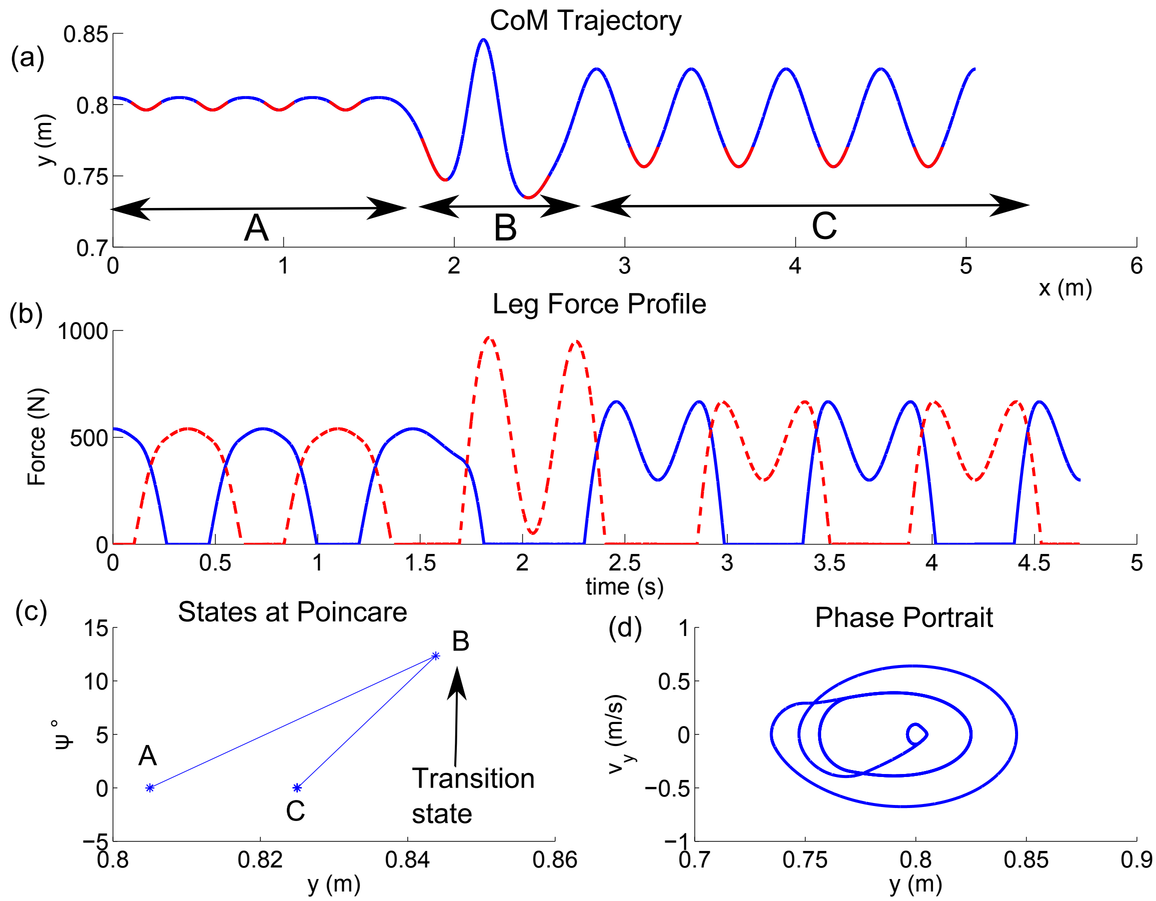

Figure 4.6: The two-step deadbeat control policy navigates the system to go to $(y, \psi) = (0.825, 0)$ from $(y, \psi) = (0.805, 0)$ through the transition state which is far from both of the initial and final states. In part (a) the CoM trajectory is shown and the force profile is depicted in part (b). The states of the system at the Poincare section is shown in part (c). The phase portrait of the system from the initial limit cycle to the final limit cycle and the transition between them are shown in part (d).

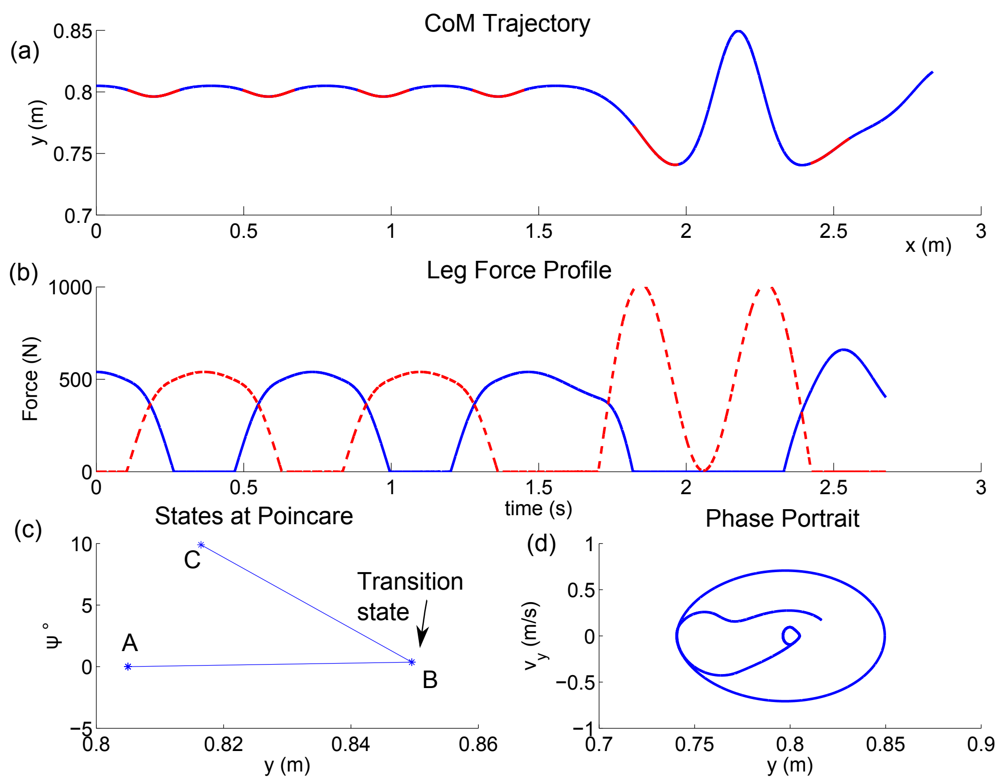

Figure 4.7: Example of the affect of noise in the touch-down angle of the swing leg. Here the noise applied to the system is around 0.5°. The system finally settles in a state far from the desired state.

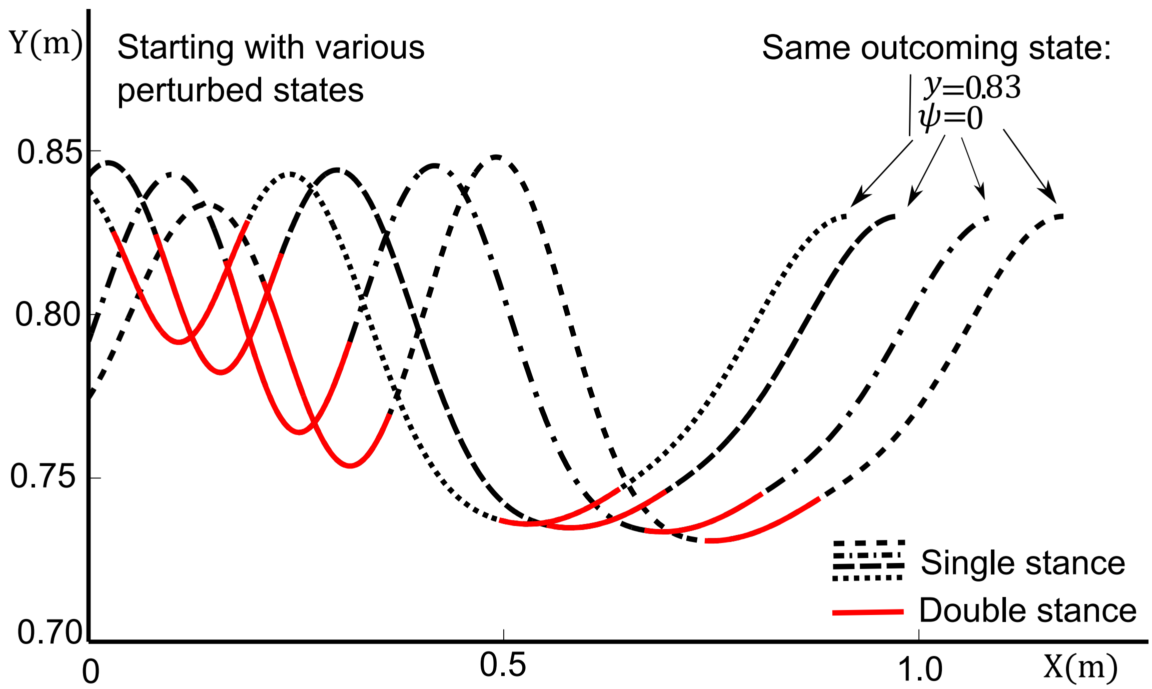

Figure 4.8: Center of mass trajectory of the bipedal spring-mass model starting from various perturbed initial conditions. For all the cases, the system settles into the desired state in two steps. The double stance phases are shown in solid red lines and the dashed black lines are the single stance phases.

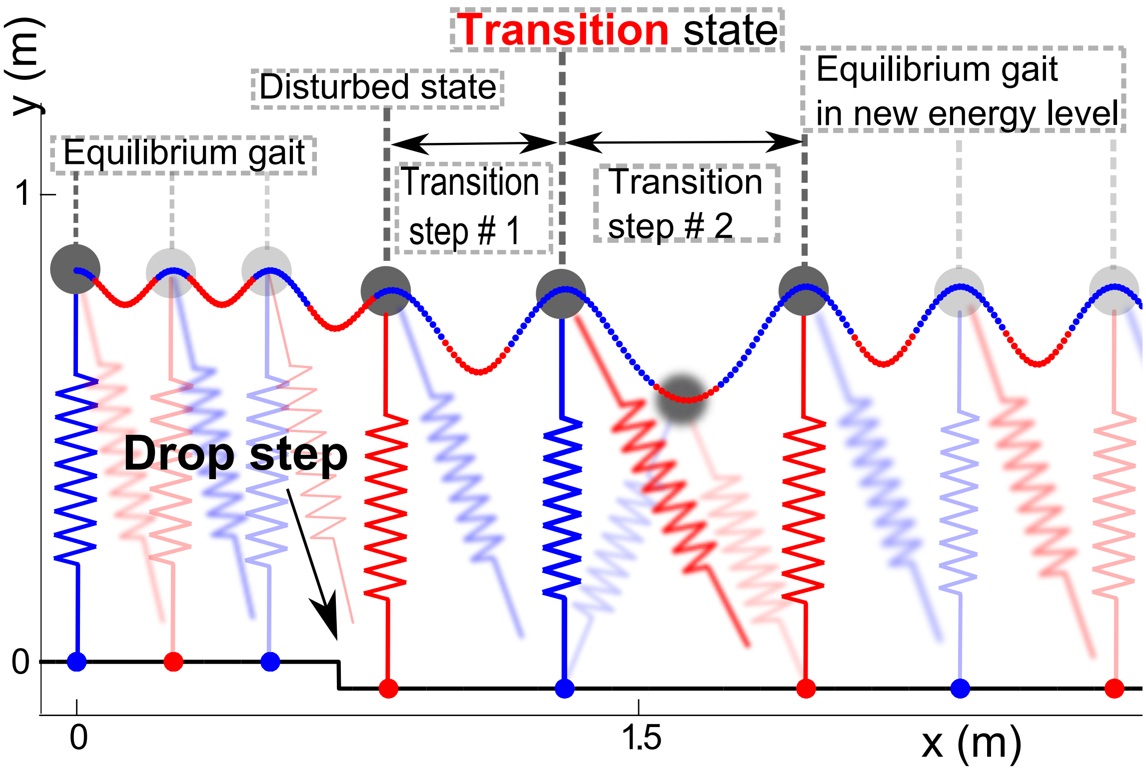

Figure 4.9: Center of mass trajectory of the bipedal spring-mass model before and after a drop step in the ground. The system does not have prior information about the size and location of the disturbance. After the drop step, the system goes to a disturbed state in the new energy level (determined by the height of the drop step). To pinpoint the desired equilibrium gait, the system first goes to a transition state and after that it pinpoints the new desired equilibrium gait.

Chapter 5 – State-based and time-based switching policies

In this chapter, new swing leg control policies are proposed for the bipedal spring-mass model and confirmed on the full order model of the robot as well as the real hardware. First, the proposed control policies are evaluated for stability and robustness at the level of reduced order model and compared with the existing swing-leg control policies. After that the resulting behavior of the bipedal spring-mass model with the proposed control policies are compared with the behavior due to the current swing leg control policies. The comparison for different scenarios show the superiority of the proposed control policies over the existing strategies. Moreover, the basins of attraction that each control policy provides for different equilibrium points are calculated and compared. Several numerical examples show the significant robustness of the proposed control policies. Finally, the validity of the analysis on the reduced order model is shown through implementing one of the most successful proposed control policies on the simulation of the full order model and on the real platform. It is shown that the proposed control policy can successfully stabilize the full order model as well as the robot itself with the expected behavior. This chapter will be submitted as a paper in collaboration with Dr. Hartmut Geyer in Robotics Institute, Carnegie Mellon University.

5.1 Introduction

We use the bipedal spring-mass model as the template for control and design of walking and running robots [2, 1] and in this paper the focus is on control for walking robots. The bipedal spring-mass model is inspired from the dynamics of human walking [6, 7] and is an extension of a more well-known model for running, called spring loaded inverted pendulum (SLIP) model [39, 40, 4, 76]. Geyer et al. [6, 7] showed that the bipedal spring-mass walking model can capture some of the important characteristics of human walking like the shape of the ground reaction force profile and the center of mass (CoM) oscillation during walking. This model has two massless elastic legs connected to a lumped mass (figure 5.1). The spring in the leg allows the system to maintain energetically conservative with no energy loss at the impacts with the ground, but the dynamics of this model is still hybrid due to the two phases that occur during walking: single support phase where only one leg is on the ground and double support phase where both legs are on the ground at the same time.

Rummel et al [8] found different types of equilibrium points with different sizes for the basins of attraction using the constant angle of attack control policy. The results of the paper give very good insights about the various equilibrium points and their stability with respect to the chosen control policy (constant angle of attack policy). However, they did not address the rate of convergence of the equilibrium points when the perturbation is not very small.

Salazar et al [53] analyzed the bipedal spring-mass model and defined concepts such as finite stability and viability. They considered constant angle of attack control

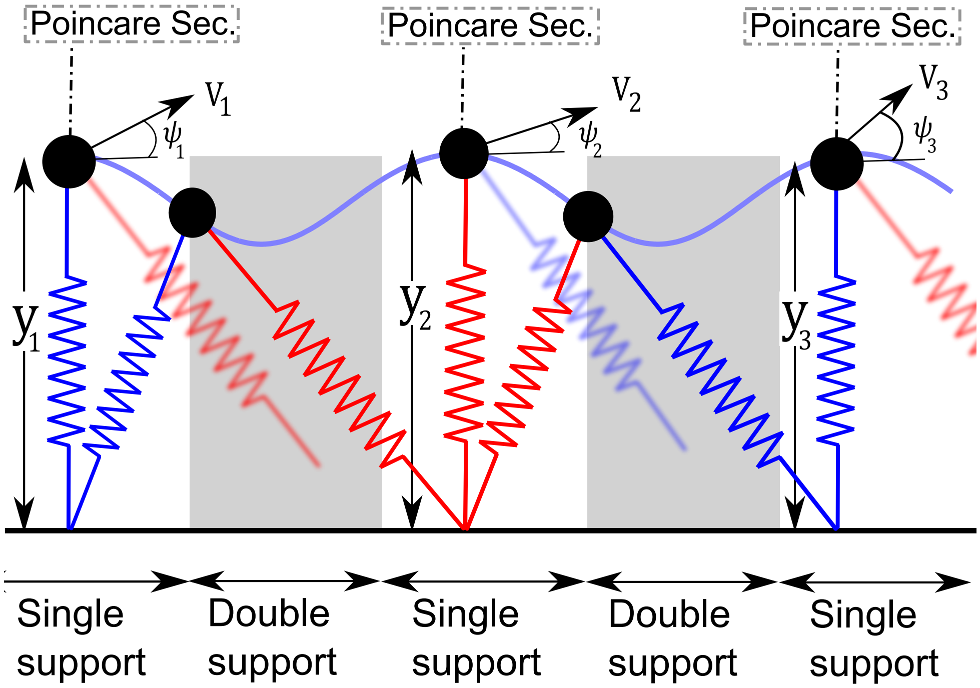

Figure 5.1: The bipedal spring-mass model with single support phase and double support phase. The Poincare section is defined during the single support phase where the stance leg has vertical orientation. The states of the system at the Poincare section are y and ψ. One step is defined from one Poincare section to the next Poincare section and the touchdown angle of the swing leg is shown by θ_1 in the first step and θ_2 in the second step.

policy for studying the stability and viability of the system. Even though they showed that it is possible to change the gait in the same energy level, the gait transition in their method does not happen in a minimum number of steps and it can take a long time until the system converges to the desired state.

Recently Maus et al [74], extended the 2D bipedal spring-mass model to 3D and investigated the walking in circle. They demonstrated that the model is capable of explaining certain behaviors that are observed from blindfolded or disoriented people during walking.

Andrada et al. [75] showed that keeping the angle between the two legs constant can lead to a robust and finite stable ground running gaits.

The spring-mass model has been also used for controlling the full body model of robots [58], and very recently Garofalo et al [77] used this model to control a fully actuated robot. It should be noted that the advantage of the spring-mass model is more prominent on the robots with tuned springs in the legs.

In this study, first the mathematical model of the bipedal spring-mass model is presented. Then the current control policies for the swing leg of the model are reviewed. After that, the new control strategies for the swing leg are presented. To show the stability of the proposed and current control policies, the magnitude of the eigenvalues are calculated and compared with each other. For the stable control policies, the resultant basins of attraction for different policies are calculated and then compared against each other. The behavior of the system subject to initial perturbation is presented for different scenarios and finally the behavior of the system when it is walking on rough terrain is demonstrated in simulation which the energy of the system changes.

5.2 Mathematical model and formulation

We use the bipedal spring-mass model [6, 7, 53] for our simulation. This model consists of a concentrated mass connected to two elastic massless legs such that when only one leg is on the ground, it looks like an inverted pendulum (figure 5.1). From the engineering perspective, the existence of spring in the leg prevents any energy loss during impact and therefore walking with this mechanism would be energy efficient (theoretically no energy loss). It should be noted that even though with this model the leg impact does not instantaneously change the velocity of the system (contrary to other walking models [11, 70, 78, 28, 79]), the dynamics of this model is still hybrid due to the two possible phases during walking: single support phase and double support phase. Single support phase is the time that only one leg is on the ground and double support phase refers to the time when both legs are on the ground at the same time.

Single support phase dynamics:

$$\begin{Bmatrix} \ddot{x} \\ \ddot{y} \end{Bmatrix} = \begin{Bmatrix} \frac{F_1(x-x_{t1})}{m.l_1} \\ \frac{F_1(y-y_{t1})}{m.l_1} - g \end{Bmatrix} \tag{5.1}$$

Double support phase dynamics:

$$\begin{Bmatrix} \ddot{x} \\ \ddot{y} \end{Bmatrix} = \begin{Bmatrix} \frac{F_1(x-x_{t1})}{m.l_1} + \frac{F_2(x-x_{t2})}{m.l_2} \\ \frac{F_1(y-y_{t1})}{m.l_1} + \frac{F_2(y-y_{t2})}{m.l_2} - g \end{Bmatrix} \tag{5.2}$$

Where

$$F_i = k(l_0 - l_i) \quad i = 1, 2 \tag{5.3}$$

$$l_i = \sqrt{(x - x_{ti})^2 + (y - y_{ti})^2} \quad i = 1, 2 \tag{5.4}$$

In these equations, m, k and l_0 are the mass, leg stiffness and zero force leg length of the legs respectively and $g = 9.81\,\mathrm{m/s^2}$ is the gravitational acceleration. The coordinates of the center of mass (CoM) are shown by x and y and the coordinates of the toes are (x_{t1}, y_{t1}) and (x_{t2}, y_{t2}). The leg forces are F_1 and F_2 which only can be in compression.

The transition from single support phase to double support phase occurs when the condition $y = l_0 \sin(\theta)$ is fulfilled where (θ) is the touchdown angle of the swing leg which is determined from the control policy and it is the only control input for the system. The transition between the double support phase to single support phase occurs when the spring deflection of one leg returns to zero (the length of the leg becomes equal to its corresponding zero force leg length).

5.3 Control strategies

Considering that the bipedal spring-mass model is energetically conservative, the number of the independent variables during single support phase reduces to three. We can reduce the number of the states even more by using the concept of Poincare section and return map [69, 68]. One way of defining the Poincare section for walking is during the single support phase where the stance leg has vertical orientation (also known as vertical leg orientation (VLO) [8, 71]). Figure 5.1 shows the position of this Poincare section in the gait. By this definition, the number of the independent states at the Poincare section reduces to two (the height of the CoM (y) and the velocity vector orientation (ψ)). The magnitude of the velocity at the Poincare section can be calculated from the conservation of energy in the system. The whole mechanical energy can be written as follows:

$$E_n = \frac{1}{2}k(l_0 - y_n)^2 + \frac{1}{2}mv_n^2 + mgy_n \tag{5.5}$$

The analysis of the system can be simplified by using the concept of return map f acting on the Poincare section χ:

$$f : \chi \to \chi \tag{5.6}$$

Here, χ is the manifold that contains the states on the Poincare section. Therefore for the bipedal spring-mass model, the elements in χ for the nth step of walking are in the form of:

$$\boldsymbol{X_n} = \begin{Bmatrix} y_n \\ \psi_n \end{Bmatrix} \tag{5.7}$$

Which the return map f returns the states on the next Poincare section:

$$\boldsymbol{X_{n+1}} = f(\boldsymbol{X_n}) \tag{5.8}$$

The return map can be obtained from the dynamics and the control input (here: θ_n). If the map of the dynamics is shown by A then:

$$\boldsymbol{X_{n+1}} = A(\boldsymbol{X_n}, \theta_n) \tag{5.9}$$

Using a feedback controller for the control input ($\theta_n = H(\boldsymbol{X_n})$) and substituting it to the dynamics of the system, the return map is obtained:

$$\boldsymbol{X_{n+1}} = A(\boldsymbol{X_n}, H(\boldsymbol{X_n})) = f(\boldsymbol{X_n}) \tag{5.10}$$

In these equations the function H defines the orientation of the swing leg at the moment of touch-down. By changing the touch-down angle at the time of contact, the initial conditions for the beginning of the double support phase are changed and since the dynamics of the system during the double support phase and the subsequent single support phase are solely passive, the effect of the control policy at the next Poincare section is determined through the change on the initial conditions at the beginning of the double support phase. To understand the effect of the change in the transition to the next Poincare section, figure 5.2 is considered.

In this figure, the control input influences the initial conditions ($x, y, \dot{x}$ and $\dot{y}$) at the beginning of the double support phase. Since the final goal is to use the control policy on the robot and given the fact that there are some mechanical components that are ignored in the level of reduced order model, the control policy needs to be as independent as possible from the states of the system like the concept of self-stability [84, 85, 7]. For example policies like the constant angle of attack control policy [7] that provides the same touch-down angle for each step regardless of the states of the system would be less sensitive to the discrepancies in modeling than the control policies like deadbeat control that the touch-down angle depends on the states at the Poincare section. It should be noted, even for providing self-stable control policies like the constant angle of attack policy, we do require sensor data from the proprioceptive sensors, but it is important that the value of the control input (like angle of attack) is not determined from feedback calculation of the states and this makes the control policy less prone to the simplifications in modeling.

For the proposed control strategies, we investigate the switching policies between the single support phase and double support phase that are predefined functions between the initial conditions ($x, y, \dot{x}$ and $\dot{y}$) at the moment of transition (figure 5.2). It should be noted that among the four initial conditions at the beginning of the double support phase, due to the conservation of energy in the model, there are three independent variables. Also, from the practical point of view for using the initial conditions, the preference is on the control policy that requires minimal sensing from the system while providing stable and robust gaits. Therefore, we first look for control policies that require minimal proprioceptive information from the system that can create stable and robust gaits. Moreover, between the initial conditions, measuring the $\dot{x}$ and the $\dot{y}$ on the robot require differentiating the proprioceptive quantities which bring more noise and uncertainty to the transition. Therefore, using the velocity states to define the transition function is studied if we can not find transition functions based on only x and y that creates stable and robust gaits.

5.3.1 Current control policies

There are two swing leg control policies that currently are available for the control of the bipedal spring-mass model. The details of these control strategies are presented in this section.

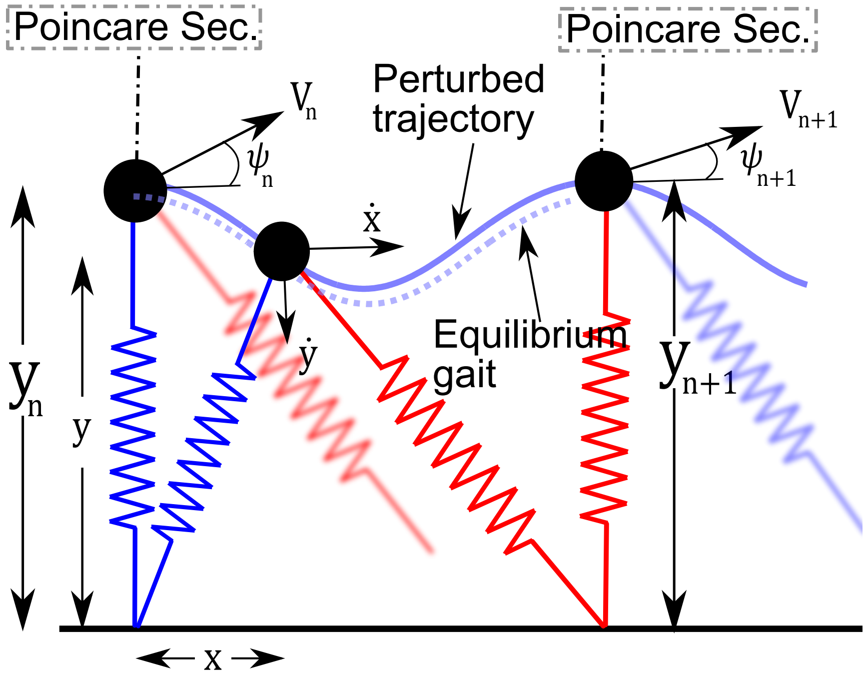

Figure 5.2: The swing leg control policy determines the initial conditions at the beginning of the double support phase ($x, y, \dot{x}$ and $\dot{y}$) and the effect of the swing leg control policy on the next Poincare section is determined through these variables because the double support phase is solely passive.

5.3.1.1 Constant angle of attack policy

The constant angle of attack control policy is the first control strategy that was proposed and investigated for the bipedal spring-mass model [7]. Inspired by the self-stable characteristic of the SLIP model for running, Geyer [7] was the first one that showed the bipedal spring-mass model can also be self-stable by keeping the angle of attack constant. Therefore, for the stable limit cycles, the system approaches the equilibrium point if it is subjected to a disturbance by only keeping the swing leg angle constant at the time of contact. The size of the basin of attraction and the convergence rate can be different for different systems and different equilibrium points. Later Rummel et al. [8] analyzed the constant angle of attack in more detail and investigated the robustness of this control policy with different leg parameters. Salazar et al. [53] introduced the concept of finite stability and viability for this control policy and showed for human like parameters, there are equilibrium points that are finite stable.

Based on this control policy the system goes to the double support phase when the height of the CoM satisfies $y = l_0 sin(\theta_{TD})$ and therefore this control policy can be categorized as a state-based switching control policy for transitioning from single support phase to double support that regulates the height of the CoM (y in figure 5.2) at the time of touch-down.

5.3.1.2 Constant aperture angle policy

Inspired by quails grounded running (walking with leg force profile similar to running with no flight phase), Andrada et al. [75] proposed that fixed angle between legs, which they called it aperture angle and is shown in figure 5.3, can lead to finite stability with a large tolerance of perturbation (which means a system with high robustness) [75].

Therefore, from engineering point of view, they proposed that grounded running gaits may be useful to avoid quick locomotor changes when facing perturbations. The simplicity of the controller is a remarkable characteristic of it, but since this control policy is very new, it is not still clear if this policy can also be useful for other types

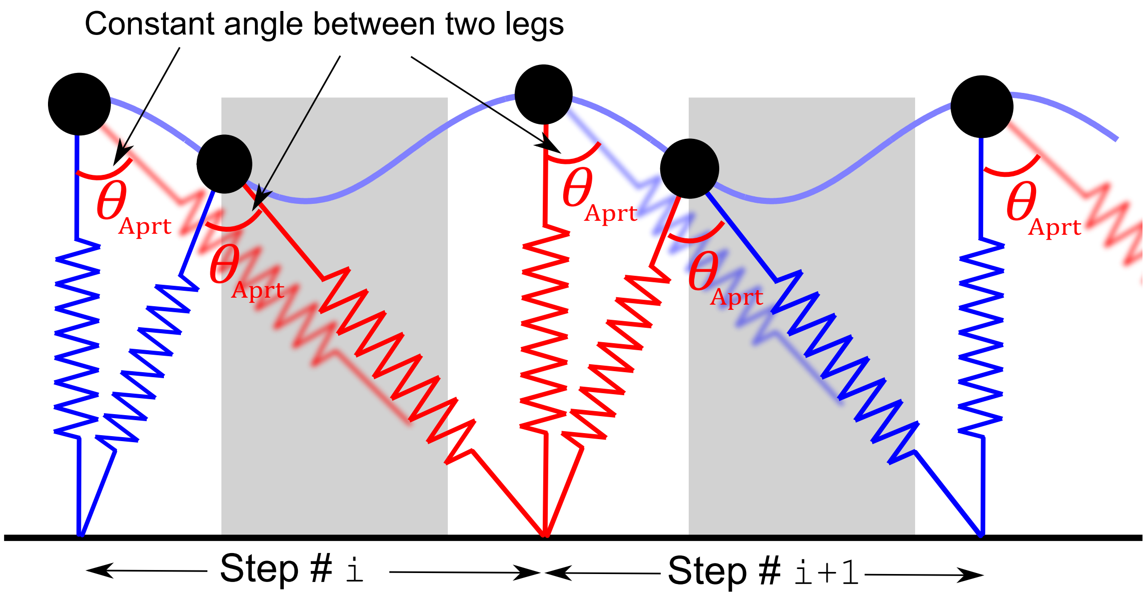

Figure 5.3: The constant aperture angle control policy. The swing leg is adjusted such that the angle between the stance leg and the swing leg remains constant.

of walking gaits (like double hump force profile) or it is only useful for grounded running gaits. Also, they reported that this policy does not necessarily stabilize the gait, it leads to finite stability which means continuing walking for more than 25 steps after the perturbation. This study is very recent, there would be useful to know lot more about this control policy, like the size of the basin of attraction, or if this policy really stabilizes some gaits and the effects of energy change on the behavior of a system under this policy and the sensitivity of the policy to the aperture angle.

The constant aperture angle policy can be interpreted as a policy that regulates a function between the x and y to define the transition from single support phase to double support phase.

5.3.2 Proposed control policies

In this section the proposed control policies for the swing leg are presented. As was mentioned earlier, the focus is on the control policies that defines a function between the proprioceptive quantities and we do not consider the derivative of these quantities due to more uncertainty that differentiatiation brings in the calculcations. There are one time-based control policy that proposes to regulate the time for the touch-down and three state-based control policies that regulate some state-dependent parameters at the moment of transition from single support to double support.

5.3.2.1 Constant CoM displacement

The first proposed control policy directly targets the horizontal position of the CoM after the Poincare section. Contrary to the constant angle of attack control policy that regulates the hieght of the CoM for the transition to double support, in this control policy here, the horizontal position of the CoM is regulated for the transition. In this policy the system transitions to double stance from single support phase when the horizontal position of the CoM reaches a predefined value after the Poincare section. Therefore, this policy regulates the horizontal position of the CoM with respect to the toe that is on the ground as it is shown in figure 5.4.

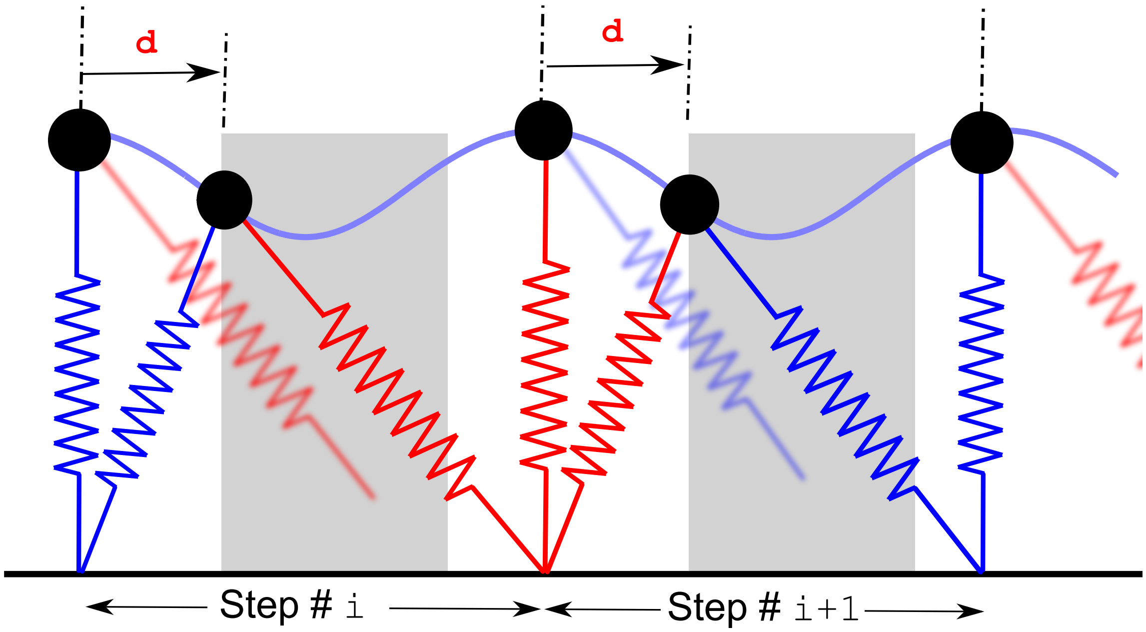

Figure 5.4: In the constant CoM displacement control policy, the transition to double support happens when the CoM reaches to a constant predefined position from the stance toe (here it is shown by d). In the presence of perturbation, the required touch-down angle of the swing leg is changed such that the toe reaches the ground.

5.3.2.2 Constant stance leg angle

The second proposed control policy defines the transition from the single support to double support based on the state of the system. In the constant stance leg angle control policy, the transition from single support to double support is determined based on the angle of the stance leg. In this policy, the swing leg hits the ground when the stance leg reaches a specific angle with a constant reference like the VLO. Figure 5.5 shows this control policy when the switching angle for the stance leg is θ_{SL} with respect to vertical orientation.

Contrary to the constant angle of attack policy that the switching condition is indirectly the height of the CoM, in this control policy, the system is defined to go to the double support phase when the line between the CoM and the contact toe on the ground reaches a predefined angle. For different equilibrium points, this angle varies therefore depends on the desired equilibrium point, the stance leg angle that determines the transition from single support to double support is adjusted.

There is a practical benefit for this control policy because it makes the swing leg slave to the movement of stance leg which then automatically handles the leg trajectory for different velocities.

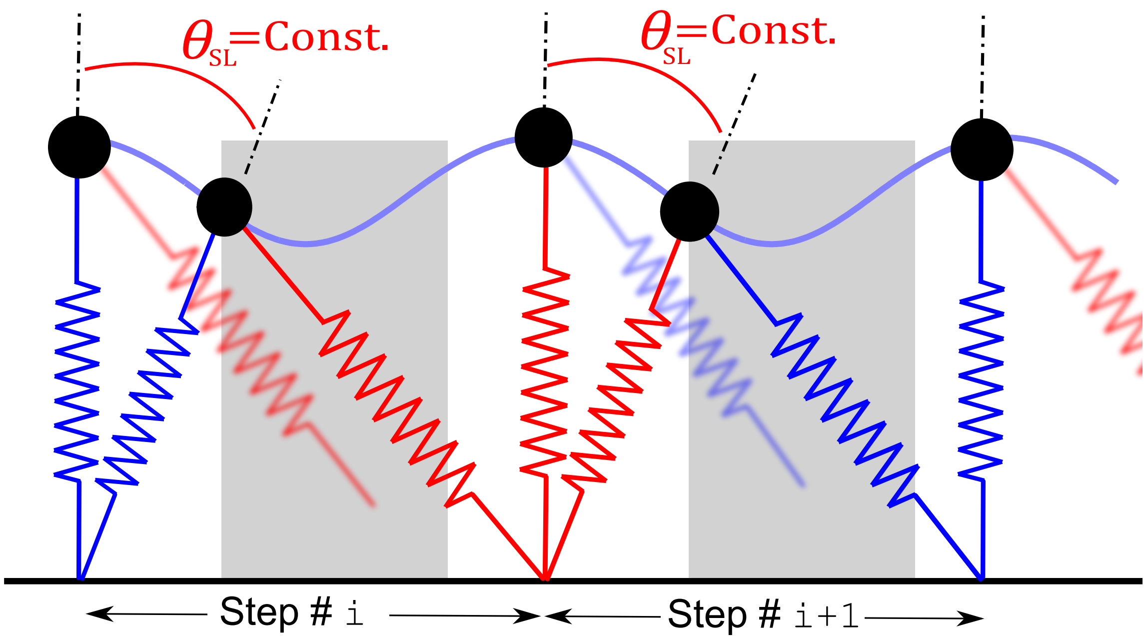

Figure 5.5: The constant stance leg angle control policy regulates the angle of the stance leg at the moment of touch-down.

In figure 5.6, the constant stance leg angle control policy is shown subjected to perturbation. If the system does not have any perturbation, the touch-down angle of the swing leg and the angle of the stance leg both correspond to the values of the equilibrium point at the moment of touch-down. In the presence of perturbation, based on the constant stance leg angle control policy, the angle of the stance leg at the moment that the system transitions to double support is the same as the stance leg angle of the equilibrium point at the beginning of its double support, but the touch-down angle of the swing leg can be different based on the geometry of the system. Figure 5.6 shows how the touch-down angle of the swing leg can be determined from the geometry of the system. It should be reminded that the initial leg length of the swing leg is known and it is supposed to be equal to l_0.

5.3.2.3 Constant stride length

The previous state based control policies use the states of the CoM to determine the beginning of the double support. In the constant stride length control policy, the step length or the distance between the toes is kept constant or regulated at each step. Therefore, the transition from single support to double support happens when the toe of the swing leg can be placed on a predefined constant distance from the toe of the stance leg. Figure 5.7 shows this control policy. Like other mentioned control policies, any perturbation at the Poincare section leads to change in the required touch-down angle for the swing leg to reach the ground.

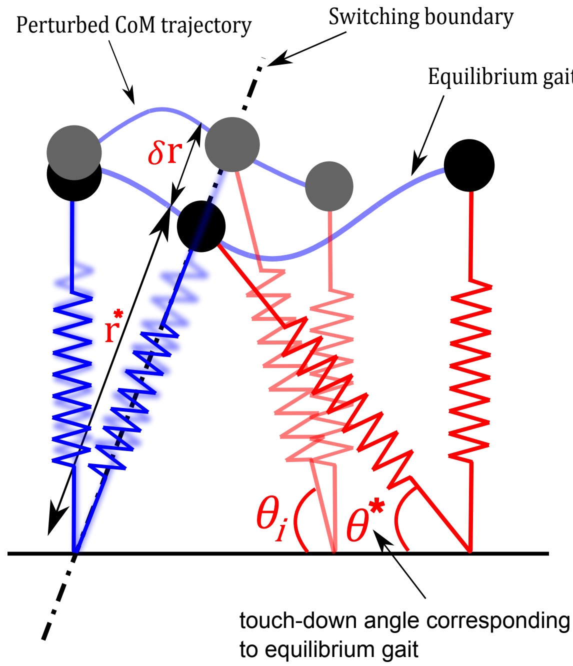

Figure 5.6: Touch-down angle of the swing leg based on the constant stance leg angle policy. In the presence of perturbation at the Poincare section, the system reaches the switching boundary with some drift from the equilibrium gait. The touch-down angle of the swing leg is determined such that the swing leg hits the ground when the CoM reaches the switching manifold.

5.3.2.4 Time-based switching policy

The other variable that can be measured with reasonable accuracy is time. Therefore, another proposed control policy is time-based switching strategy. In this control policy, the system transitions from single support to double support after a predefined specific time after the Poincare section. Therefore, this control policy regulates the time after the Poincare section or VLO. Each equilibrium point has its unique time after VLO to go to double support phase and the idea of this control policy is that if the transition time is regulated for perturbed system, the perturbation decays in

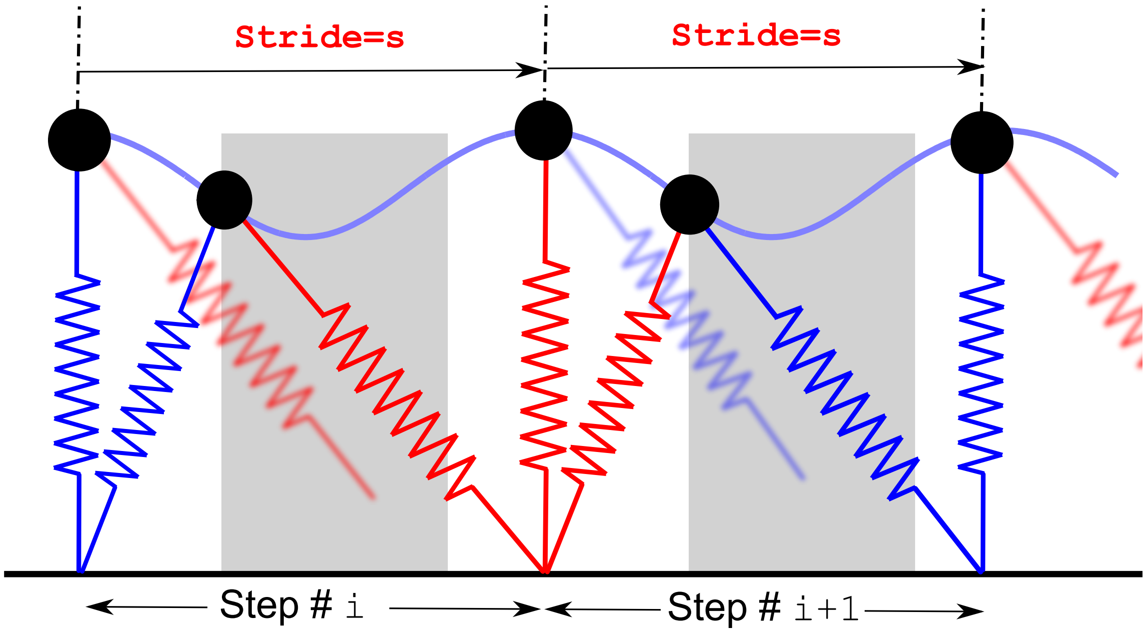

Figure 5.7: In the constant stride length control policy, the system transitions to double support when the toe of the swing leg can be placed at a predefined distance from the toe of the stance leg (here the stride length is s).

successive strides.

5.4 Method

To study the stability of the control policies, we first find the equilibrium points of the system and then find the eigenvalues of the Jacobian matrix. The equilibrium points are those states that can return themselves on the next Poincare section and satisfies the following condition:

$$\boldsymbol{X}^{\star} = f(\boldsymbol{X}^{\star}) \tag{5.11}$$

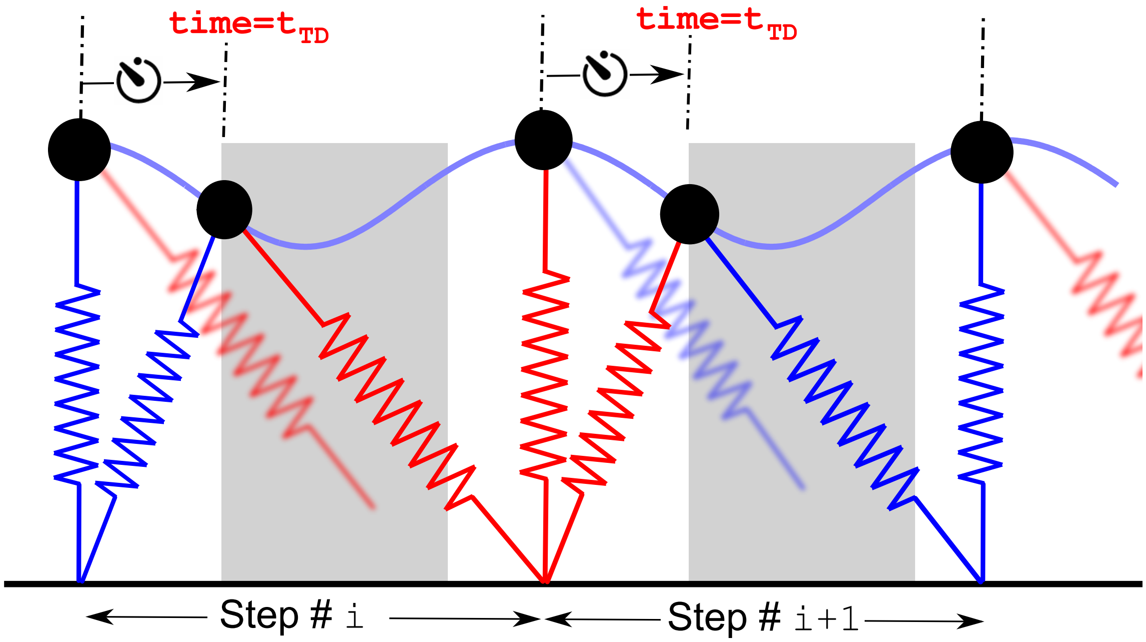

Figure 5.8: The constant touch-down time control policy regulates the time after the Poincare section. The system transitions from single support to double support when a predefined and constant time passes after the VLO.

In this equation $X^{\star}$ is the equilibrium point and f is the return map. We investigate the behavior of the equilibrium points of the bipedal spring mass model under different control policies and compare the results.

To accomplish the simulations, the model was implemented in Matlab (R2014a, Mathworks Inc., Natick, MA, USA) and the following properties for the robot (table 5.1) were assumed. To solve the differential equations, ode45 was used with relative and absolute tolerances equal to 1e-11.

Table 5.1: Properties of the spring-mass robot

Parameter	**Description**	**Value**
m	robot mass	$58.0kg$
k	leg spring stiffness	$14000\frac{N}{m}$
l_0	initial leg length	$0.9m$

5.4.1 Stability analysis

Stability of a control policy can be determined from the eigenvalues of the Jacobian matrix. For nonlinear systems, the Jacobian matrix is obtained by differentiating the equations of motion with respect to the states around the equilibrium points. If the magnitude of the eigenvalues are all less than 1, the system is stable and if the maximum magnitude of the eigenvalues is greater than 1, the system is unstable.

5.5 Simulation results and discussion

Stability analysis starts by calculating the eigenvalues of the Jacobian matrix of the system under various control policies around the equilibrium points. For this purpose the eigenvalues of the bipedal spring-mass model in various energy levels are calculated and compared. The energy levels are chosen such that slow walking, medium speed walking, fast walking and very fast walking can be achieved. It should be noticed that in the analysis here, transition from single support to double support can happen regardless of the direction of the velocity of the CoM. Therefore, grounded running (running force profile without flight phase and with double support) can happen in the analysis. Also, some equilibrium points can be repeated by different distinct control inputs and therefore the eigenvalues correspond to each of them are different. For example there are two touch-down angles that return $(y, \psi) = (0.88, 0)$ at energy level $E = 510J$.

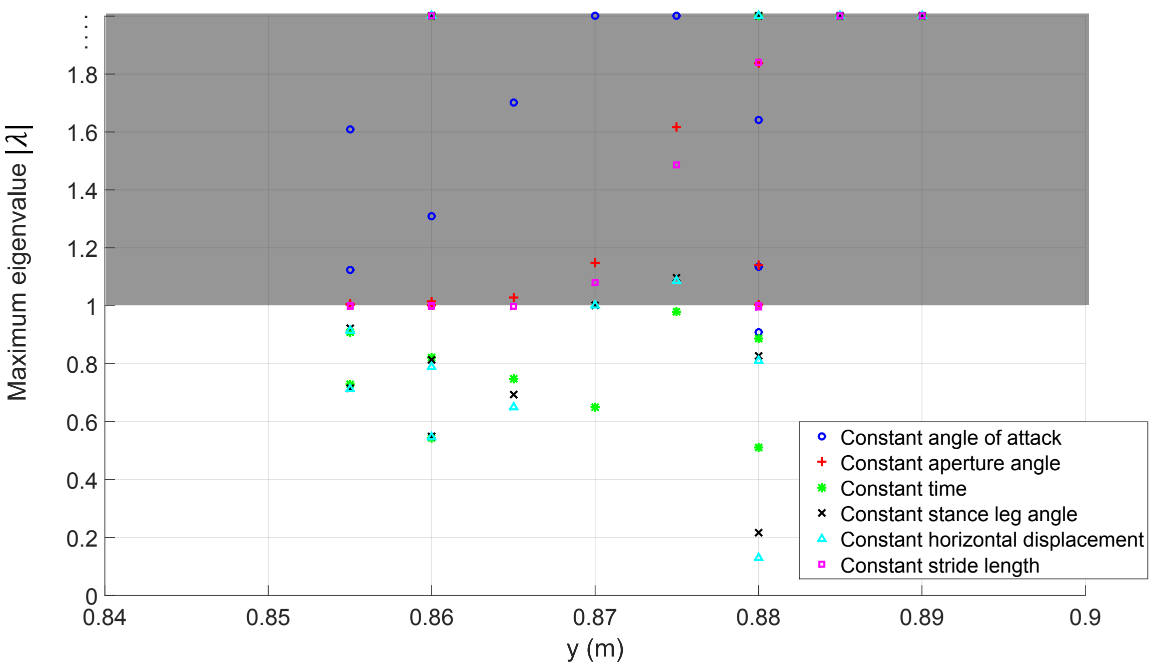

Figure 5.9: The maximum eigenvalues of the Jacobian matrix for energy level $E = 510J$ with the control policies. The constant stance leg angle policy, the constant horizontal displacement policy and the constant time policy are stable for most of the equilibrium points.

The first energy level that we investigate is $E = 510J$ for the system parameter mentioned in table 5.1. This energy level is equivalent to average horizontal speed of around $v_x = 0.5\frac{m}{s}$. The symmetric equilibrium points are shown for this energy level in figure 5.9 with the maximum eigenvalues of the Jacobian matrix. The shaded area in the figure distinguishes the unstable eigenvalues that are more than one. The maximum magnitude for the eigenvalues is assumed to be 2, meaning that if the magnitude of the eigenvalue is greater than 2, it is set to 2. As can be seen in this figure, the constant angle of attack policy is only stable for one equilibrium point ($y = 0.88$). The proposed control policies are stable for most of the equilibrium points. The constant stride length policy is in the marginal stability region and with behavior like the constant aperture angle control policy.

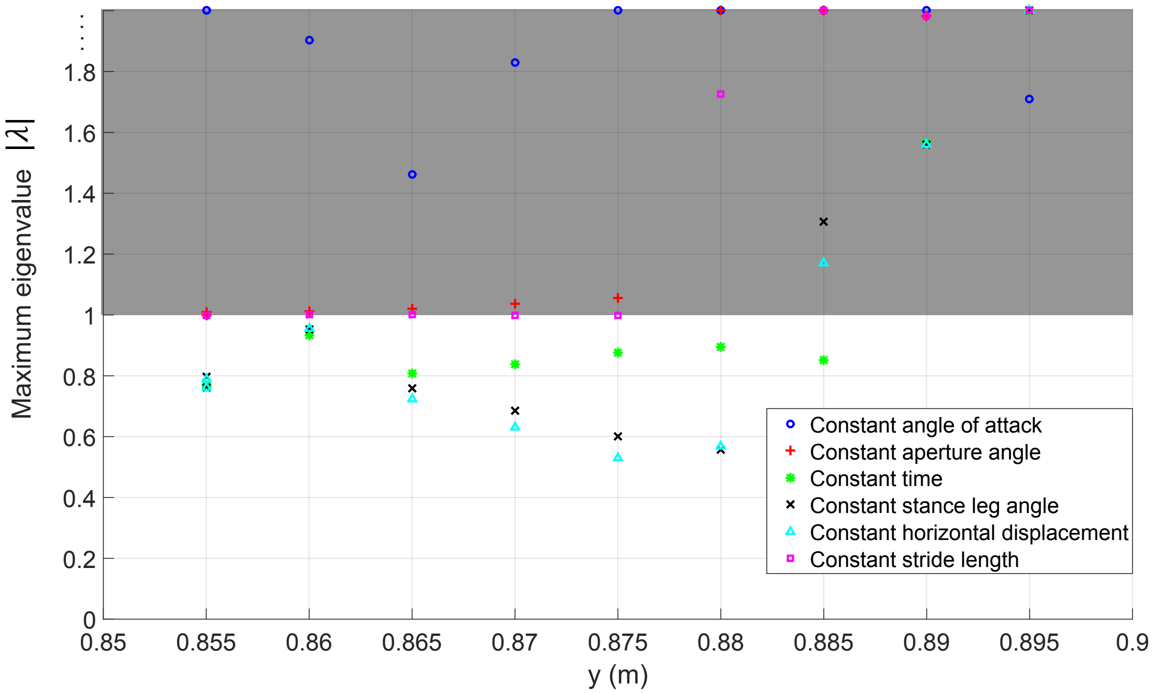

Figure 5.10: The maximum magnitude of the eigenvalues of the Jacobian matrix for energy level $E = 515J$ for the control policies. The constant angle of attack control policy is always unstable, but other strategies perform stable walking.

In figure 5.10, the maximum eigenvalues are shown for slightly greater energy level ($E = 515J$). In this energy level, like before, the three proposed control policies (constant stance leg angle, constant touch-down time and constant CoM position) perform well while the constant angle of attack policy is always unstable and the constant aperture angle control policy is at the marginal stability and slightly unstable. The stability of the constant stride length control policy is comparable to the constant aperture angle control policy. Even though most of the times the constant stance leg angle and the constant horizontal displacement control policies give smaller eigenvalue than the constant touch-down time policy, but sometimes (for example $y = 0.885$), the constant time control policy is the only stable strategy.

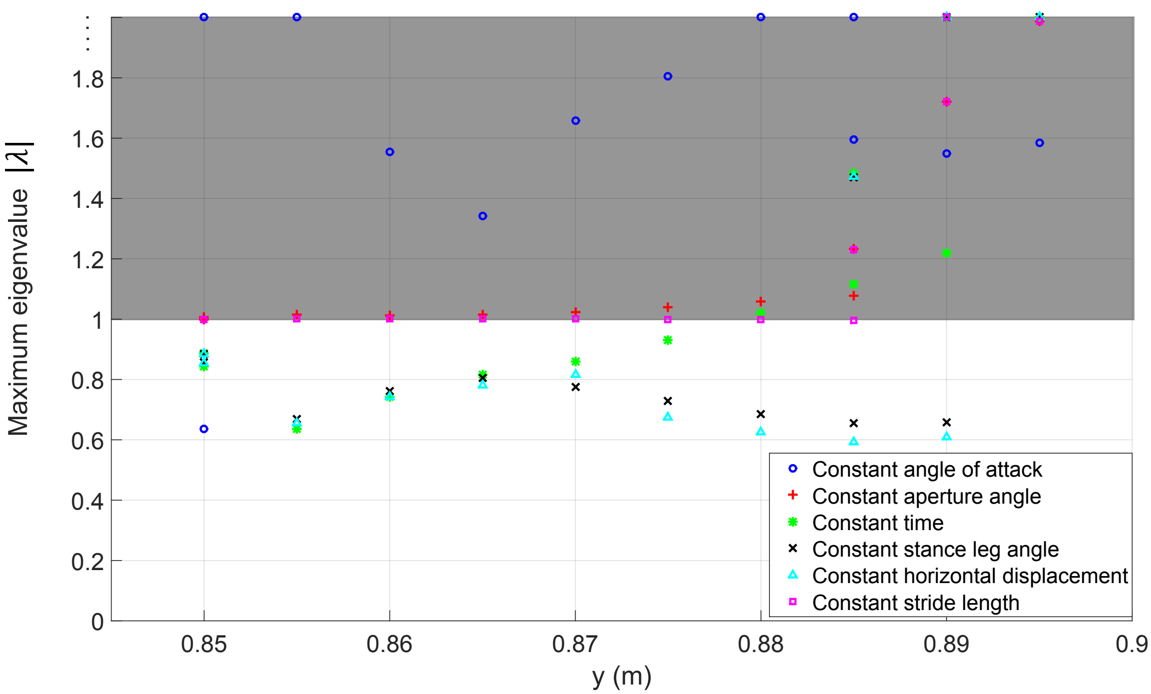

Figure 5.11: Stability analysis of the control policies through the magnitude of the eigenvalues of the Jacobian matrix for energy level E=520 J.

As the energy level of the system increases, the advantage of the two of the proposed control policies highlights more. In figures 5.11 and 5.12, the maximum eigenvalues of the system are shown for medium speed walking. The advantage of the constant stance leg angle control policy and the constant horizontal displacement control policy are clearly shown in these figures. The same trend for the behavior

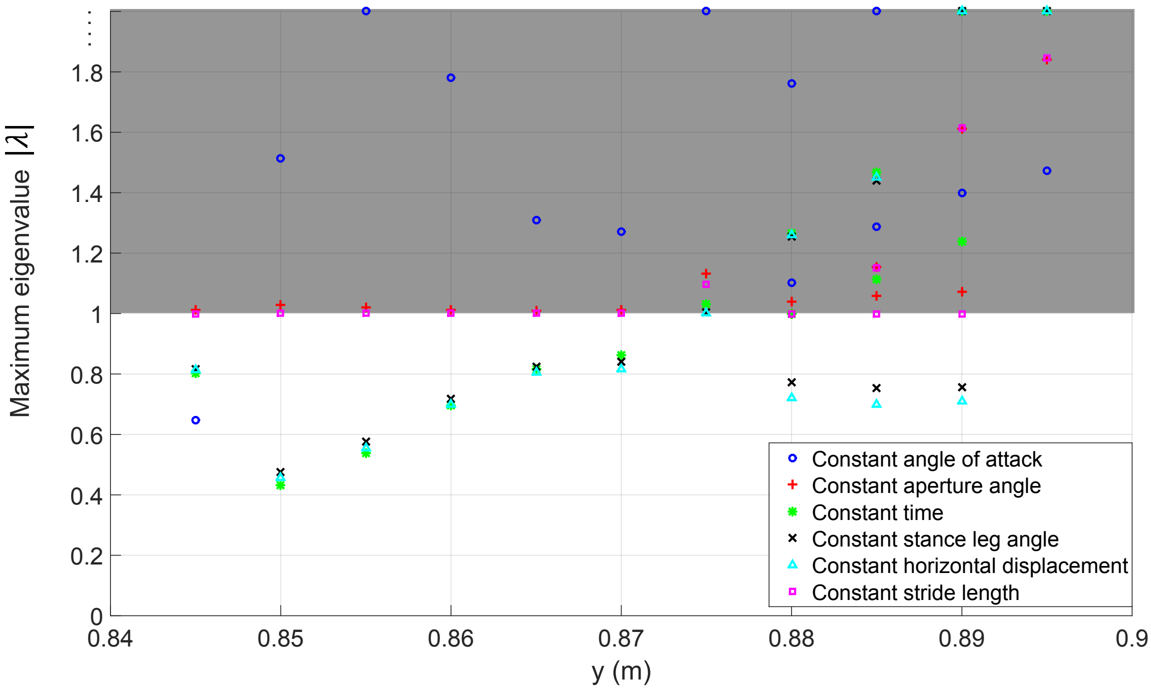

Figure 5.12: Magnitude of the eigenvalues of the Jacobian matrix for the stability analysis of the control policies for energy level E=525 J. The proposed control policies can stabilize the gait.

of the constant aperture angle and constant stride length can be seen. The constant touch-down time control policy is appropriate for some of the equilibrium points. Very interesting behavior is that the constant touch-down angle control policy is nearly always unstable except in one equilibrium point.

For very fast walking gaits, energy levels in figures 5.13, 5.14 and 5.15 are studied. The equilibrium gaits in these energy levels can only be grounded running and the forward speeds are very high for regular walking (more than $3\frac{m}{s}$). The constant touch-down angle policy always fail at these energy levels. The constant aperture angle and the constant stride length control policies show similar eigenvalues and stay at the marginal stability. Other proposed control policies are very similar in the magnitude of the eigenvalue and as the energy of the system increases, they approach to marginal stability from the stable side.

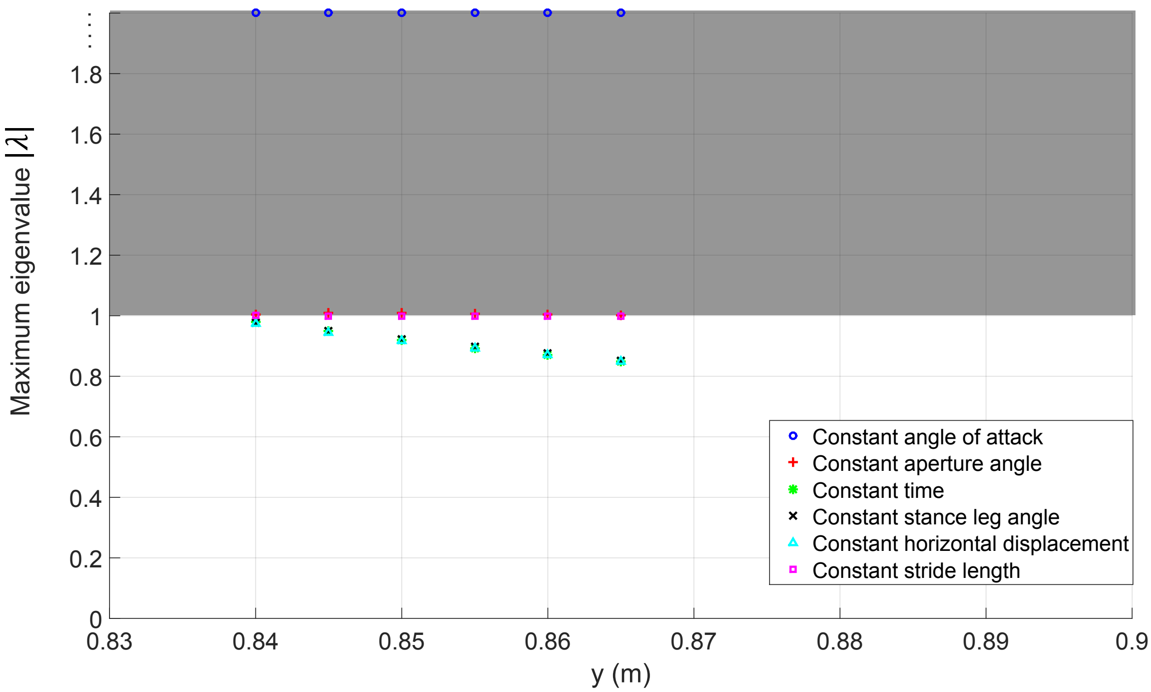

Figure 5.13: The stability analysis of the control policies for high energy level E=800 J.

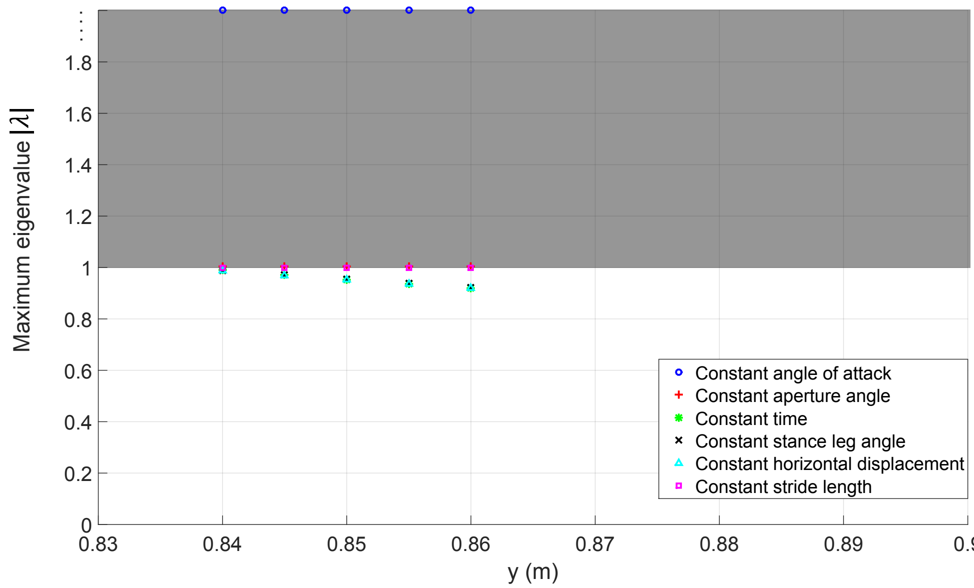

Figure 5.14: The magnitude of the eigenvalues for high energy level E=1000 J. The magnitude of the eigenvalues are approaching 1 from stable side.

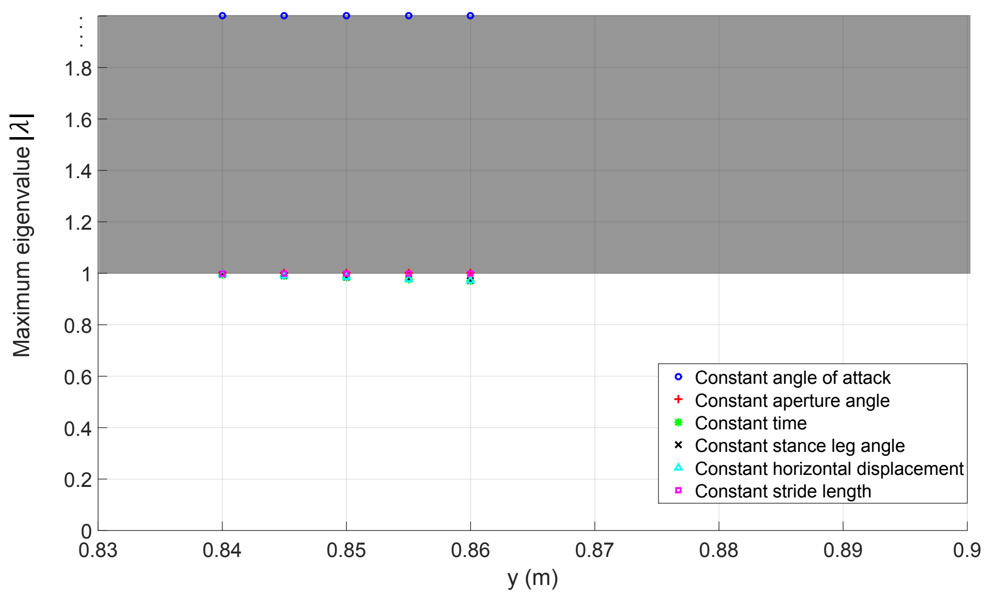

Figure 5.15: The magnitude of the eigenvalues are equal to 1 for very high energy level E=2000 J.

After investigating the magnitude of the eigenvalues for different equilibrium points and various control policies, here the basin of attraction of the control policies are investigated. The importance of the basin of attraction is that it shows why some of the control strategies can reject large perturbations and some of them are prone to disturbances. The domain in the state space that the control policy can successfully recover to the desired equilibrium point is called basin of attraction. Now, we investigate the size and shape of the basin of attraction that the proposed and current control policies create for some of the equilibrium points. We find the states that can continue walking for at least 50 steps. Therefore, if a state can continue walking for 50 steps without converging to the equilibrium point, it is still categorized as a state in the basin of attraction. For finding the basin of attraction, the states in the workspace are checked under the control policy. If the model can continue walking for more than 50 steps starting with a state in workspace, that state is considered as a point in the basin of attraction. The search starts from the desired equilibrium point and continues radially from that until a state that can not continue walking for 50 steps, therefore the states in the basin of attraction look like the shape of a spoke.

The analysis starts with the constant stance leg angle control policy. The basin of attraction for this control policy is large with respect to the whole state space that walking can be defined. In figures 5.16 and 5.17 the basins of attraction for two equilibrium points with the constant stance leg angle control policy is shown. The area of the basins of attraction is at least about 70% of the whole walking state space. Therefore, even fairly large disturbances can be rejected by this control

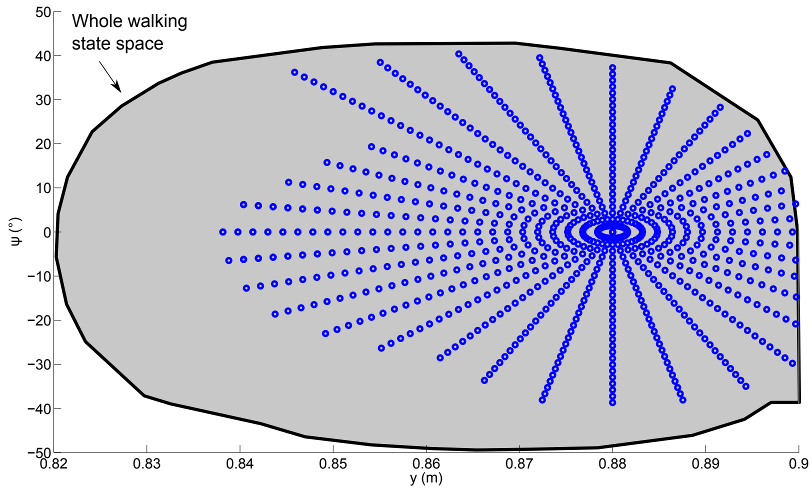

Figure 5.16: The gray area with black boundary shows the whole state space for walking. The blue circles are the states that can return to the desired equilibrium point at $(y, \psi) = (0.88, 0)$ using the constant stance leg angle control policy. The basin of attraction of this control policy is the region in the state space that contains all of these states.

policy (within the domain that the disturbance can be rejected by touch-down angle control).

After the constant stance leg angle control policy, the power of the constant touch-down time control policy is shown in figures 5.18 and 5.19. The size of the basins of attraction for this control policy are greater than the constant stance leg angle control policy. Therefore, the system can sustain bigger disturbances, but the size of the basin of attraction does not indicate how fast the system reject the perturbation.

Figure 5.20 shows the basin of attraction for the constant horizontal position of the CoM. The size of the basin of attraction in this control policy with respect to the whole walking state space, shows that this control policy can reject even large disturbances.

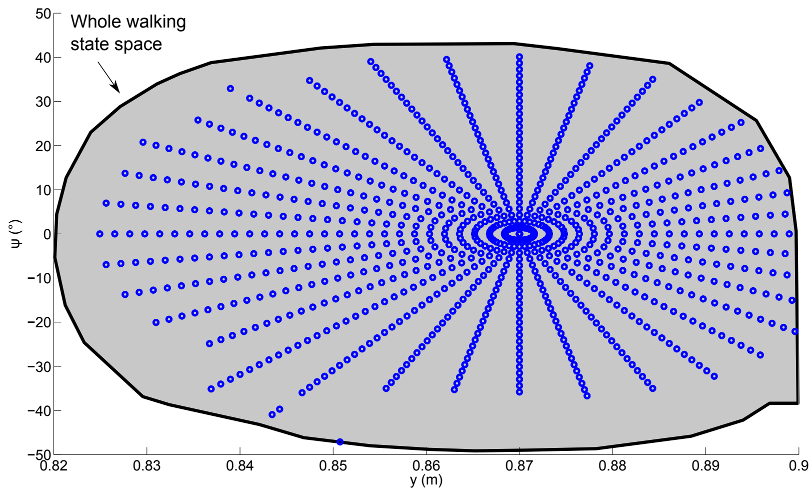

Figure 5.17: The blue circles are the states that can return to the desired equilibrium point at $(y, \psi) = (0.87, 0)$ using the constant stance leg angle control policy. The whole walking state space is the gray area with black boundary and the basin of attraction of the control policy is the region in the state space that contains all of the blue circles.

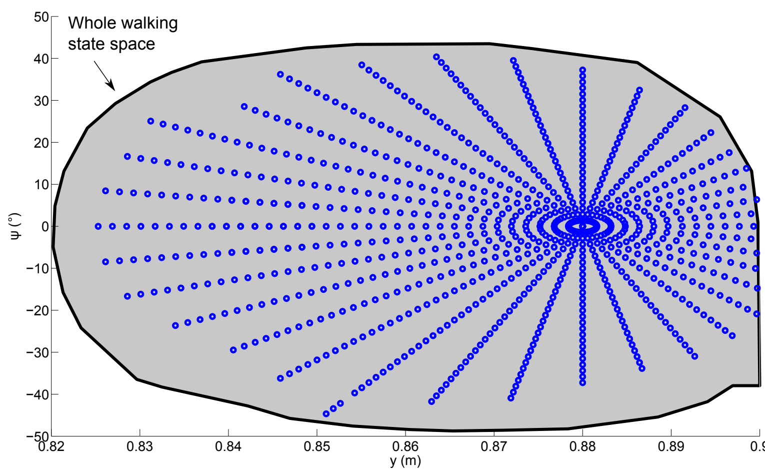

Figure 5.18: The basin of attraction of the constant touch-down time control policy for the equilibrium gait $(y, \psi) = (0.88, 0)$. This region contains the blue circles in the state space.

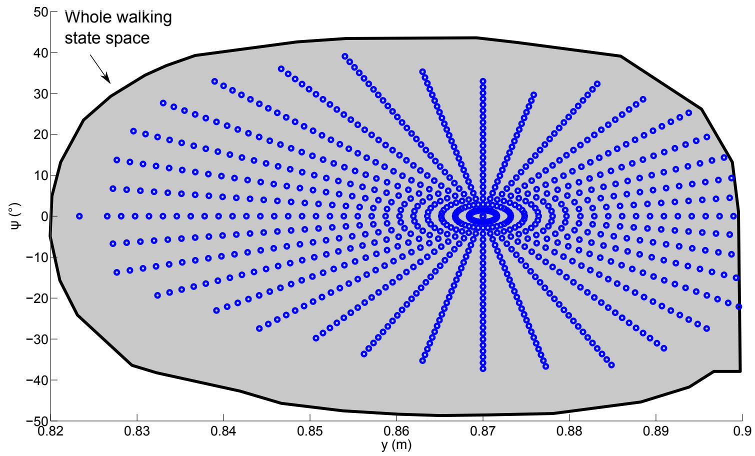

Figure 5.19: The constant touch-down time control policy makes the blue circles to converge to the desired equilibrium gait which here is $(y, \psi) = (0.87, 0)$.

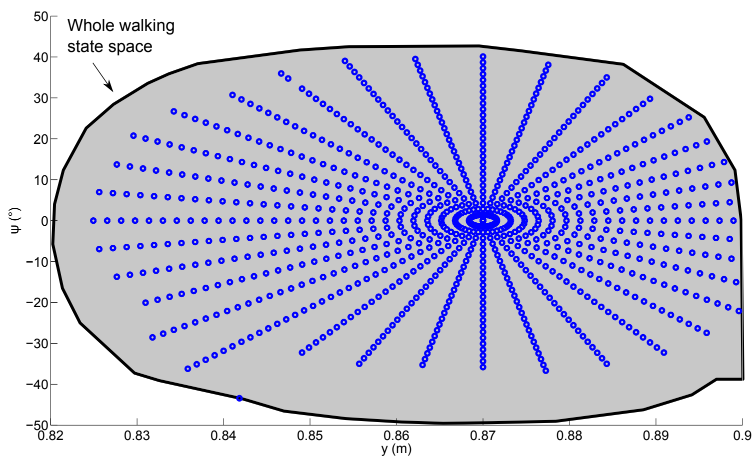

Figure 5.20: The blue circles here are the states that can converge to the desired equilibrium point at $(y, \psi) = (0.87, 0)$ using the constant CoM position control policy. Compared to the whole walking state space which is the gray area with black boundary, the basin of attraction of the control policy is the region that contains the blue circles.

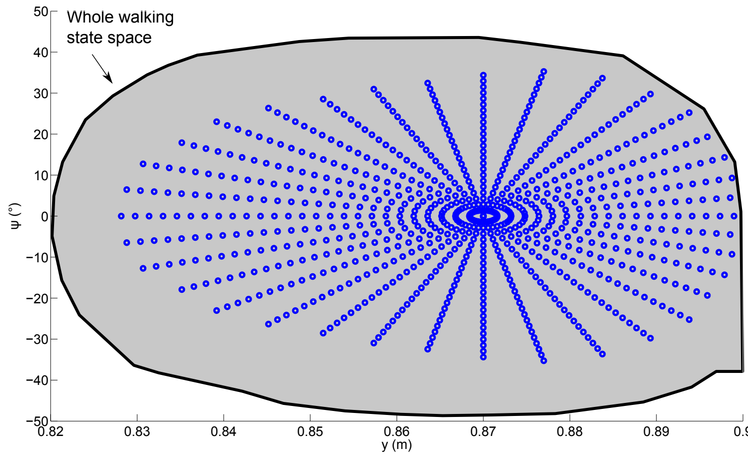

Figure 5.21: The constant stride length control policy returns the blue circles to the desired equilibrium point $(y, \psi) = (0.87, 0)$ or keep the system walking for at least 50 steps.

The basin of attraction of the constant stride length control policy is shown in figure 5.21 for equilibrium point $(y, \psi) = (0.87, 0)$. Even though the magnitude of the eigenvalue is not well below 1, but the size of the basin of attraction shows that this control policy can keep the system walking for several steps and not fall due to large disturbances.

The constant aperture angle control policy can reject or sustain perturbations shown in figure 5.22. It was shown that the constant aperture angle control policy does not necessarily converge to the desired equilibrium gait, but the system can continue walking without falling with this control policy.

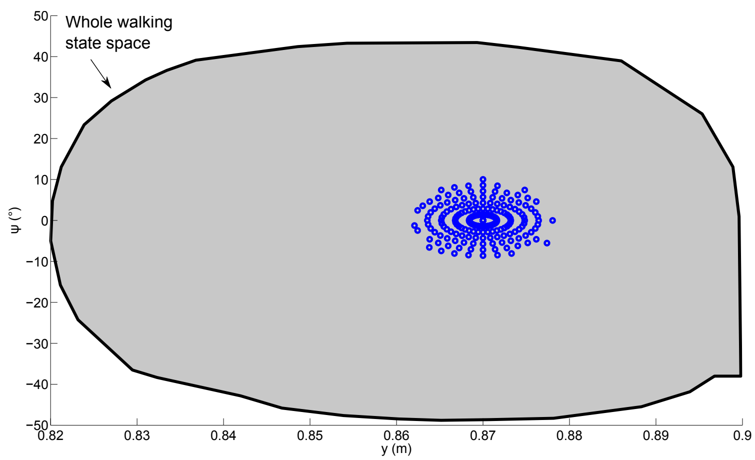

Figure 5.22: The constant aperture angle control policy returns the blue circles to the desired equilibrium point which is $(y, \psi) = (0.87, 0)$ or keep the system to walk at least for 50 steps.

Here, the basins of attraction of the control policies are compared for two equilibrium points. The results show that the constant aperture angle control policy can not provide large basin of attraction for the equilibrium points. After that the constant stride length control policy provides the smallest basin of attraction for the equilibrium points, however the size of the constant stride length control policy is more than 3 times greater than the constant aperture angle policy. The proposed control policies like regulating the touch-down time and the stance leg angle and the CoM position provide similar and large basins of attraction that can assure most of the disturbances would be handled by the control policy.

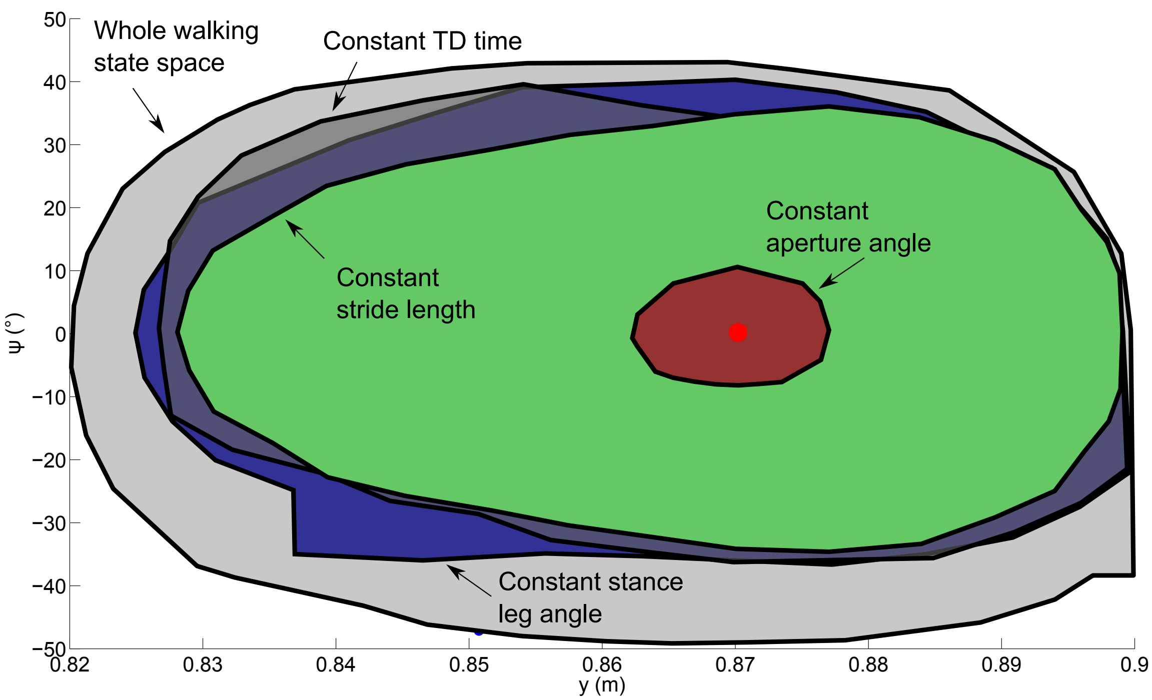

Figure 5.23: The comparison of the size of the basins of attraction for the various control policies that return to the equilibrium point $(y, \psi) = (0.87, 0)$. The constant aperture angle control policy has the smallest basin of attraction and for the other three control policies here, the size of the basins of attraction are close to each other.

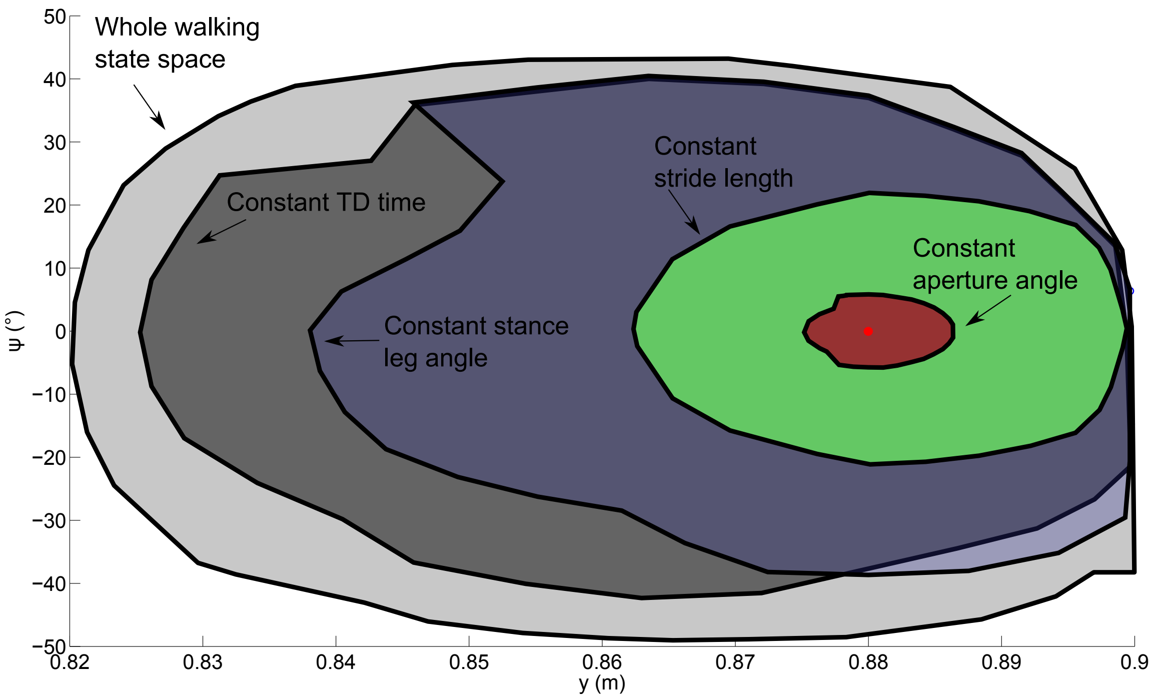

Figure 5.24: The comparison of the basins of attraction. The constant aperture angle control policy has the smallest basin of attraction and the constant touch-down time control policy gives the larges basin of attraction for this equilibrium point.

After the stability analysis and investigating the basins of attractions of the control policies, now the behavior of the policies are studied for different equilibrium points in various energy levels. Even though the magnitude of the eigenvalue does not necessarily show the rate of convergence, in some cases it can be a good measure for the rate of convergence.

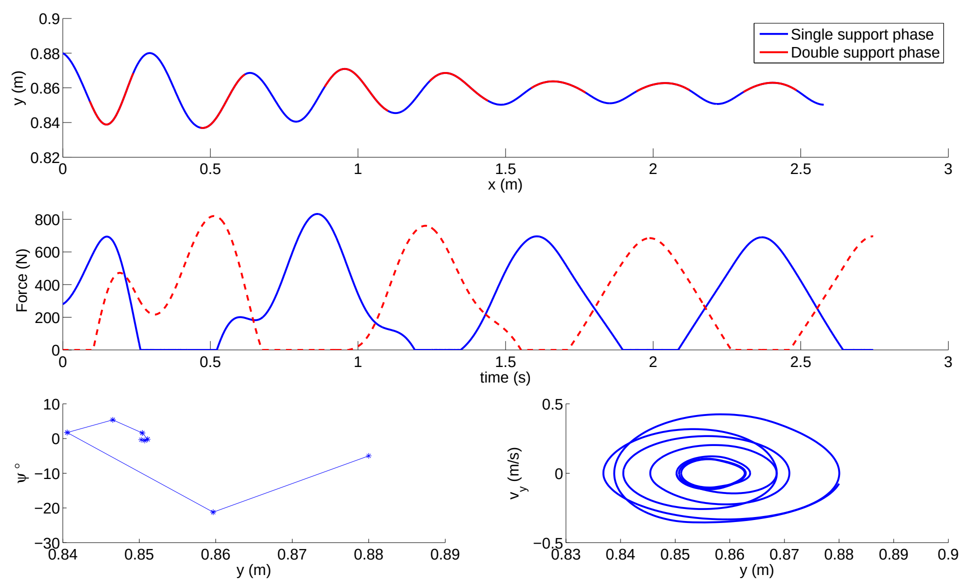

Figure 5.25: The constant stance leg angle control policy for equilibrium point $(y, \psi) = (0.85, 0)$. The initial perturbation is $(y, \psi) = (0.88, -5)$ and the system converges in about 4 steps.

For the first example, the behavior of the system with the constant stance leg angle control policy is shown in figure 5.25. The analysis starts with an initial perturbed state $(y, \psi) = (0.88, -5)$ that is far from the desired equilibrium point $(y, \psi) = (0.85, 0)$, but the system converges to the desired equilibrium point in about 4 steps. The desired equilibrium gait is located in the region of grounded running gaits. The resultant force profile of the desired equilibrium gait confirms the grounded running gait and the CoM trajectory of the system shows the double support at the peak of the height of CoM in each gait.

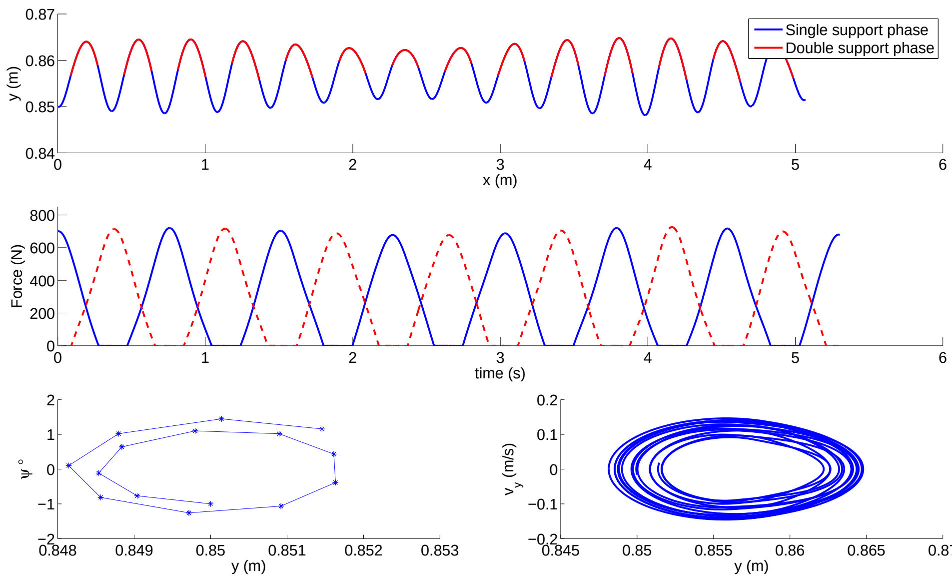

Figure 5.26: The behavior of the constant aperture angle control policy. The initial perturbation is $(y, \psi) = (0.85, -1)$ which is close to the desired equilibrium point. The system gradually diverges from the desired equilibrium point.

The behavior of the constant aperture angle control policy is shown in figure 5.26. As the basin of attraction of this control policy shows, the domain in which the initial perturbed state can be chosen, is not as large as other control policies. Since the system can not recover from big perturbations, the initial perturbation in this case is chosen $(y, \psi) = (0.85, -1)$ to show the behavior of the system. As can be seen in figure 5.26, the system gradually diverges from the desired equilibrium point as was expected from the eigenvalue of the system which is slightly greater than 1 but the process takes some steps until failure. This result is compatible with the behavior that Andrada et. al [75] reported in their paper.

Figure 5.27 shows the behavior of the constant stride length control policy. In this policy, the system does not converge to the desired equilibrium gait because the magnitude of the eigenvalue is about 1 and therefore it is marginally stable. The behavior of the system is like oscillating around the desired equilibrium point like 1-DOF spring-mass system without damping around its fixed point. The advantage of this control policy over the constant aperture angle control policy is that in this strategy the system does not diverge from the desired equilibrium point.

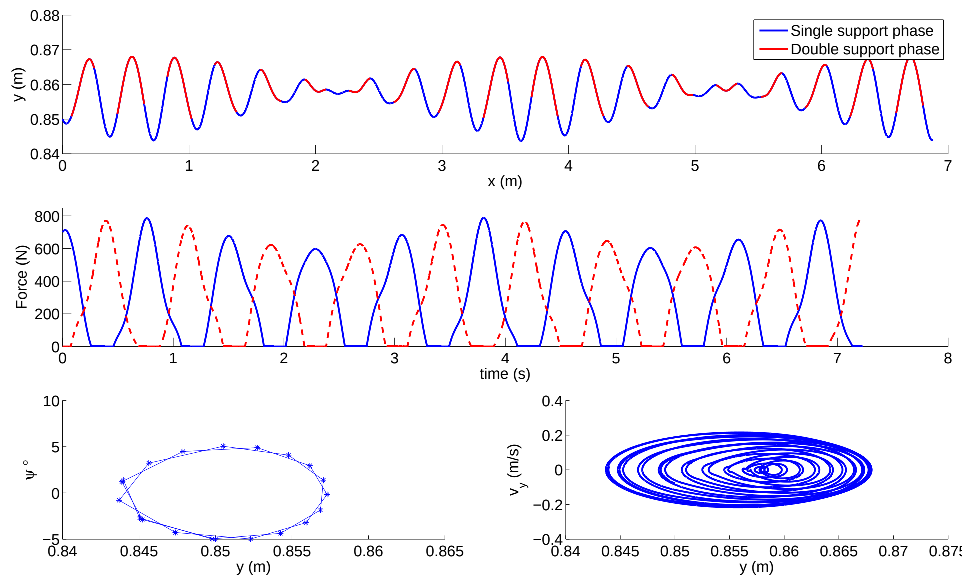

Figure 5.27: In constant stride length control policy, the system is marginally stable and oscillates around the desired equilibrium point.

The behavior of the constant touch-down time control policy is shown in figure 5.28. Despite a large initial perturbation, the system recovers from the perturbation

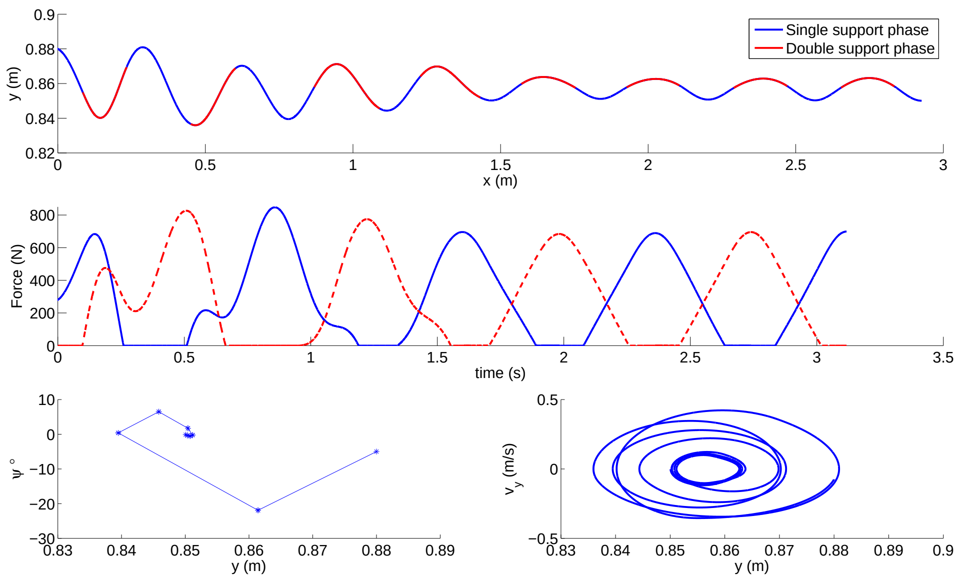

Figure 5.28: The constant touch-down time control policy recovers from initial perturbation in about 4 steps.

in about 4 steps and settles to the desired equilibrium point $(y, \psi) = (0.85, 0)$. The convergence rate is similar to the constant stance leg angle for this equilibrium point as the magnitude of the eigenvalues suggest. As can be seen in the CoM trajectory, the transition from the perturbed initial condition to the final equilibrium point is gradual and smooth.

The constant horizontal displacement control policy also shows converging behavior with large perturbations. Figure 5.29 shows the behavior of this policy under a large initial perturbation. This policy converges quickly to the desired equilibrium point as was expected from the magnitude of its eigenvalues. The behavior of this control policy on the bipedal spring-mass model is similar to the constant stance leg angle policy, but the touch-down time and the conditions at the moment

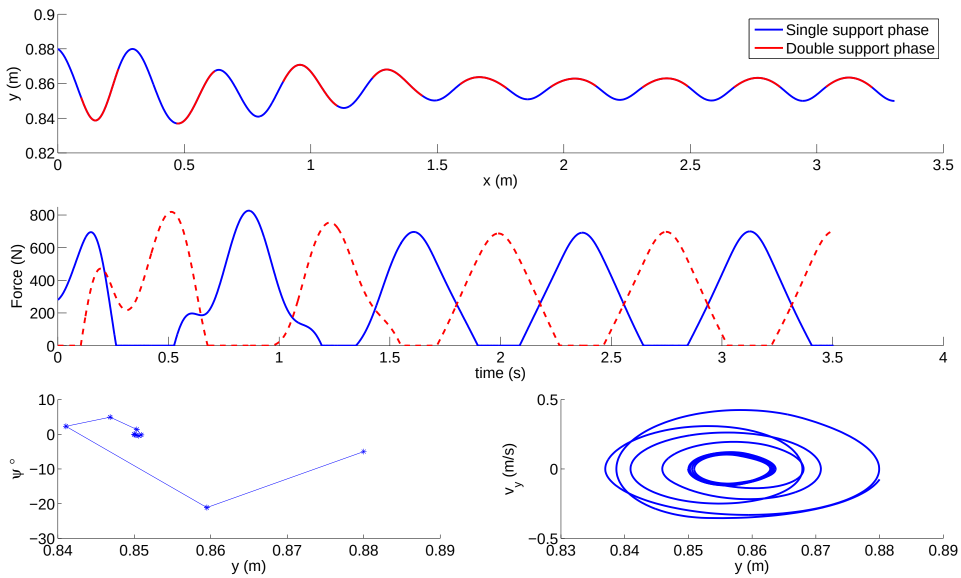

Figure 5.29: The system converges fast to the desired equilibrium point using the constant CoM horizontal displacement. The CoM trajectory and the change in the force profile are gradual to the desired limit cycle.

of touch-down are different for each control policy.

For the constant angle of attack policy, we expect an unstable behavior from the stability analysis of the system as the magnitude of the eigenvalue for this policy suggests. In figure 5.30 the unstable behavior of the constant angle of attack control policy is well depicted. Even though the initial perturbation is chosen close to the desired equilibrium point, the system diverges very quickly from the equilibrium point and becomes unstable. In the CoM trajectory with this control policy, after few steps, the system diverges and becomes unstable.

Now, we investigate the behavior of the control policies for another type of equilibrium points. So far, the examples were for grounded running equilibrium points.

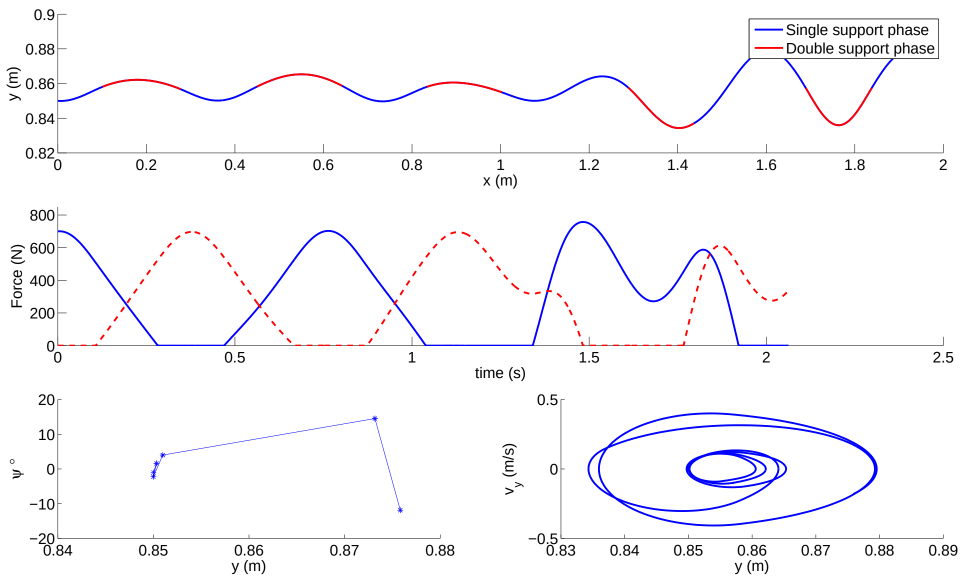

Figure 5.30: The constant angle of attack control policy diverges from the desired equilibrium point.

Here, we investigate the behavior of the bipedal spring-mass model for equilibrium gaits with double-hump force profile. The energy level of the system is assumed to be equal to $E = 525J$, and we focus on the behavior of the symmetric equilibrium points (like $(y, \psi) = (0.88, 0)$) under various control policies.

The analysis starts with the constant stance leg angle control policy. The behavior of this control strategy is shown in figure 5.31. As can be seen in this figure, the system recovers from the perturbation and converges to the desired equilibrium point. The convergence rate is not as fast as it was before for grounded running equilibrium gaits, but the transition is smooth and gradual and the system settles exactly on the desired equilibrium point. The behavior of the system under this control policy is like oscillating around the desired gait and gradually converges and settles to the

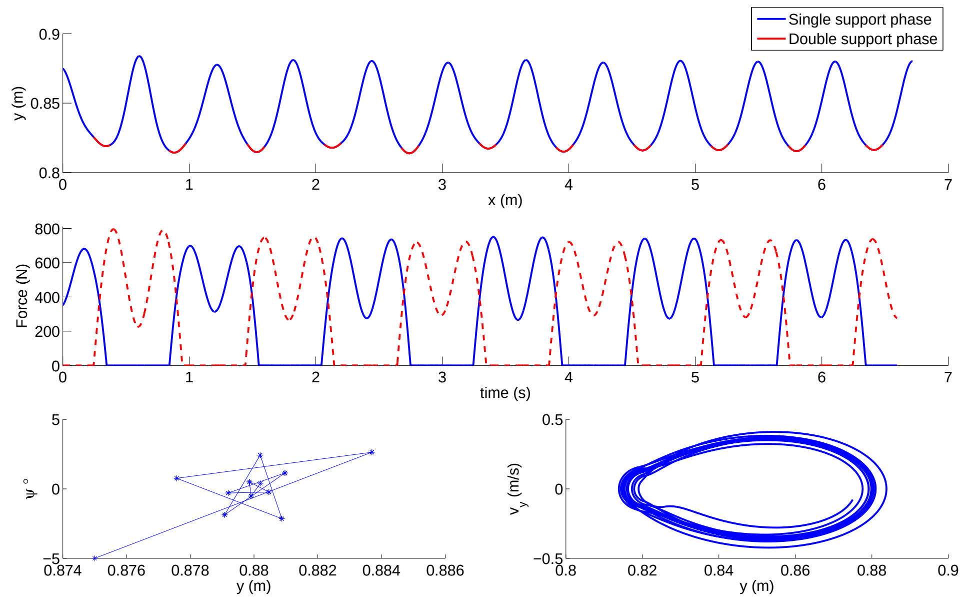

Figure 5.31: The constant stance leg angle control policy for the desired equilibrium gait $(y, \psi) = (0.88, 0)$.

desired equilibrium point.

Figure 5.32 shows the behavior of the constant aperture angle policy under initial perturbation around a double-hump force profile equilibrium gait. The stability analysis showed that this policy is not asymptotically stable, but the system can walk for several steps before falling. Since the magnitude of its eigenvalues is greater then 1, in each step the error increases and the system gets further from the desired equilibrium point. If the magnitude of the eigenvalue is close to 1, it allows the system to walk for some steps before falling. As can be seen in figure 5.32, the CoM trajectory is not smooth during walking and the error increases gradually, but the system can walk for several steps before falling and therefore can be categorized as finite stable gait.

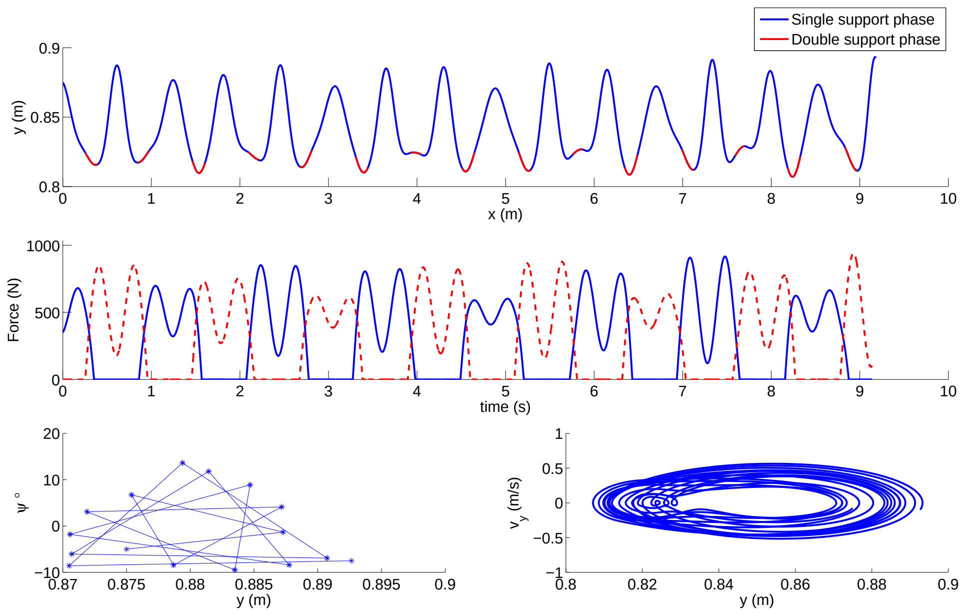

Figure 5.32: The constant aperture angle control policy is unstable but can walk for several steps before falling. The desired equilibrium point is $(y, \psi) = (0.88, 0)$ and the system oscillates around that point and gradually diverges from that.

As the stability analysis of the control policies showed, the stability behavior of the constant stride length control policy is similar to the constant aperture angle control policy. Since the magnitude of the eigenvalues is about 1, the system does not dissipate the perturbation and it does not converge to the desired equilibrium point and oscillates around it. In the constant stride length control policy as shown in figure 5.33, the system has marginal stability and therefore the perturbation remains unchanged or negligibly change after each step. This is the reason why the system can walk for several steps before falling and hence in the sense of stability for walking can be categorized as finite stable gait. The CoM trajectory of the system is not ideal, but it is smoother than the constant aperture angle control policy.

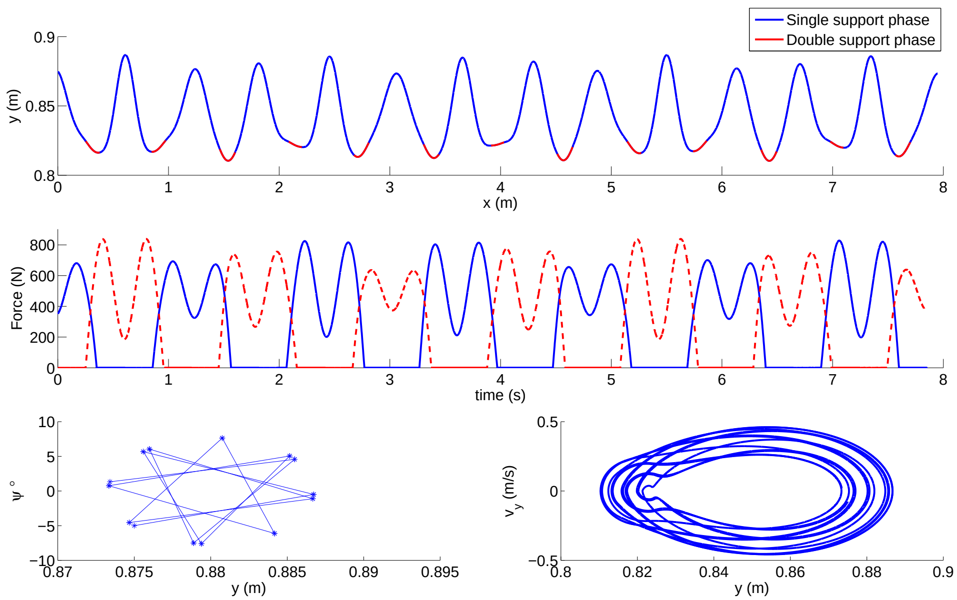

Figure 5.33: The constant stride length control policy is marginally stable and therefore it oscillates around the desired equilibrium point but does not settle into the desired gait.

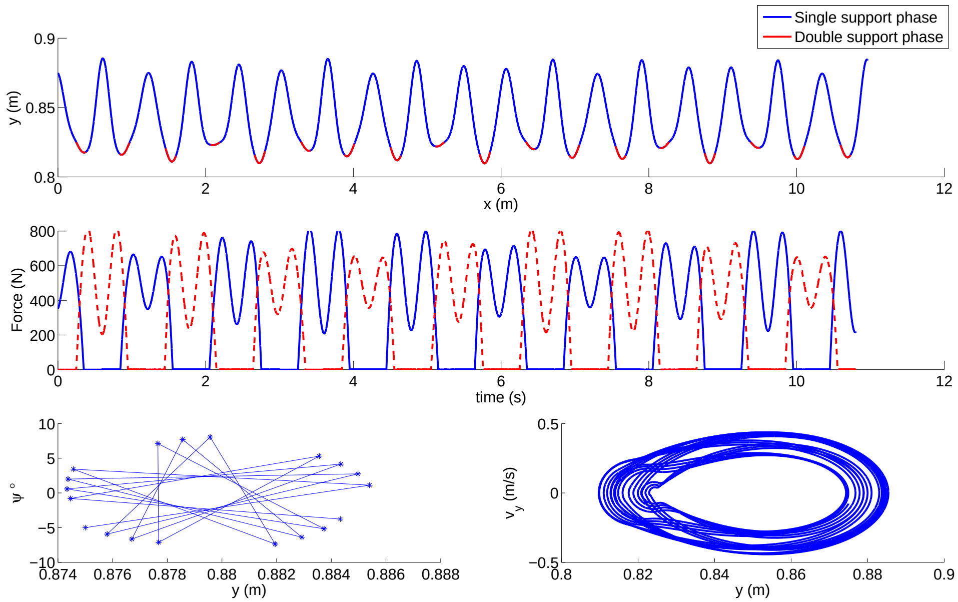

Figure 5.34: The constant touch-down time control policy for double-hump force profile equilibrium gait. The system does not converge to the desired equilibrium point and oscillates around it.

The behavior of the system with the constant touch-down time control policy is shown in figure 5.34. Even though this control policy was stable very well for the grounded running gait, but as can be seen here, the stability of this control strategy is not well converging to the desired equilibrium point. The eigenvalue of the system for this control policy suggests that the system is unstable, but as can be seen in this figure, the system can accomplish several walking steps with descent behavior before falling.

Figure 5.35, shows the behavior of the constant horizontal displacement control policy around a M-shaped force profile equilibrium point. After the initial perturbation in the state, the system recovers quickly from the disturbance and converges

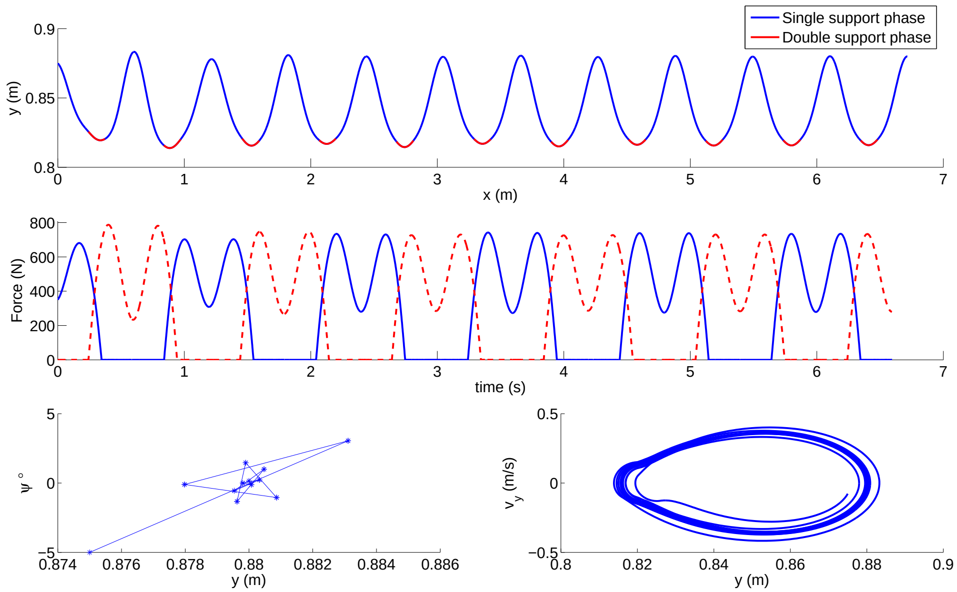

Figure 5.35: The constant horizontal displacement control policy quickly recovers from the initial perturbation.

to the desired equilibrium point. The transition from the perturbed state to the desired limit cycle is smooth and gradual, but the convergence rate is smaller than the grounded running equilibrium points.

For the last example of studying the behavior of the system under the swing leg control policies, the response of the bipedal spring-mass model with the constant angle of attack control policy. In figure 5.36, the behavior of the constant angle of attack control policy is depicted. The eigenvalues of the system predict that the system is unstable and amplifies the perturbations in each step. The simulation shows that the system diverges very quickly from small initial perturbations. Even though the initial perturbation from the desired equilibrium point is small, but the system diverges very quickly and falls suggesting that using the constant angle of

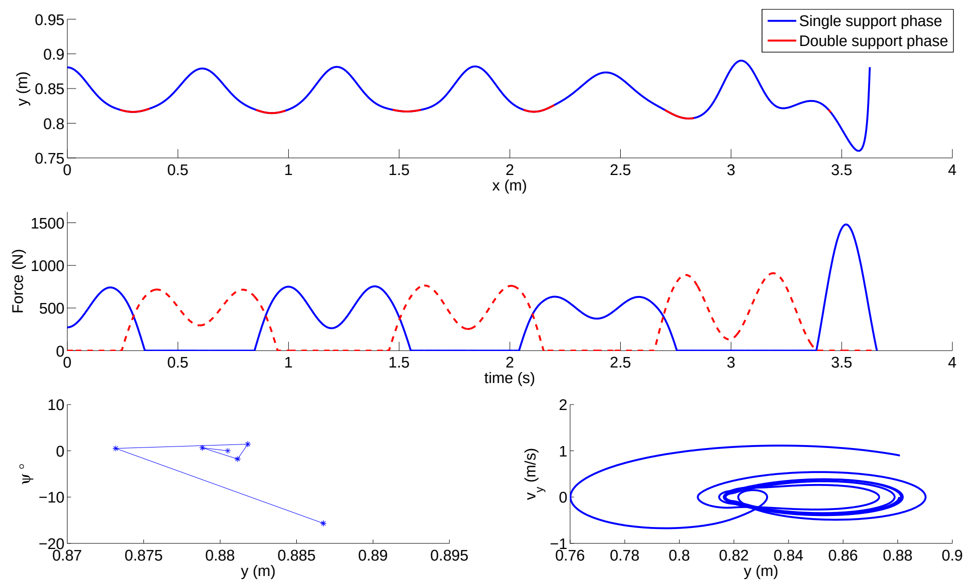

Figure 5.36: The constant angle of attack control policy. The system diverges very quickly from very small initial perturbation and falls.

attack control policy is not useful for these types of equilibrium gaits.

To show the capability of the proposed control polices for walking over rough terrain, an example of the bipedal spring-mass model waking on rough terrain is presented in figure 5.37. In this example, the switching manifold for the transition from single support phase to double support phase is the touch-down time. Therefore, the system regulates the time after the VLO until entering the double support phase regardless of the ground level without any prior information of the disturbances. By regulating the time the system converges to different types of equilibrium gaits in different energy levels. As can be seen in the figure, the control policy can handle the disturbances and makes it to converge to the corresponding equilibrium point at each energy level. The leg force profile of the system during walking over rough terrain is shown in figure 5.38. When the energy of the system increases due to the decrease in ground height, the desired equilibrium gait at the predefined touch-down time approaches grounded running type of equilibrium gait and as the energy of the system decreases, the desired equilibrium gait approaches the double-hump force profile type of equilibrium gait.

5.6 Full body model simulation

In this section one of the best proposed control policies is implemented on the full order model of the robot in the presence of moderately large noise. For the control policy, the constant stance leg angle is chosen for the implementation because this strategy showed a stable and very robust behavior at the level of the reduced order model (the bipedal spring-mass model). The full body model of the robot is shown

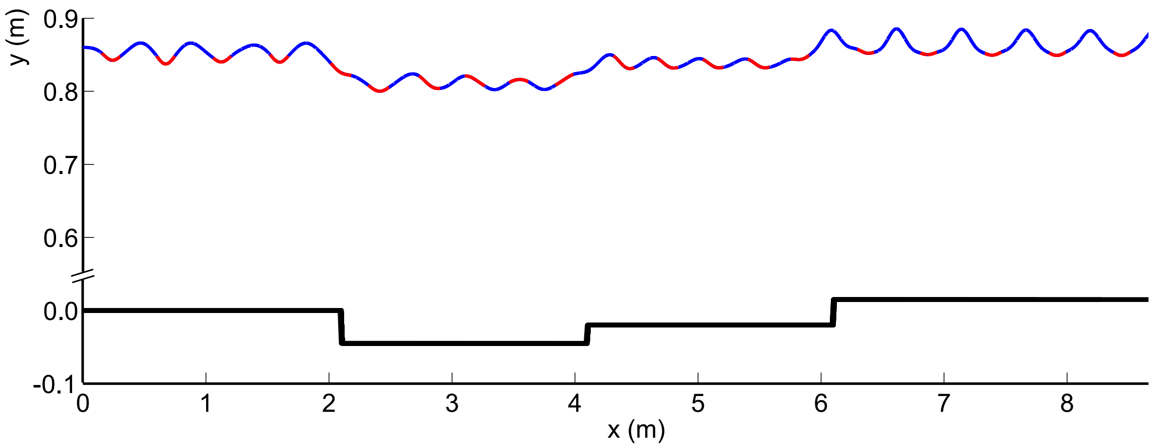

Figure 5.37: Center of mass trajectory of the bipedal spring-mass model during walking over rough terrain.

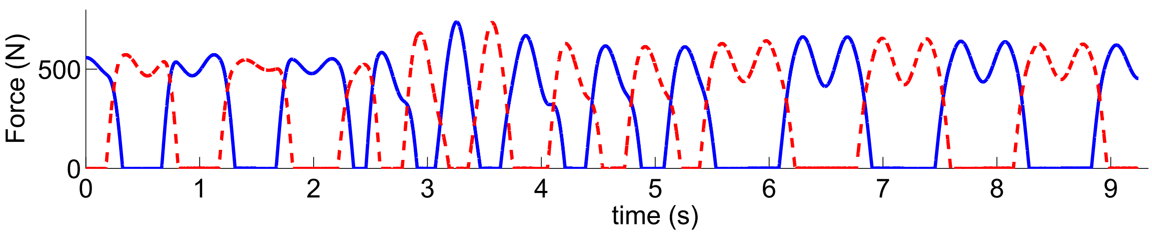

Figure 5.38: Leg force profiles during walking over rough terrain.

in figures 5.39 and 5.40. In this model, all the details of the model and the behavior of the ground as well as the impact model are included and modeled. Moreover, to simulate the noises in the sensors, moderately big Gaussian noises are added to all the measurements. The Simulink model of the controller and the full order model is shown in figure 5.41.

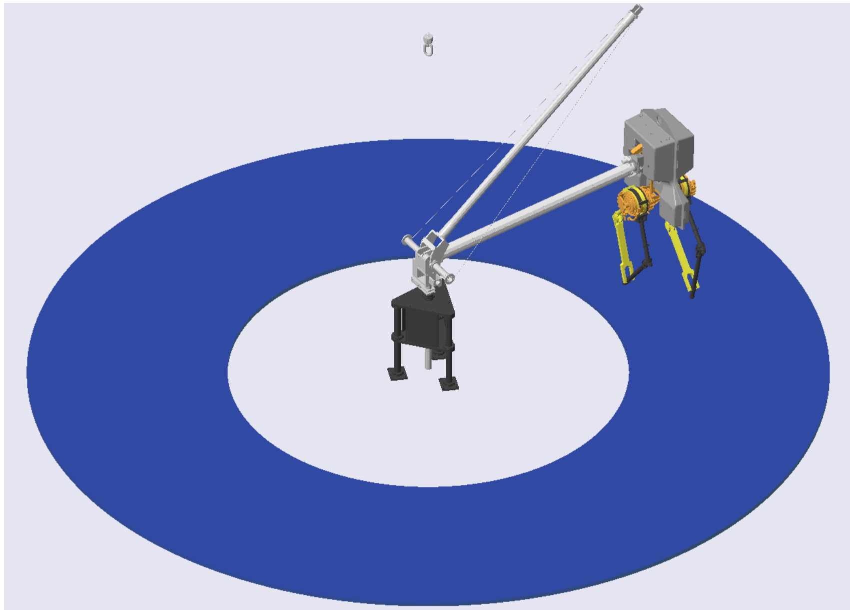

Figure 5.39: The full order model of the robot in 3D view.

5.7 Experimental results

After showing the applicability of the control policies at the level of reduced order model and the success in controlling the full order model of the robot including sensor noise, the applicability of the constant stance leg angle control policy is investigated on our robot ATRIAS [1] with locked torso to the boom. The stance leg angle is chosen because in most of the analysis, this control policy was stable for most of the equilibrium gaits and the size of the basin of attraction for this control strategy is large. Moreover, the implementation of this control policy is simple and it can be easily implemented on the real platform by just slaving the swing leg to the stance leg angle such that when the stance leg reaches a predefined value, the swing leg hits the ground. Figures 5.47 and 5.48 show the results from the ground reaction forces

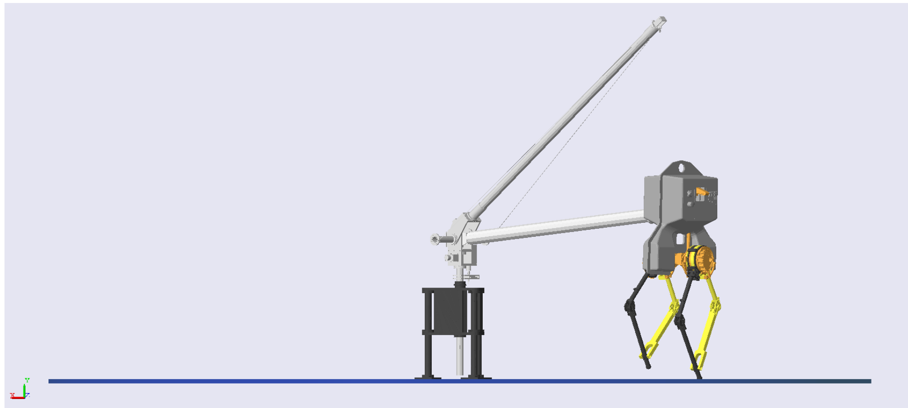

Figure 5.40: The full order model of the robot from a 2D view.

with this control policy for two experiments. As can be seen in these figures, the strategy stabilizes the gait after few steps. The fact that in the experiment the robot walks in a circle creates difference in the force profiles of the two legs. The leg that is located inside the circle moves faster than the other leg during stance phase and therefore there is a slight difference between the force profiles.

5.8 Conclusions

In this chapter we started from theory and concept of template (the bipedal spring-mass model) and successfully showed the applicability of the concept on real robot. We first derived the control policies at the level of reduced order model and then successfully applied one of the them (as an example) on the full order model of our spring-mass robot ATRIAS and after that we showed that it successfully stabilizes the real robot.

Four new swing leg control policies were proposed and compared with the existing

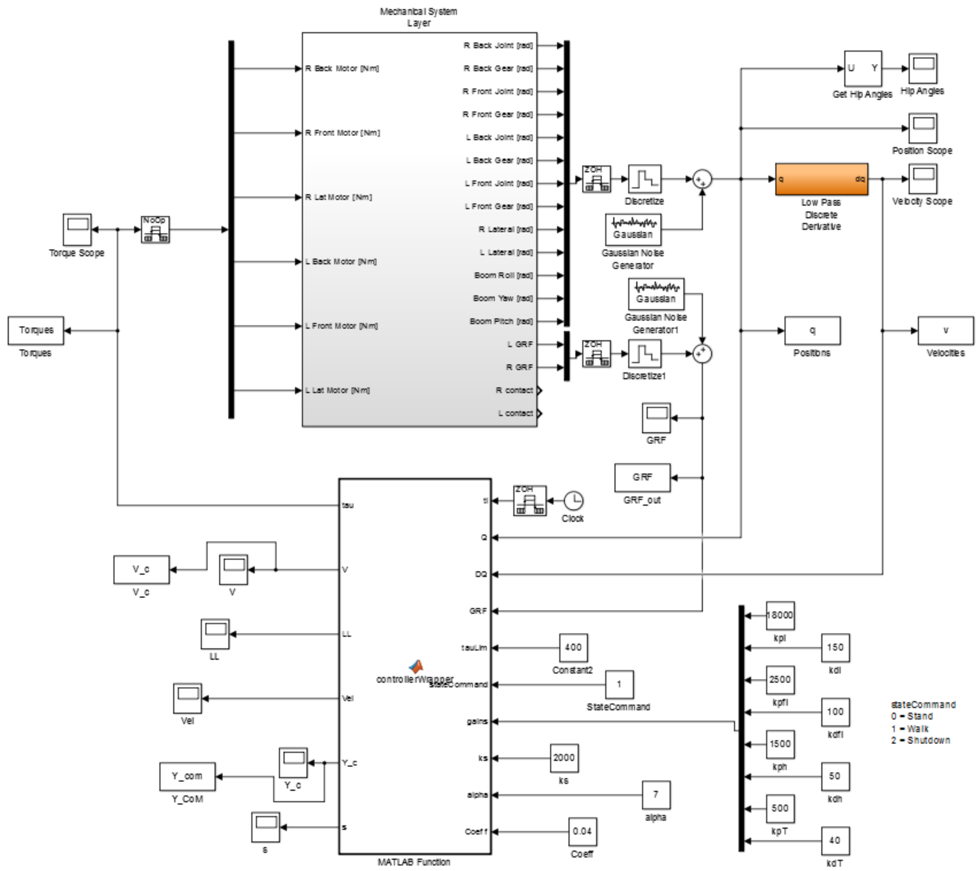

Figure 5.41: The Simulink blocks for the full order simulation. There are noises that are added to simulate the noise in the sensors.

swing leg control policies for the bipedal spring-mass model. The stability analysis of these control policies for different energy levels showed that the proposed control strategies are stable for most of the equilibrium gaits compared to the current control policies. Moreover, the size of the basin of attraction for the proposed control policies are large which guarantees that the controllers can handle large disturbances as far as the disturbance can be handled by only touch-down angle control of the

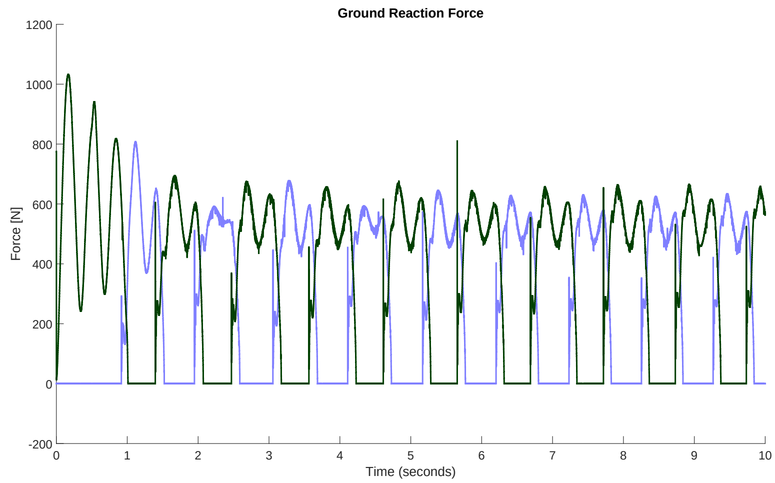

Figure 5.42: The ground reaction force in the vertical direction. After the initial perturbation, the robot converges to the limit cycle after few steps.

swing leg. The behavior of the system with the proposed control policies showed that for grounded running type of equilibrium points, the rate of convergence is faster than the equilibrium gaits with double hump force profile type. The reason is that for grounded running equilibrium gaits the double stance phase starts sooner and hence it does not allow the perturbations at the Poincare section to deviate the system significantly from the unperturbed CoM trajectory and since after the double stance phase the system is purely passive, the system with grounded running equilibrium gaits has smaller perturbations at the beginning of the double support phase. The simulation also showed that even though the bipedal spring-mass model is energetically conservative, it can be used for rough ground and converges to different equilibrium gaits in different energy levels. After the full investigation of the control policies at the level of reduced order model, we chose one of the policies as an example and implemented on full order model (anchor) of our robot. Finally, the

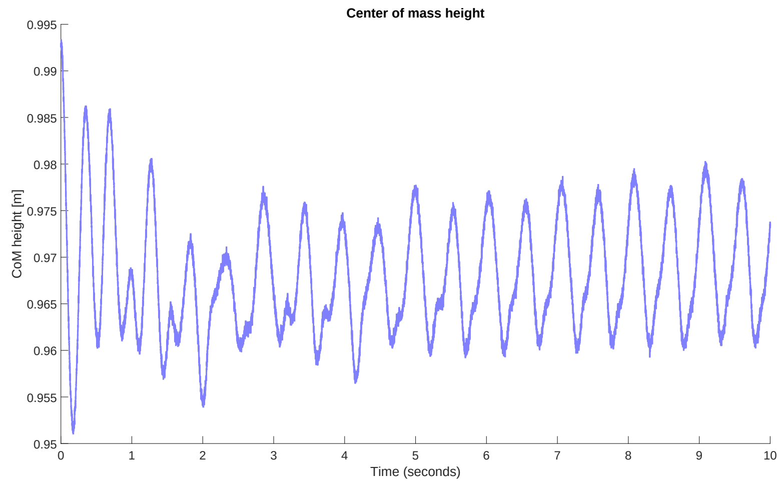

Figure 5.43: The CoM height of the robot after the initial perturbation. The robot converges to the desired limit cycle after few steps.

control policy was implemented on our spring-mass robot ATRIAS with locked torso and the same behavior that was predicted from the template and confirmed from the anchor, was observed on the robot.

5.9 Future Work

The control policies proposed in this chapter use the functions between the states of the system that have physical meaning like the stance leg angle or stride length. For the future work, an optimized function between the states for the moment of touch-down can be found to maximize the rate of convergence and the size of the basin of attraction. Moreover, the applicability of using the velocities of the CoM can also be investigated including the uncertainty that they bring to the policy.

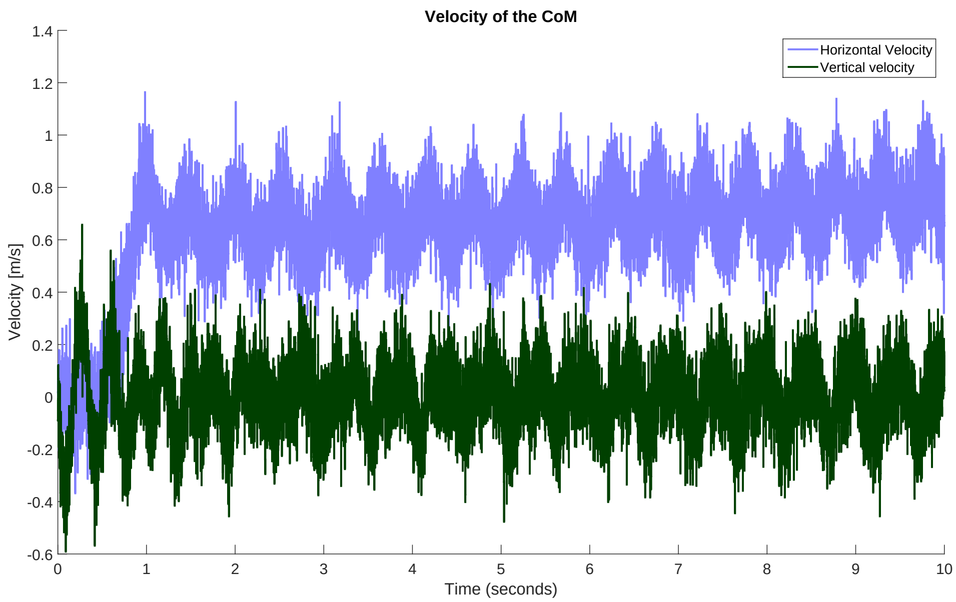

Figure 5.44: The vertical and horizontal velocities of the CoM. The robot starts with a push in the beginning which is considered as the perturbed initial condition.

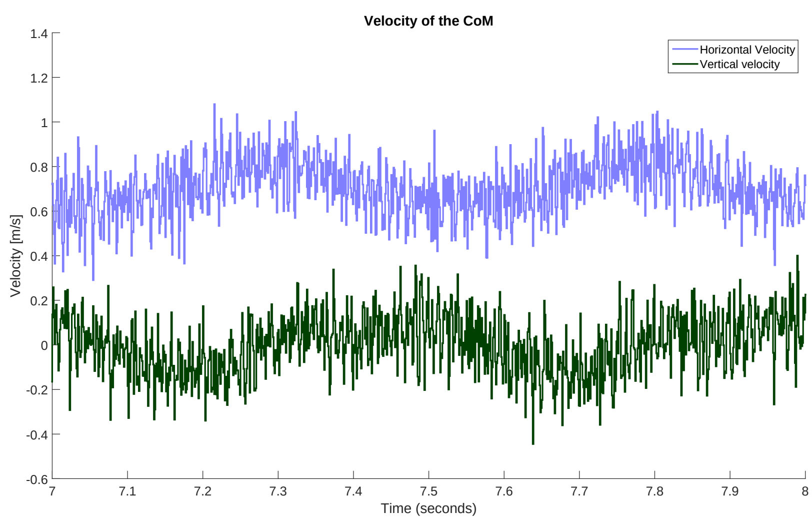

Figure 5.45: The vertical and horizontal velocities of the CoM when it is settled to the limit cycle.

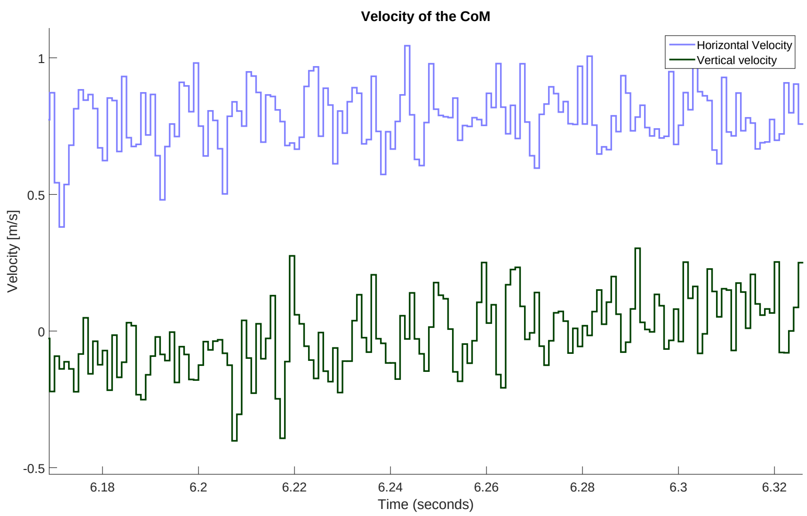

Figure 5.46: A close snapshot of the velocity to show the discrete characteristic of the signals and the magnitude of the noise in the simulation.

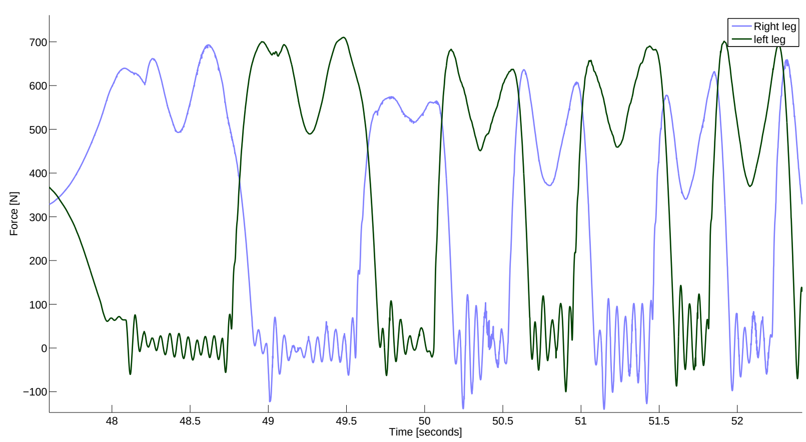

Figure 5.47: The force profile from the robot experiment using the constant stance leg angle control policy for the swing leg.

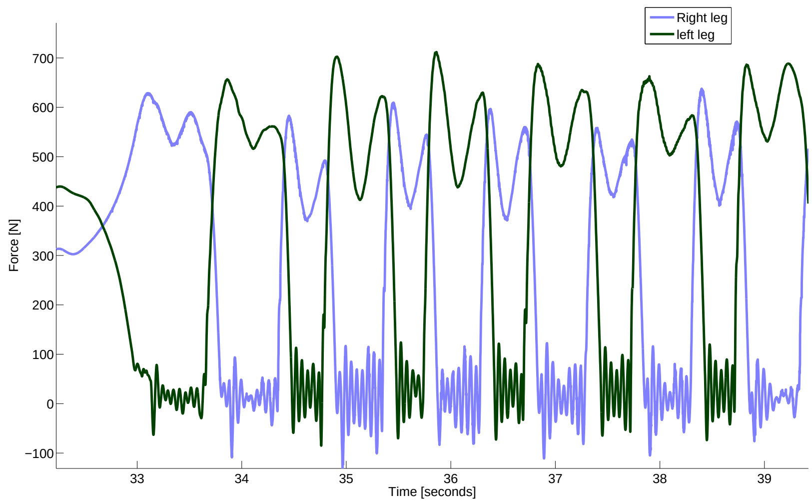

Figure 5.48: The force profile from the robot experiment using the constant stance leg angle control policy for the swing leg.

Chapter 6 – Feed-forward control technique

In this chapter, a new control strategy is presented for the walking of spring-mass robots that stabilizes the system to the desired equilibrium gait and manages the energy level of the system. The control technique is a feed-forward function based on time for stance phase and for the swing leg the time of the touch-down after the Poincare section is kept constant. The feed-forward function changes the zero force leg length of the stance leg based on a predefined sinusoidal function of time which can be analogous to the central pattern generator (CPG) control policy. For the model two cases are assumed, the bipedal spring-mass system and the bipedal spring-mass model with damping in parallel to the spring in the leg. The results show that even though for the system with damping in the leg the efficiency of the system slightly decreases, the stability and the rate of convergence improves significantly. Since the effect of damping is significant in the stability of the gait, it can also be virtually created by the actuators as virtual damping in the system.

6.1 Introduction

Humans and animals can start walking in natural environment since very young age, but despite remarkable advances in the field of legged locomotion with very advanced sensors and complicated control tools, robots do not perform as efficient and robust as baby animals. This fact has attracted the attention of the researchers to understand the principles of locomotion in animals and replicate the same dynamics and behavior on the legged robots. To achieve this goal, bio-inspired models have been proposed to describe the important features of animals' locomotion and create the same dynamics on the robots. The spring loaded inverted pendulum (SLIP) was one of the first models that was proposed for running [39] and recently it was extended to the bipedal spring-mass model [6] for walking. In this chapter, the bipedal spring-mass model is used as the basis for the passive behavior of the system with an actuator in series with the spring in the leg to be able to handle the energy management.

McGeer [9] was the first one that showed walking does not require high tech sensors or complicated control commands. In his passive walker there was no sensor in the system and the gravitational force acted like a feed-forward force to the system (feed-forward force (gravity) based on the states of the system). A similar logic was accepted by Schmitt and Clark [54] for stance phase control policy for running SLIP. In their method, the flight phase control policy used a feedback control based on the previous take-off angle and was independent of the stance phase controller and the stance phase controller was a feed-forward function that adds and removes energy regardless of the states of the system. They gained the inspiration for their control policy from the behavior of cockroaches [86] and grounded running birds [87]. Later, Miller et al. [88] showed the potential of this strategy on a mono-pod robot.

Inspired by Schmitt and Clark [54] control policy for running, we investigate the applicability of the feed-forward control strategy for walking. The plan is to extend the policy to the systems with and without some physical or virtual damping in parallel to the spring in the bipedal spring-mass model.

The inclusion of damping in the system will be investigated for two reasons: First is that all real systems have some inherent damping and second is that if the analysis shows that the existence of damping is useful for the stability and robustness of the system, the effect of damping can be generated in the software by the actuators. It is acknowledged that assuming virtual damping in the controller and providing the same effect by the actuators requires feedback from velocity and may reduce the efficiency of the system with respect to the undamped situation.

In this section we investigate how a feed-forward stance phase control policy stabilizes the bipedal spring-mass walking model. For this purpose, one of the control policies that was investigated before as the swing leg control strategy is used as the swing leg policy for the model and for the stance phase policy, a feed-forward sinusoidal function is used to change the zero force leg length of the leg.

6.2 Method

We use the actuated bipedal spring-mass model as the bipedal extension of the actuated SLIP model introduced before in [10, 47]. The actuated bipedal spring-mass model is shown in figure 6.1 and the equations of motion for this model can be modified as follows:

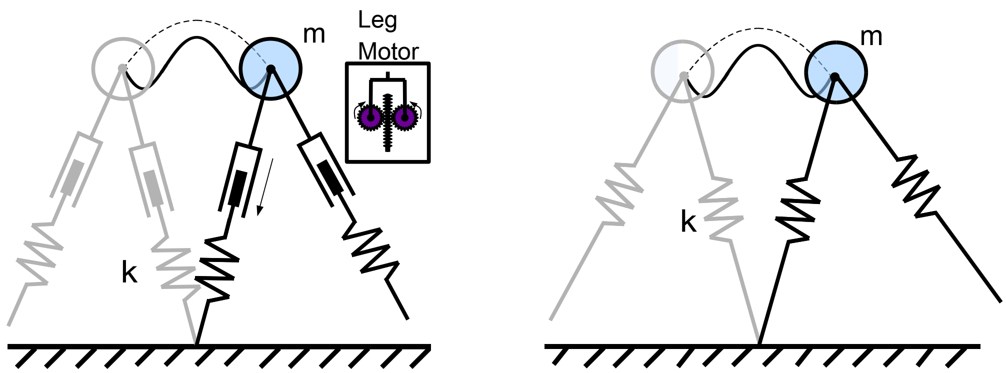

Figure 6.1: left: The model of the robot with the leg motor to change the zero force leg length during the stance phase. When the motor is kept locked (zero mechanical energy), it provides the same behavior of the equivalent conservative bipedal spring-mass model that is shown in the right.

For single support phase dynamics:

$$\begin{Bmatrix} \ddot{x} \\ \ddot{y} \end{Bmatrix} = \begin{Bmatrix} \frac{F_1(x-x_{t1})}{m.l_1} \\ \frac{F_1(y-y_{t1})}{m.l_1} - g \end{Bmatrix} \tag{6.1}$$

For double support phase dynamics:

$$\begin{Bmatrix} \ddot{x} \\ \ddot{y} \end{Bmatrix} = \begin{Bmatrix} \frac{F_1(x-x_{t1})}{m.l_1} + \frac{F_2(x-x_{t2})}{m.l_2} \\ \frac{F_1(y-y_{t1})}{m.l_1} + \frac{F_2(y-y_{t2})}{m.l_2} - g \end{Bmatrix} \tag{6.2}$$

Where

$$F_i = k(\tilde{l_0}(t) - l_i(t)) + c(\dot{\tilde{l_0}}(t) - \dot{l}_i(t)) \quad i = 1, 2 \tag{6.3}$$

$$l_i = \sqrt{(x - x_{ti})^2 + (y - y_{ti})^2} \quad i = 1, 2 \tag{6.4}$$

To have a feed-forward function for the change of the zero force leg length during stance phase, the actuator dynamics is ignored and the change in the rest leg length is assumed instantaneous. Here we assume that the zero force leg length is changed based on the following function:

$$\tilde{l_0}(t) = l_0 - l_{dev} sin(\omega t) \tag{6.5}$$

The derivative of the zero force leg length with respect to time is as follows:

$$\dot{\tilde{l_0}}(t) = -l_{dev} \omega cos(\omega t) \tag{6.6}$$

In this equation $\tilde{l_0}(t)$ is the zero force leg length of the stance leg at time t and l_0 is the original rest length of the leg correspond to the zero actuator length. The amplitude of the leg length change is shown by l_{dev} and the frequency of the leg length change is denoted by ω. As can be seen in equation 6.5, the change of the leg length does not depend on the state of the system and is based on time as well as its derivative. Since the leg force during the stance is always in compression, shortening the leg means dissipating some energy and extending the leg means gaining some energy. Therefore, like in Schmitt and Clark [54] policy for running, for the exact desired gait, the robot loses some energy in the beginning of the touch-down and later during the stance, it gains the energy it lost before such that at the end the whole energy of the system remains the same. If the system has more energy than the desired energy level then the leg leaves the ground earlier and therefore it loses more energy in the beginning than it receives from the actuators later.

For the swing leg control, we use the constant touch-down time control policy as described in chapter 5, to be a function of time similar to the stance phase. Moreover, the constant touch-down time control policy has shown successful results in stabilizing the bipedal spring-mass model.

6.3 Results

The results of the numerical simulations are presented in this section for two separate scenarios: system without damping and damped model. The results show that the system converges to asymmetric equilibrium gait in the presence of damping and can converge to both symmetric and asymmetric equilibrium gaits for undamped system. The parameters that affect the analysis are the touch-down time t_{TD}, frequency of the leg length change during the stance phase ω, the amplitude of the leg length change during the stance phase l_{dev} and the amount of damping in the system c. By changing either of the aforementioned parameters, the system converges to different equilibrium point in different energy level.

6.3.1 Undamped system

We start the analysis with the case that there is not any physical damping in the system and therefore the system is conservative if the actuators are kept locked during the stance phase. Therefore, the only sources of energy change in the model are the leg actuators. For the first case, shown in figures 6.2 and 6.3, the system starts with a perturbed state to transition to the desired state in lower energy level than the initial state. The transitioning to the desired state in this case is similar to recovering from a drop step when the perturbed system has higher energy level than the desired state.

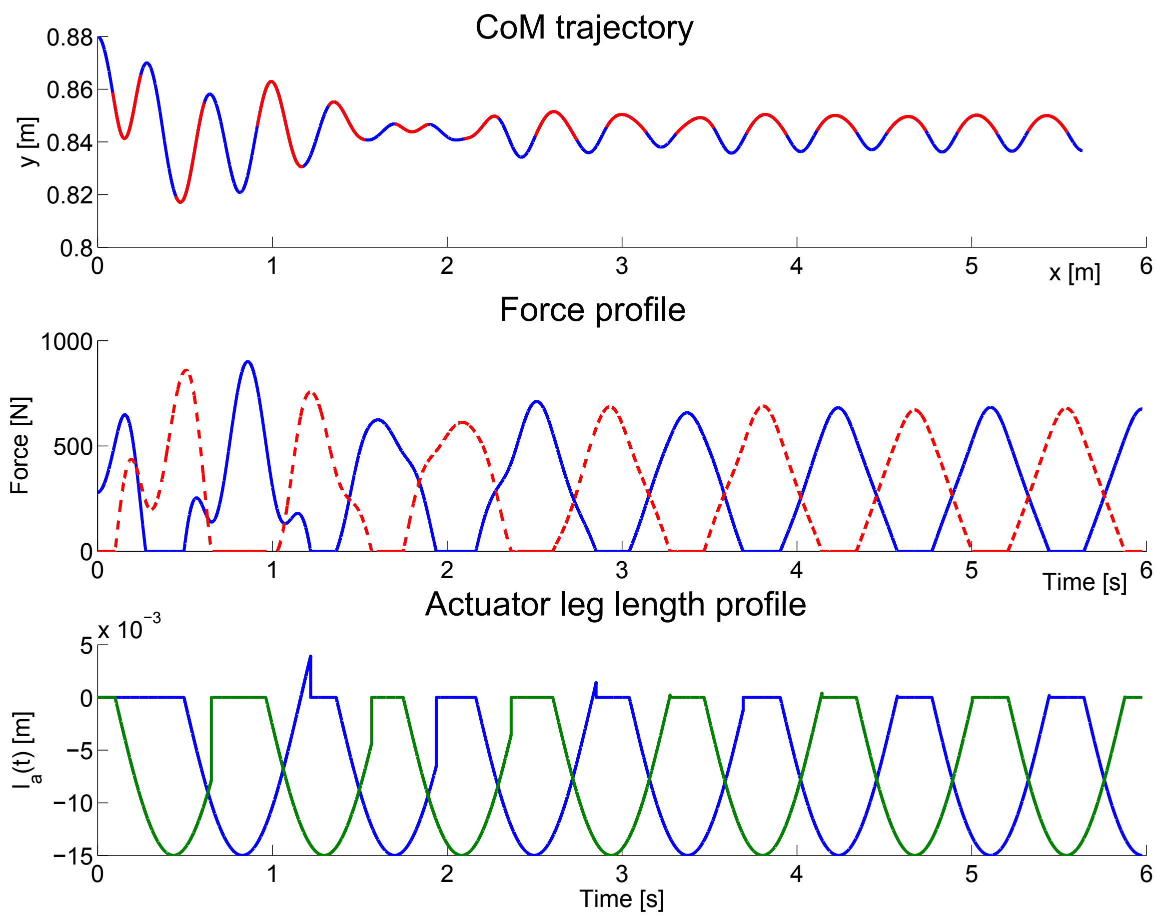

Figure 6.2: The behavior of the bipedal spring-mass model using the feed-forward stance phase control strategy. The model starts with a perturbed state and converges to the desired equilibrium point. The actuator leg length profile is not matched with the gait for the initial steps and then they get aligned.

For the second example of the undamped case, the desired equilibrium point has higher energy level than the initial perturbed state. The results for this case are

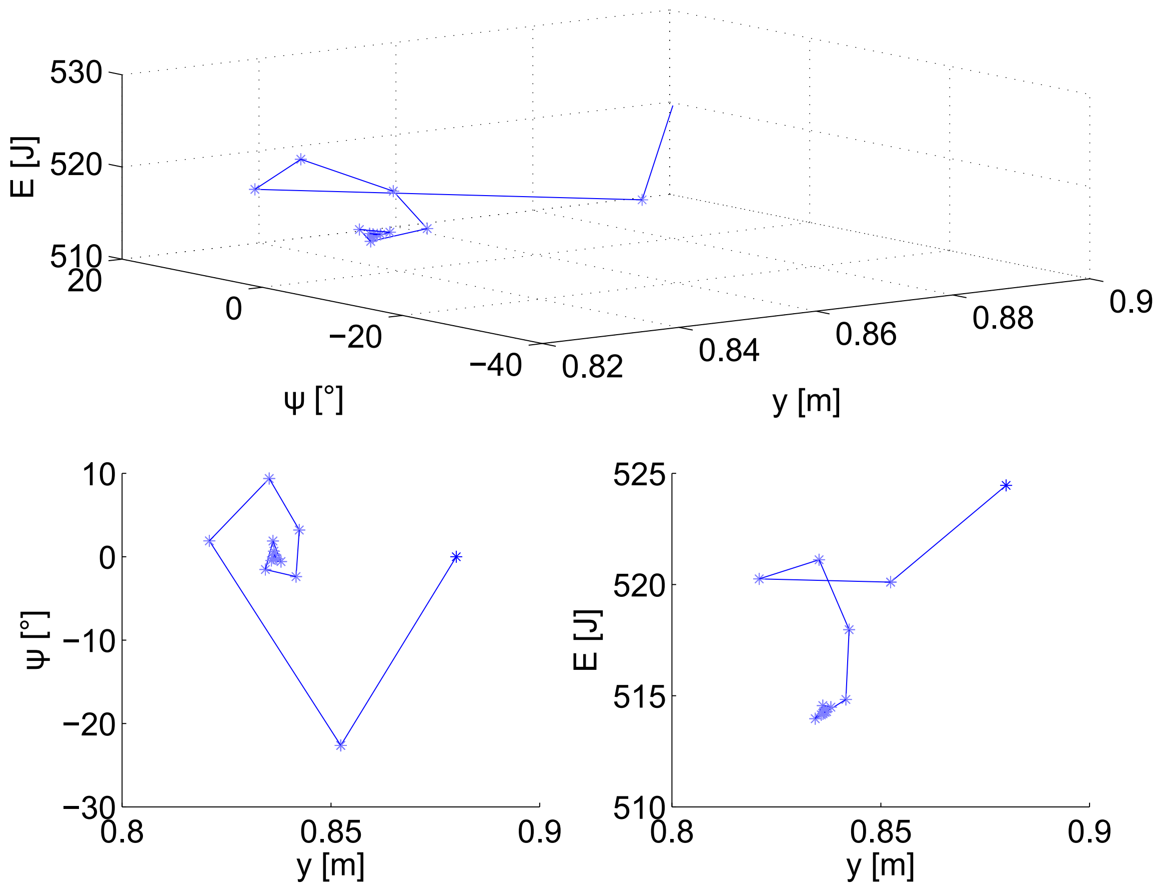

Figure 6.3: The states of the system at the Poincare section. The perturbed state at the beginning has higher energy than the desired equilibrium point.

shown in figures 6.4 and 6.5. The case of having the desired state in higher energy level is like walking over a step and recovering from the perturbation. By adjusting the frequency and the touch-down time, asymmetric equilibrium point with higher energy level can be achieved. The actuator leg length is not aligned with the gait in the beginning and after few steps the actuator leg length profile gets compatible with the gait and the system monotonically gains energy until the desired equilibrium gait. In this case, unlike the previous example, the actuator leg length profile is not symmetric with respect to the mid-stance even though the system is physically undamped. Therefore the actuator adds and removes the same amount of energy in each gait, but the first half with shorter duration, the rate of removing energy is higher than the second half of the stance phase.

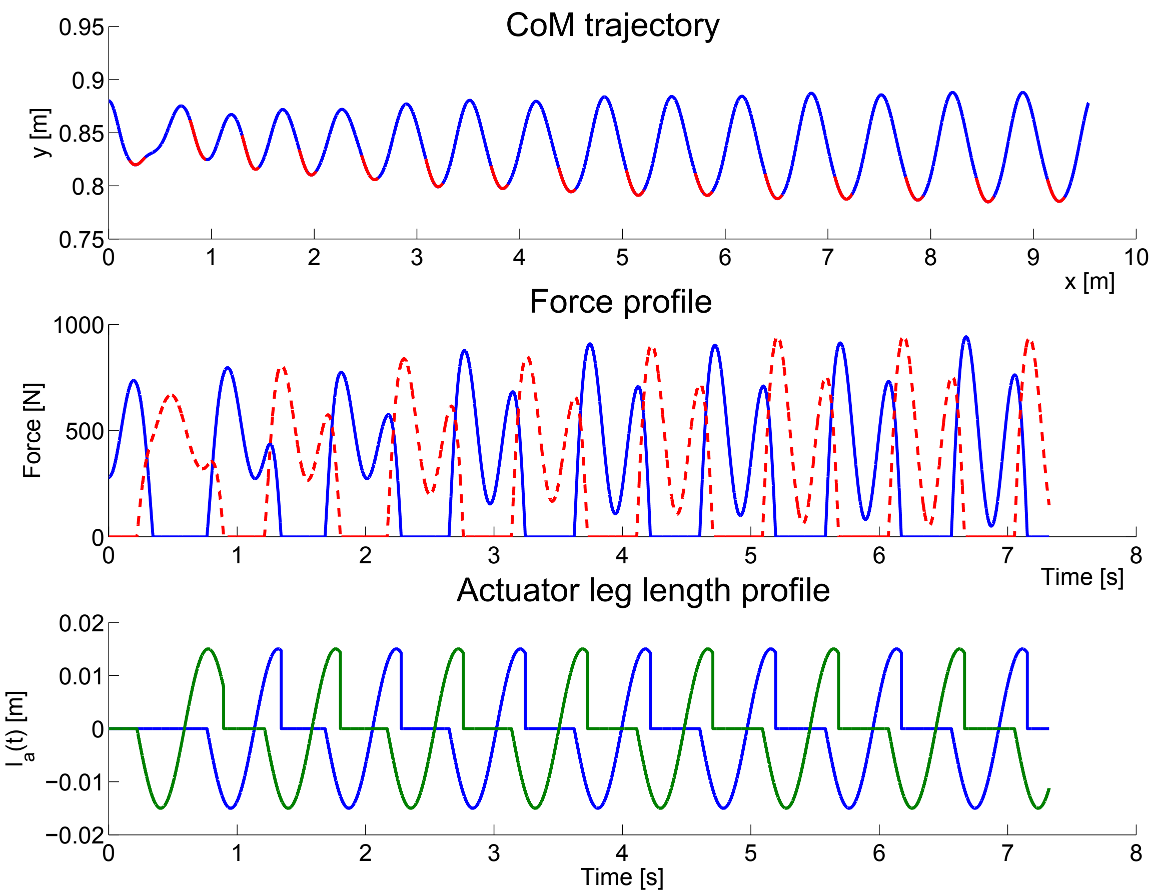

Figure 6.4: By adjusting the frequency and the touch-down time, the system can converge to asymmetric equilibrium point. The actuator leg length is not aligned with the gait in the beginning of the perturbation.

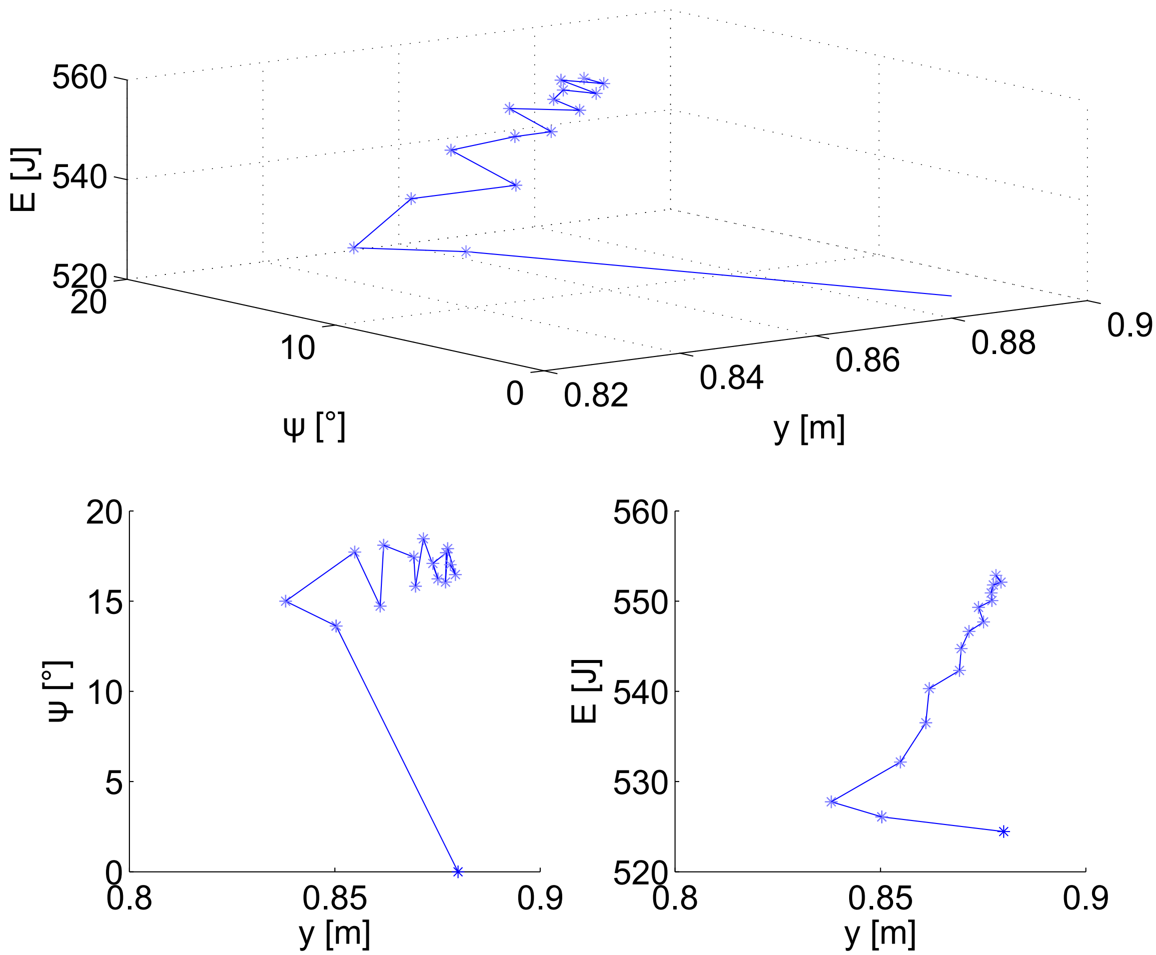

Figure 6.5: The states of the system at the Poincare section including the energy level of the system. The desired equilibrium gait is asymmetric in higher energy level.

6.3.2 System with damping

In the presence of damping, the behavior of the system improves even though the efficiency may sometimes degrade. In the following examples, two cases are studied that a physical damping exists in the leg. For the first example, the desired equilibrium gait is asymmetric double hump with higher energy level than the initial perturbed state. The results are shown in figures 6.6 and 6.7. The rate that the system converges to the desired equilibrium gait is faster than the undamped situation and the system converges to the desired equilibrium gait. It can be seen that the actuator leg length profile is not symmetric with respect to the mid-stance because the actuator should compensate for the energy that the damper dissipates in each gait.

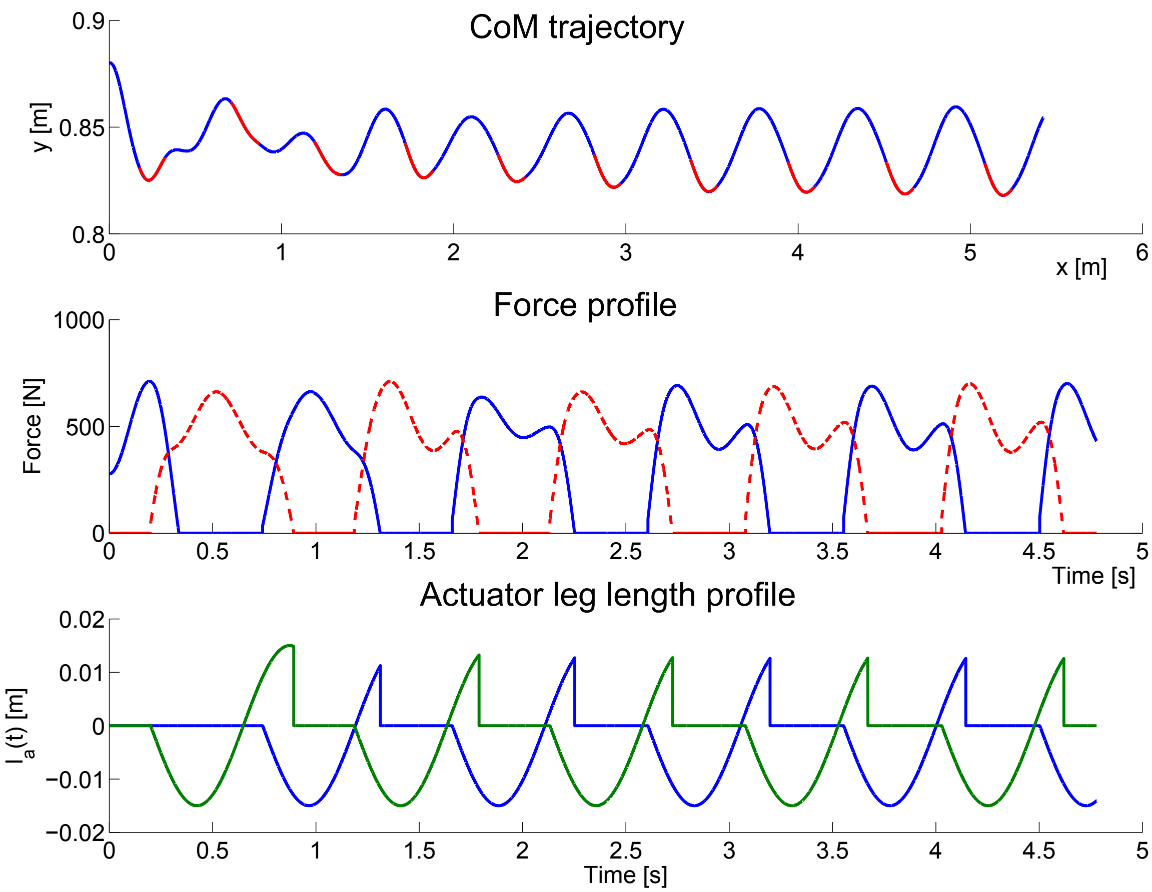

Figure 6.6: The center of mass trajectory, force profile and the actuator leg length of the bipedal spring-mass model in the presence of $\zeta = 5\%$ damping in parallel to the spring. The system starts from a perturbed state and after 5 steps converges to the desired equilibrium point with the desired energy level.

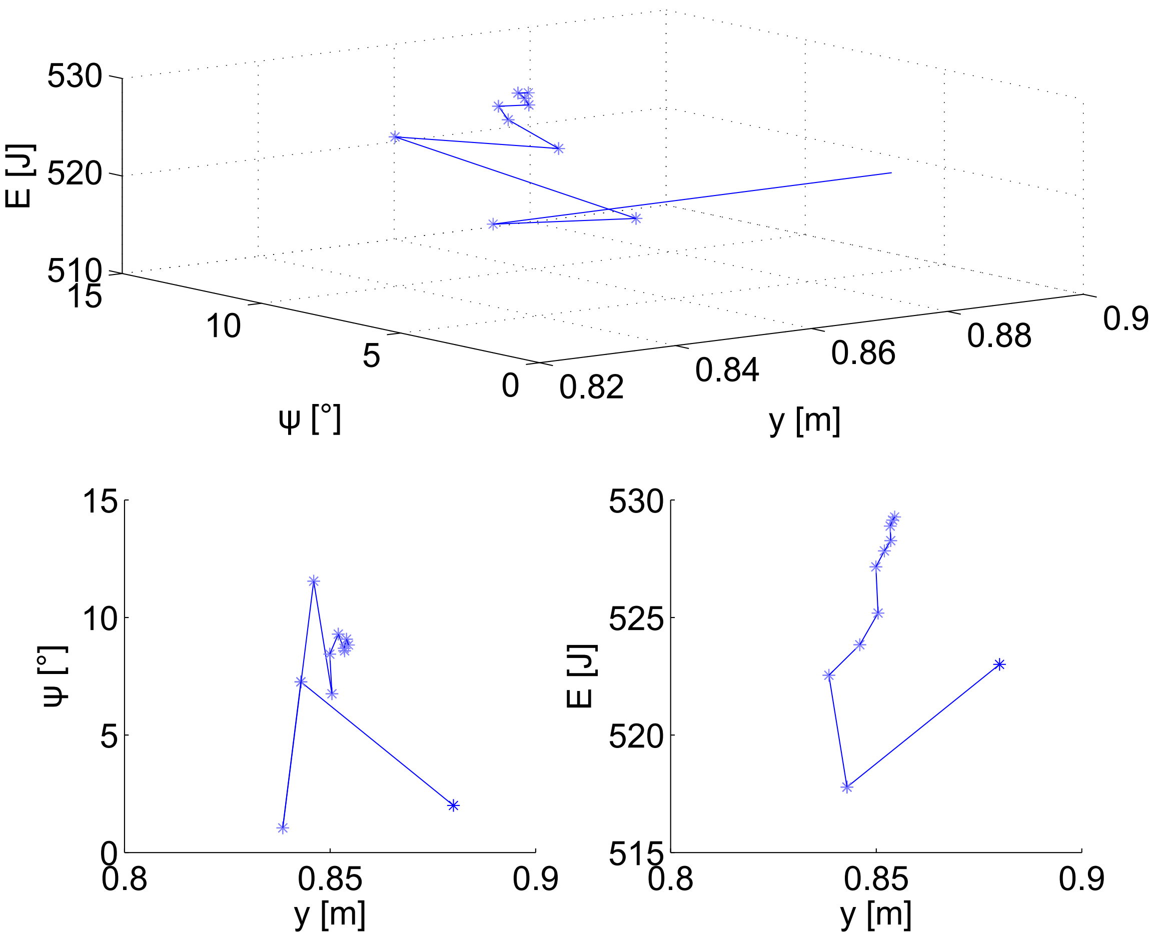

Figure 6.7: The change of the Poincare section states from a perturbed state to the desired equilibrium gait in higher energy level than the initial perturbed state.

For the second example, the desired equilibrium gait is grounded running with higher energy level. The results for this case are shown in figures 6.8 and 6.9. The system converges to the equilibrium point after about 5 steps.

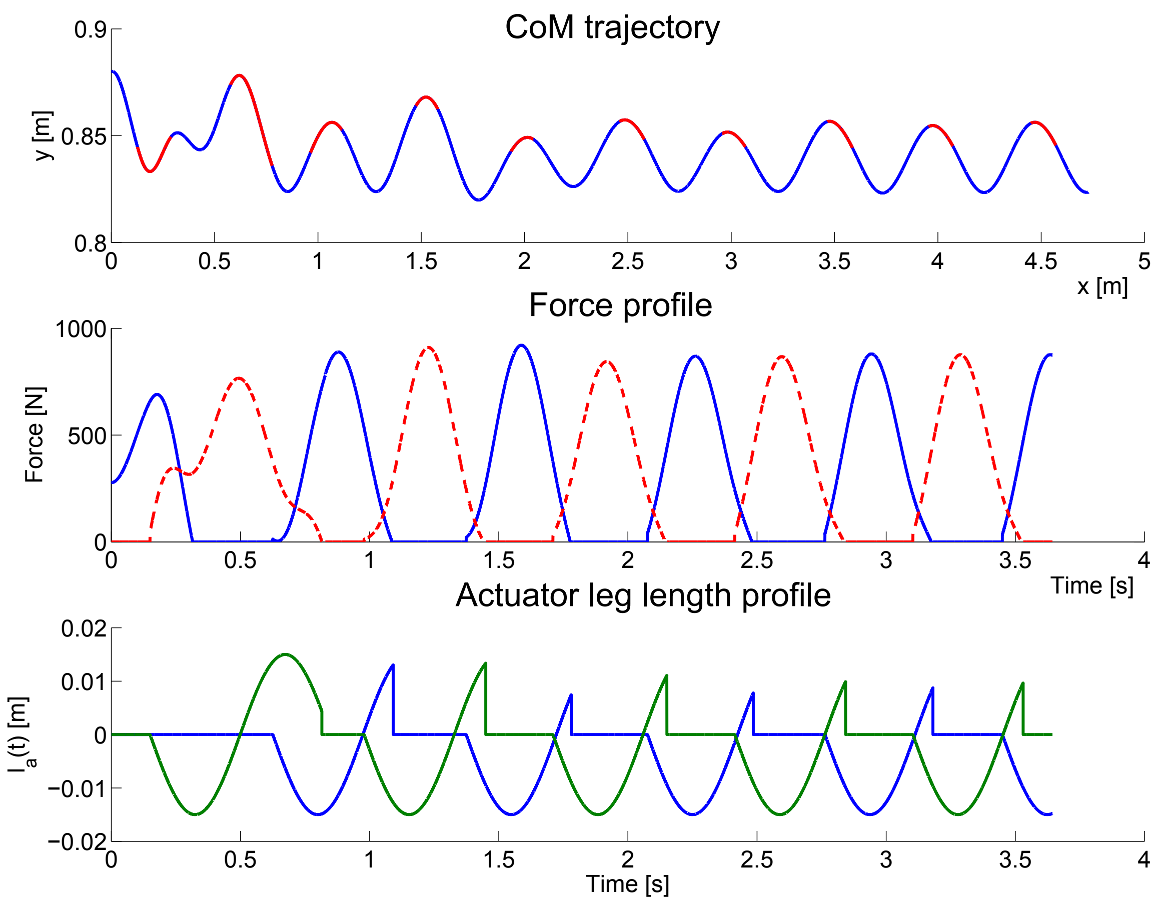

Figure 6.8: The behavior of the bipedal spring-mass model in the presence of damping and using the feed-forward stance phase control strategy. The desired equilibrium point is grounded running state with higher energy level than the initial perturbed state. In the presence of damping, the actuator leg length is not symmetric and the positive work done by the actuator is bigger than the negative work.

6.4 Simulation on the full order model

In this section the proposed control policy is implemented on the full order model of the robot in the presence of moderately large noise. For the swing leg control policy, the constant stance leg angle is chosen for the implementation and the stance phase

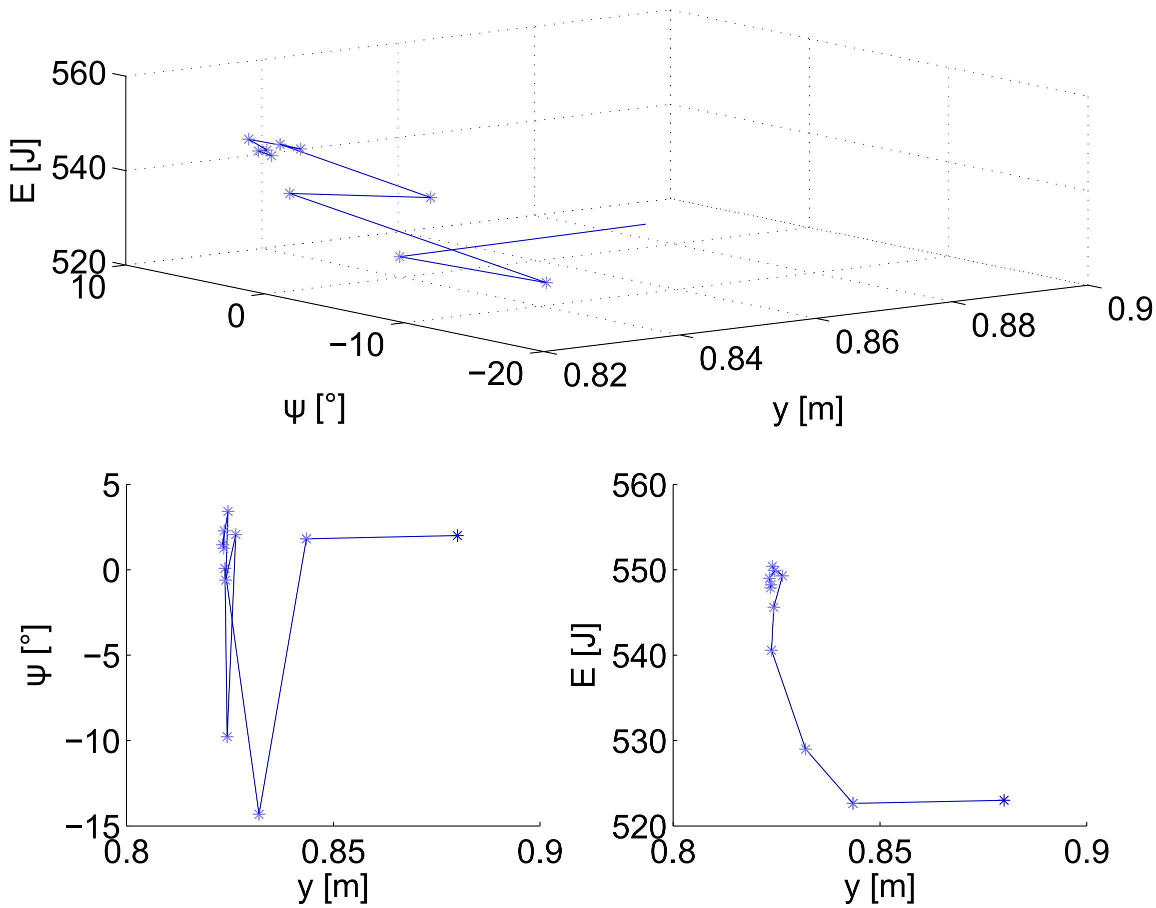

Figure 6.9: The states at the Poincare section and energy level of the system in the presence of $\zeta = 5\%$ damping in parallel to the spring and using feed-forward stance phase control strategy. The desired state is in higher energy level than the initial state.

control policy is the sinusoidal feed-forward function of the zero force leg length. The full body model of the robot is shown in figures 5.39 and 5.40 in chapter 5. This control policy can successfully stabilize the full order model and the resultant ground reaction force from this simulation is shown in figure 6.10.

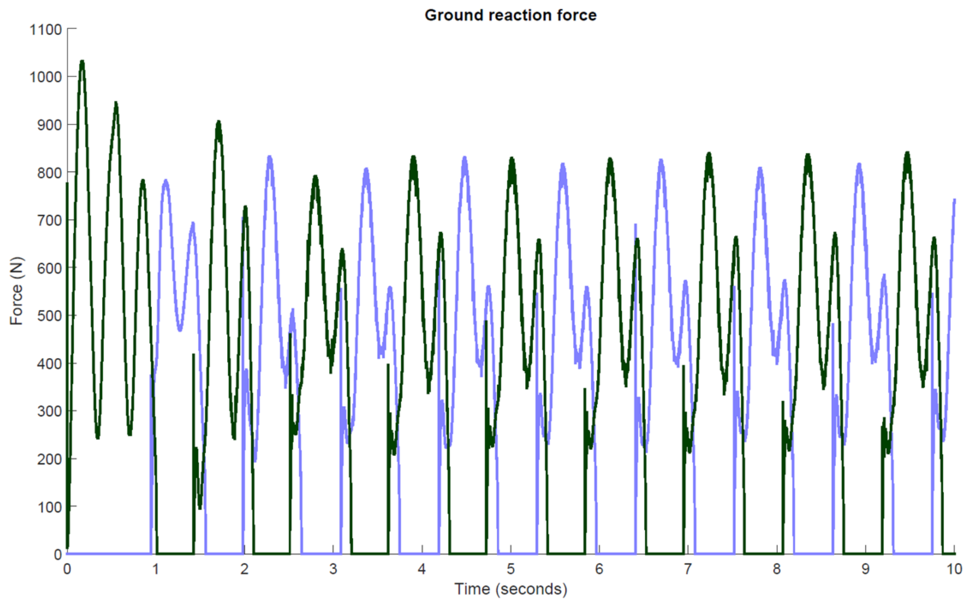

Figure 6.10: The vertical ground reaction force from the feed-forward control policy implemented on the full order model of the robot. The asymmetric shape of the ground reaction force is the same as the force profile that we expect from the reduced order model.

6.5 Conclusion

In this chapter, a new control strategy was proposed for spring-mass walking robots that can stabilize the gait and manages the energy of the system. For the stance phase, a feed-forward function based on time was used and for the swing leg policy, the constant touch-down time strategy presented in chapter 5 was used. The simulation results showed that the control policy can indeed stabilize the bipedal spring-mass model to the desired gait and desired energy level. If the energy of the gait is more than the desired energy that corresponds to the swing leg touch-down time and the stance phase parameters (amplitude and frequency of the feed-forward function), the leg leaves the ground earlier and therefore it leads to losing more energy during the stance than gaining energy. Although the simulation results show that losing or gaining energy is not a monotonic function, but in general as a whole this is the stabilizing reason for the energy of the gait. Moreover, for the spring-mass model with some physical damping in parallel to the spring, the stability of the control policy was enhanced and the rate of convergence increases as well. The damping in the leg can be physical damping or can be virtually created by the actuators.

6.6 Future work

The next step is to implement this control strategy on the spring-mass legged robot. Reformulating this concept based on the states of the system (like the stance leg angle) instead of time is another extension to this control policy.

Chapter 7 – Bio-inspired swing leg control for spring-mass robots running on ground with unexpected height disturbance

We proposed three swing leg control policies for spring-mass running robots, inspired by experimental data from our recent collaborative work on ground running birds. Previous investigations suggest that animals may prioritize injury avoidance and/or efficiency as their objective function during running rather than maintaining limit-cycle stability. Therefore, in this study we targeted structural capacity (maximum leg force to avoid damage) and efficiency as the main goals for our control policies, since these objective functions are crucial to reduce motor size and structure weight. Each proposed policy controls the leg angle as a function of time during flight phase such that its objective function during the subsequent stance phase is regulated. The three objective functions that are regulated in the control policies are i) the leg peak force, ii) the axial impulse, and iii) the leg actuator work. It should be noted that each control policy regulates one single objective function. Surprisingly, all three swing leg control policies result in nearly identical subsequent stance phase dynamics. This implies that the implementation of any of the proposed control policies would satisfy both goals (damage avoidance and efficiency) at once. Furthermore, all three control policies require a

surprisingly simple leg angle adjustment: leg retraction with constant angular acceleration. This work was published as a paper in Bioinspiration & Biomimetics journal (2013) in collaboration with Dr. Monica A. Daley at Royal Veterinary College, London.

7.1 Introduction

We seek to understand the principles of legged locomotion and to implement them on robots. Recent years have seen remarkable advances in dynamic legged robots, including Rhex, a rough-terrain hexapod [61, 62], Bigdog, a rough terrain quadruped [89], MABEL, a biped that can negotiate uneven terrain [90], ATRIAS, a bio-inspired actuated spring-mass robot [2], and PETMAN, a versatile humanoid biped. These robots highlight the emerging potential for legged robotic technology; however, none of these machines can compete with animal performance and efficiency. In natural environments animals frequently negotiate potholes, steps and obstacles remarkably, while running. Because we do not yet understand the fundamental principles of locomotion that enable such performance, we cannot reproduce these behaviors in machines [91]. In this study we seek to identify reasonable objective functions animals might care about, and use them to control a spring-mass running robot. To gain insight into the goals birds may care about during running, we investigated guinea fowl running data (figure 7.1) and interpreted the importance of those goals for real machines.

There are two reasons why we focus on swing leg control: i) The flight phase

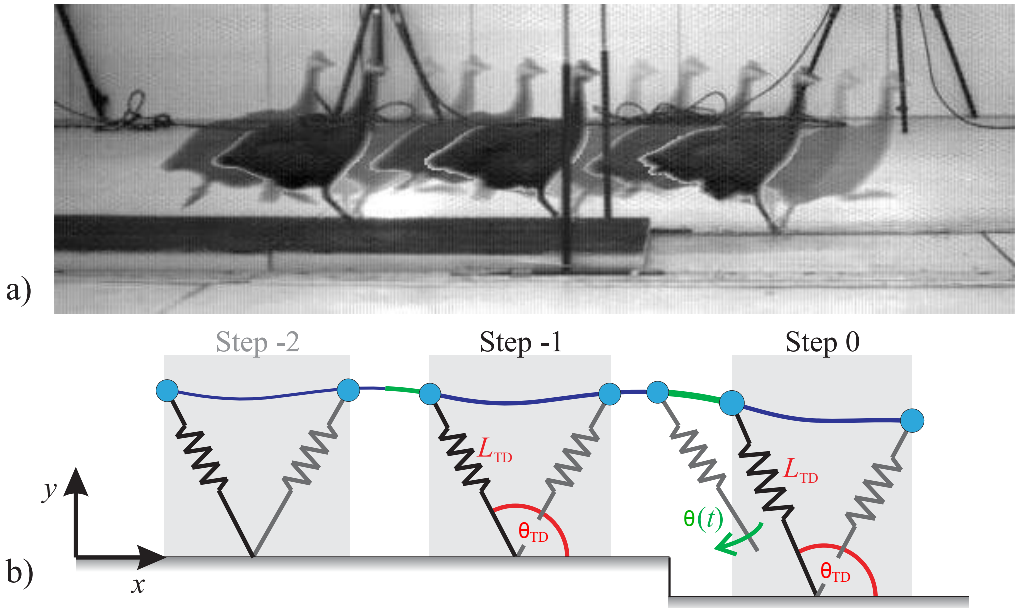

Figure 7.1: Illustration of experiment setup on the guinea fowl running over a step down (a), and schematic drawing of the SLIP model (b). The gray areas indicate the stance phases, and the blue line represents the CoM trajectory [3].

determines the landing conditions, which have huge effects on stance dynamics, and ii) adjusting the leg parameters during flight is very energy efficient because there are no ground reaction forces to overcome during flight to move the leg. The effect of swing leg control methods on the dynamics of a spring-mass system has been investigated in previous literature [6, 4, 42, 43, 5]. From a biologist's perspective, animal running data reveal that the initial leg loading during stance is very sensitive to its landing conditions, which are determined by the flight phase [92, 93, 94, 95]. Daley et al. [87] showed that for running guinea fowl, the variation in leg contact angles explains 80% of the variation in stance impulse after an unexpected pothole. From a roboticist's point of view, using a feed-forward control strategy minimizes the need for sensing, which makes these techniques easy to implement in robots.

Previous theoretical studies of swing leg control suggest a trade-off between objectives like disturbance rejection, stability, maximum leg force and impact losses. For example, a constant leg retraction velocity in late swing improves stability in both quadrupeds [96] and bipeds [42]. Similarly, increasing the leg length in late swing can improve stability and robustness [43]. Whereas low leg retraction velocities improve the robustness against variations in terrain height, high leg retraction velocities minimize peak forces and improve ground speed matching [97, 44]. Alternatively, a feed-forward swing leg control policy can be applied to the spring-loaded inverted pendulum (SLIP) model to maintain steady state running (equilibrium gait), regardless of ground height changes [98]. While maintaining steady state running results in symmetric trajectories even in the presence of ground height changes, it also results in high leg forces and high leg actuator work (electric consumption of the electric motor) during the perturbed step. Karssen et al. [99] determined the optimal swing leg retraction rate that maximizes disturbance rejection, and minimizes impact losses and foot slipping. They considered a predefined constant leg retraction rate for running and concluded that there exists no unique retraction rate that optimizes all goals mentioned above at the same time. Especially for high forward speeds, a compromise between disturbance rejection and energy losses is inevitable. Recently, Ernst et al. [5] demonstrated how leg stiffness may affect the self-stability of a running robot. They proposed a control strategy that updates the leg stiffness based on the fall time or vertical velocity of the center of mass (CoM).

The equilibrium (symmetric) gait policy is a well-investigated swing leg control policy for spring-mass robots [98, 5]. This policy ensures that the robot's CoM trajectory is symmetric with respect to the vertical axis, which is defined by mid-stance (touch down and take off conditions are symmetrical). Therefore, on flat ground each step is identical to the previous step, resulting in a periodic gait pattern. By choosing the appropriate initial leg angle (touch down leg angle) for each velocity vector $\boldsymbol{v} = (v_{\mathrm{x}}, v_{\mathrm{y}})^T$, a symmetric gait can be obtained. This policy continuously updates the leg angle based on the CoM velocity vector during flight such that whenever the leg hits the ground, a symmetric CoM trajectory is maintained. In the presence of a drop, however, the required mechanical capacity (leg force for example) can increase drastically, and may exceed the ultimate leg capacity. Therefore, the equilibrium gait policy may not be a practical control strategy for spring-mass robots.

Inspired by our findings from a previous study on guinea fowl negotiating a drop perturbation [3], we propose three candidates for the objective function of the swing leg control policy. The objective functions are: i) maintaining constant peak force, ii) maintaining constant leg axial impulse, and iii) maintaining constant leg actuator work. Each control policy adjusts the leg angle during flight such that its objective function during the subsequent stance phase is regulated. The first swing leg control policy ensures that the leg peak force in the following stance phase is the same as the peak force of the previous step. The second policy keeps the axial impulse of the upcoming passive stance phase the same as the axial impulse of the previous step. The last control policy focuses on economy by maintaining constant electrical work to keep the motor, which is in series with the spring, locked (providing zero mechanical work and thus a conservative passive stance phase). In this case the actuator requires the same electric energy for the drop step and flat ground. We compare these control policies with equilibrium gait policy and against each other.

The results show that the equilibrium gait policy requires more energy and leg force capacity than the proposed control policies. For economically designed robots that are operating at (or close to) their maximum mechanical capacity, any drop in the ground may cause damage, or the robot could even fall if the motors are not strong enough. Moreover, it turns out that with a simple swing leg control policy, retracting the leg with constant angular acceleration, both goals (optimizing mechanical demand and energy efficiency) could be met at once.

7.2 Bioinspiration

We are inspired by the robust and efficient running of animals. Guinea fowl, for example, locomote highly agile, robust and efficient in natural environments (uneven terrain). We want to identify control policies that make running legged robots perform as proficiently as animals like guinea fowl.

Our strategy is to exploit results from experiments that have been conducted by Blum etal [3] on guinea fowl negotiating a drop perturbation, and hypothesize policies these birds may follow during running. The experimental setup they used is shown in figure 7.1.

The results suggest that the leg touch-down angle may be the main parameter that guinea fowl control during flight phase. Furthermore, force data show that leg peak forces and axial impulses are nearly constant during level running and in the presence of a drop [3].

7.3 Methods

In this section we describe the model that we use in this study and our proposed control policies. We use the spring-loaded inverted pendulum (SLIP) model (section 7.3.1) as the model for our running robot, and our hypothesized control policies (section 7.3.2) will be applied on this model during running. We assume the system is running on level ground and without any prior information, an unknown disturbance in the ground occurs. Each control policy regulates an objective function (section 7.3.2) to handle the disturbance.

We focus on step-down disturbances through all of our simulations because the only challenge for step-up disturbances is a geometric constraint between the toe and the ground that may lead to a stumble or a fall. Once the geometric constraint for step-up disturbances is solved (by changing the length of the swing leg and adjusting the leg angle accordingly), an equilibrium gait can be obtained without suffering leg force or work increase. We will discuss this case more in stability analysis section (section 7.5.1) and in the discussion section as well.

7.3.1 Model

We consider the spring-loaded inverted pendulum (SLIP) [39, 100], because the passive model of the spring-mass robot is similar to the SLIP model. The SLIP model is a well-known template for studying legged locomotion [40]. This model is based on the ubiquitous center of mass trajectory that animals have during running. Both humans and birds can deviate from SLIP dynamics for very large disturbances; yet, numerous studies [101, 102, 92, 4, 43, 103, 104] have investigated human locomotion in response to terrain perturbations and found that humans follow SLIP like behavior for a range of disturbances. It should be noted that animals and actual spring-mass running robots have leg actuators in series with a spring (figure 7.2) to compensate for the energy loss due to friction and impacts. However, the mechanical energy generated/dissipated by the motor is low, and thus the system can be accounted as a passive conservative SLIP model. Because the model is passive during stance phase we do not need the leg motor in our simulation, but its existence can not be ignored. Therefore, we keep the leg motor locked (zero mechanical work) to have a conservative system (SLIP-like) and consider a criteria for the required electric energy.

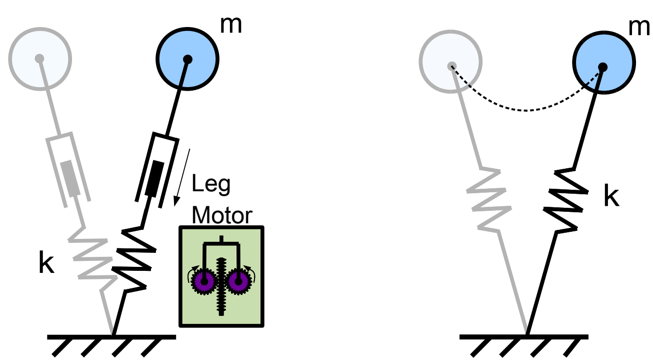

Figure 7.2: left: The model of the robot with the leg motor. The reason of the leg motor existence is to add energy into the system when some energy is lost due to impact or friction. Here, this motor is kept locked (zero mechanical energy) to provide the equivalent conservative SLIP model that is shown in the right.

During flight phase of running the CoM describes a ballistic curve, determined by the gravitational force. Therefore, the only leg parameters that can be controlled during the flight phase are the landing conditions for the upcoming stance phase. The transition from flight to stance occurs when the landing condition $y = L_0 \sin(\theta_{\mathrm{TD}})$ is fulfilled. During stance phase the equation of motion for a passive SLIP model is given by

$$m\ddot{\boldsymbol{r}} = k_{\mathrm{Leg}} \left(\frac{L_0}{r} - 1 \right) \boldsymbol{r} - m\boldsymbol{g},$$

with $\boldsymbol{r} = (x, y)^T$ being the position of the point mass with respect to the foot point, r its absolute value and $\boldsymbol{g} = (0, g)^T$ the gravitational acceleration, with $g = 9.81\,\mathrm{m/s^2}$. Take off occurs when the spring deflection returns to zero. The system is energetically conservative and due to the massless leg there are no impact or friction losses in the system.

The model was implemented in Matlab (R2012a, Mathworks Inc., Natick, MA, USA). To accomplish the simulations, following properties for the robot (table 7.1) were assumed.

Table 7.1: Properties of the spring-mass robot

Parameter	**Description**	**Value**
m	robot mass	$38.0kg$
k_{leg}	leg spring stiffness	$3900\frac{N}{m}$
v_{0x}	initial horizontal velocity	$3.5\frac{m}{s}$
h_0	initial CoM height	$57cm$
δ_{gnd}	ground disturbance	$-10cm$

7.3.2 Proposed control Strategies

Inspired by the running behavior of birds mentioned in section 7.2, we propose three swing leg control policies. We focus on flight phase control policies because, contrary to stance control, we can theoretically do no work and still control the gait. Therefore, the controllers are economically efficient. Leg angle during flight is the only parameter that is changed in all three proposed control policies. Each policy controls the trajectory of the leg angle as a function of time $\theta(t)$ (or vertical velocity) such that its objective function is regulated in the upcoming passive stance phase. The objective function for each policy is i) the leg peak force, ii) the axial impulse, or iii) the leg actuator electric work. Therefore, each control policy adjusts the leg angle during flight at each instant to keep its objective function the same as in the previous step. When there is no ground height disturbance (level running), all control policies result in equilibrium gait.

We assume that our model has no information about the location and the size of the drop perturbation, and the leg angle is adjusted continuously starting at the instant of the expected touch down in anticipation of ground contact. Therefore, on flat ground, equilibrium gait is obtained. In the presence of a drop, however, the leg angle is adjusted at each instant such that the objective function is regulated in the subsequent stance phase. It should be noted that no control is applied during stance, which is purely passive.

7.3.2.1 Constant peak force policy

The first proposed control strategy is to regulate the peak force during running. The constant leg peak force control policy adjusts the leg angle during flight such that the resulting leg peak force during stance of any drop step remains the same as for level running. This control policy allows for running robots to operate at their maximum capacity on even terrain and relinquishes the need to reserve some of the mechanical capacity, motor torque and structural strength for the drop step, and hence yields to lighter and more efficient robots. Experimental data show that running birds maintain nearly constant peak forces during running and in the presence of a drop ([3]). It should be noted that the controller does not need any information about the size and location of the drop (minimal sensing), since the leg angle is adjusted continuously during the flight phase such that the leg peak force gets regulated.

In the presence of a drop, the leg angle retracts towards the ground. Contrary to equilibrium gait policy, as indicated in appendix 7.7, constant peak force policy always retracts the leg to fulfill its objective function. This behavior helps to reach the ground sooner and hence prevents the vertical velocity from increasing further. The reason that the leg is retracted before hitting the ground in this control policy is as follows: As the robot falls, the vertical velocity of the CoM increases and consequently the velocity vector rotates towards the leg. To avoid an increase of the peak force, the angle between the velocity vector and the leg direction needs to be increased. To increase this angle, the leg has to be retracted even faster than the rotation of the velocity vector towards the leg.

7.3.2.2 Constant axial impulse policy

The axial impulse is another objective function that we propose to be regulated during running. We chose the axial impulse, because this function considers both leg force and leg work at the same time (our two goals), maintains consistent energy storage in the spring, and is also able to reproduce the observed animal behavior. The constant leg impulse control policy provides the same axial impulse for the drop step as during level running by adjusting the leg angle during flight. This control policy - like the constant peak force control policy - retracts the leg at the presence of a drop perturbation, regulating the axial impulse to be the same as during level running.

The mathematical formula for the axial impulse is:

$$I = \int_0^{t_s} F \, \mathrm{d}t,$$

where, F is the force in leg direction and t_s the stance time.

7.3.2.3 Constant leg work policy

Our third proposed control policy, constant leg work policy, directly targets the efficiency of the system. The motivation for this objective function comes from observation from animals running on natural environment and still they are very efficient.

It should be noted that the connection of muscles and tendons in animals is similar to the connection of a motor in series with a leg spring for running robots. Although the whole system remains energetically conservative and the generated/dissipated mechanical work is zero, the leg actuator requires electric energy to hold a fixed position.

To regulate the electric work for this control policy in the drop step, the leg angle is adjusted such that the electric energy of the leg actuator is the same as for level running. The consumed electric energy to keep the motor locked during the stance phase is the integral of the power over time

$$EW = \int_0^{t_s} \|P\| \,\mathrm{d}t$$

Since the power in the electric motors is equal to $P = V \cdot I$, and $V = R \cdot I$, by considering the relation between the torque and current in electric motors, the required electric energy can be obtained. It should be noted that from the robotics point of view, when negative mechanical work is generated, it should be treated differently because of the energy loss in the system. Since in this study the leg motor is kept locked during the stance phase, no negative work is produced. Therefore the consumed electrical energy is proportional to the integral of the torque squared over stance time. We use this integral as the criteria for the actuator electric work. The mathematical formula for this criteria is defined as the following function which has been used as the cost function for optimization problems in other studies [105, 106, 107]:

$$W = \int_0^{t_s} F^2 \,\mathrm{d}t$$

Here, W is the work criteria that is proportional to the consumed electric energy to keep the leg motor locked. The leg force is shown by F and the stance time is t_s. This control policy that regulated the actuator electric energy- like the two previous control policies - retracts the leg in the presence of a drop to keep the leg actuator work constant and consequently, like before, the leg reaches the ground sooner because of the steeper leg angle at the time of the touch-down. It should be noted that the required energy for the swing leg is not significant because the SLIP model has a massless leg (and hence the robots that are designed based on this model have very light legs and the motors to move these light legs have small inertias), and consequently no force and energy are needed for the leg rotation (or very small for real world robots).

7.4 Results

In this section we investigate, in simulation, the success of the control policies in the presence of a hidden drop step, and then compare the three proposed control policies against the equilibrium gait policy (see Appendix) and against each other. Since the system follows its passive dynamics during stance, the difference in the behavior of the system for each policy comes only from the different touch-down angles.

As figure 7.3 shows, the overall shape of the CoM trajectories during the drop step are very similar for the three proposed control policies and clearly different from the equilibrium gait policy. In this figure the CoM trajectories of the step before the drop and the drop step itself are shown. Because the robot does not have any information about the disturbed step, the step before the drop is the identical to level running. All three control policies could successfully pass the drop step, and the robot did not fall. The constant force control policy causes the model to touch the ground slightly sooner than the other two policies, and hence results in a a lower CoM height and less vertical velocity.

The CoM trajectories in figure 7.3 imply that the robot accelerates horizontally in the drop step for all three of the proposed control policies, while for equilibrium gait policy the robot maintains the same forward speed as before. It should be noted that, although part of the potential energy of the system is redirected into horizontal kinetic energy, since the velocity contributes quadratically to kinetic energy, the resulting horizontal velocity after take-off does not increase drastically..

The leg force profiles are shown in figure 7.4. The leg peak force in the drop step for equilibrium gait policy increases by 45% compared to level running, while for the proposed control policies it remains nearly constant. For both constant impulse and constant work policy, the leg peak force increases slightly.

The axial impulse decreases slightly in the drop step for both constant peak force and constant actuator work policy (figure 7.5), but increases by 60% for equilibrium gait policy.

Figure 7.6 compares the efficiency of the control polices based on required electric energy. The constant axial impulse policy requires 7% more electric work for the drop step than during level running, while the constant peak force policy needs the least electric energy in the drop step (about 5% less than during level running). Whereas the proposed control policies require nearly the same amount of electric energy in

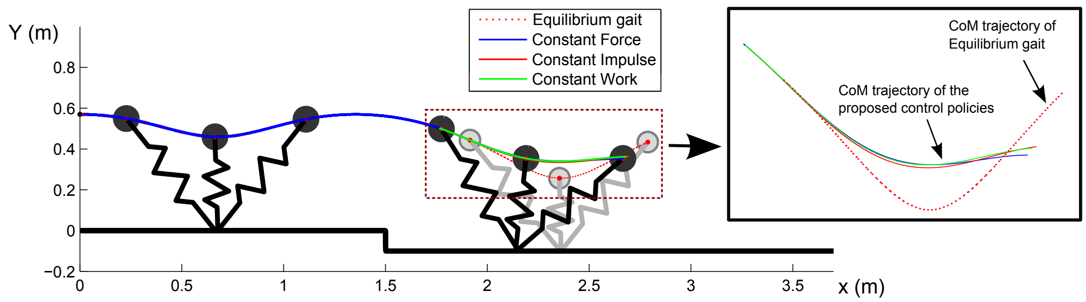

Figure 7.3: CoM trajectories of the robot subjected to the three proposed control policies and equilibrium gait control policy. For the proposed control policies the height of the CoM is lower at take-off respect to touch-down and equilibrium which implies that the system would have higher forward speed at take-off. This is the same behavior that we observe from animals.

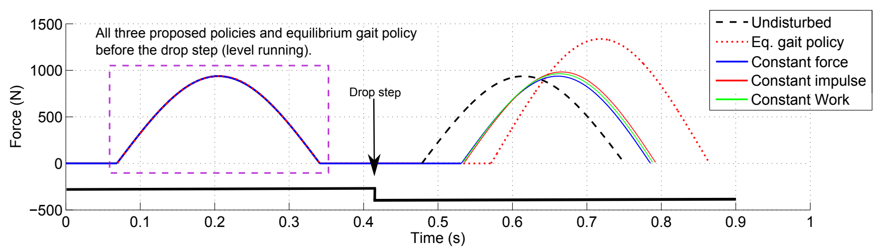

Figure 7.4: Axial force profiles for the three proposed control policies and the equilibrium gait control policy and undisturbed situation. The peak force in equilibrium gait control policy increases about %45 respect to the undisturbed peak force. The beginning of the force profiles show that the equilibrium gait policy reaches the ground the last.

the drop step as during level running, the required electric energy for the equilibrium gait policy in the drop step is more than 200% of what is required for level running.

Figure 7.7 shows that the general behavior of the system with the proposed control policies is consistent for different leg stiffness and drop heights. The system can recover from higher drop heights when the leg stiffness is greater, which means the robustness of the system increases for these control policies with increasing the

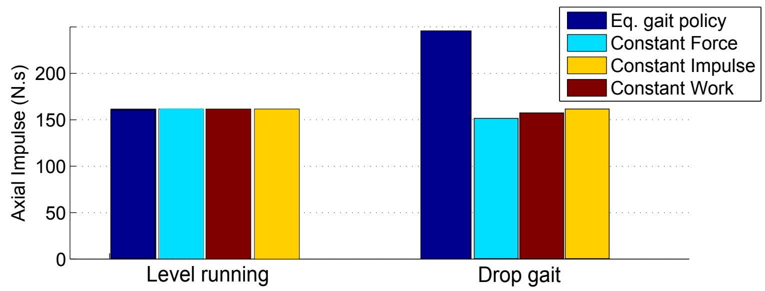

Figure 7.5: Axial impulse in the leg during the stance phase for level ground and drop step. The axial impulse for drop step with equilibrium gait control policy is much higher than the level running. For the constant peak force and constant work policies, the axial impulse in drop step decreases a little bit respect to the level running.

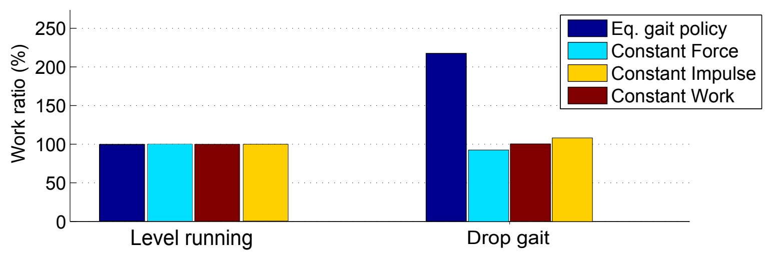

Figure 7.6: Actuator electric work criteria to keep the motor locked during the stance phase. The required work for drop step with equilibrium gait control policy is much higher than the level running (more than 2 times), but the required electric work with constant peak force control policy is nearly the same as level running.

leg stiffness. For the peak force control policy, as an example, the CoM trajectory trends of the system for different drop heights are shown in figure 7.8.

A comparison of the touch-down angles for each control policy is shown in figure 7.9. This figure qualitatively illustrates how the control policies choose leg angles through a range of vertical velocities. In this figure the proposed control policies are depicted in the peak force, impulse and leg work contour lines. Moving along each

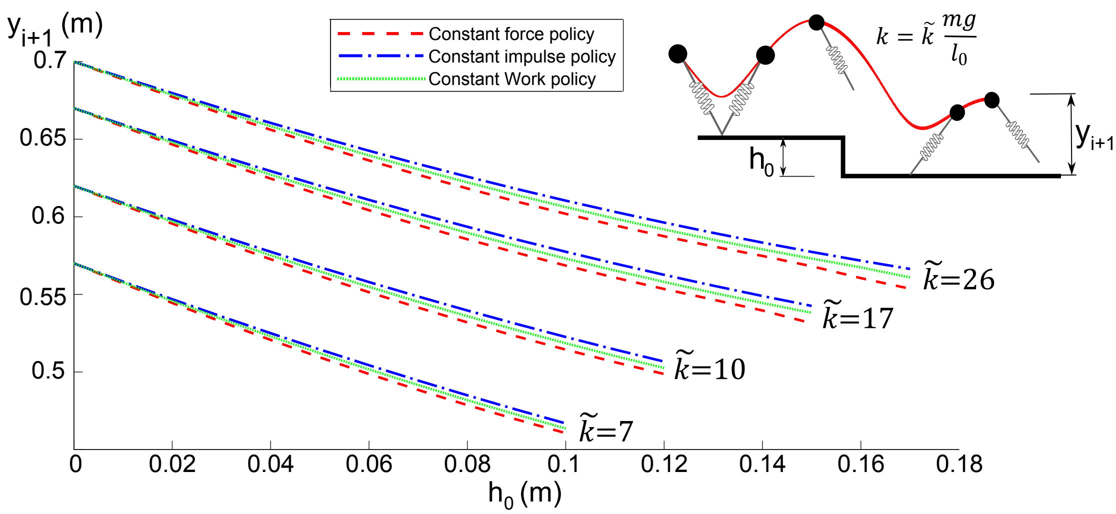

Figure 7.7: The effect of the leg stiffness and drop height on the behavior of the system with the proposed control policies. The behavior of the system is consistent for different leg stiffness and drop heights.

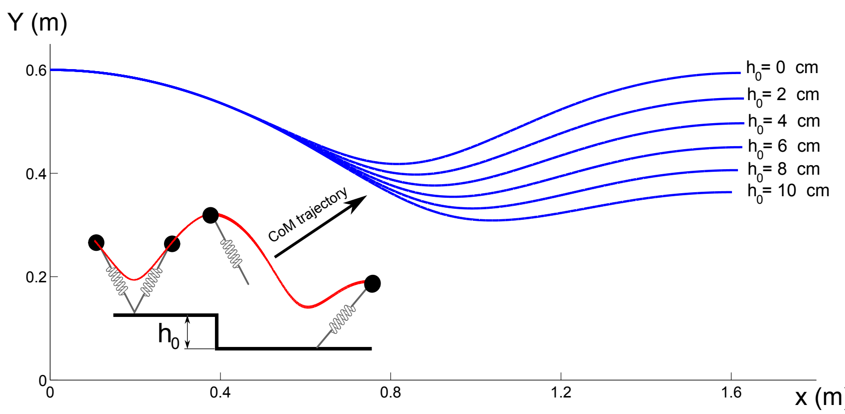

Figure 7.8: CoM trajectory trend of the system with different drop heights. In animals running, the same behavior for the CoM trajectory is observed [3]

contour line means following the corresponding control policy. During level running, all three proposed control policies and the equilibrium gait policy exhibit the same behavior, illustrated by the gray big circle in the figure. The small colored circles show the touch down conditions of the robot following each of the control policies in the drop step. As the vertical velocity increases, the contour lines diverge from each other, which implies a more different behavior of the system for each control policy in larger drops.

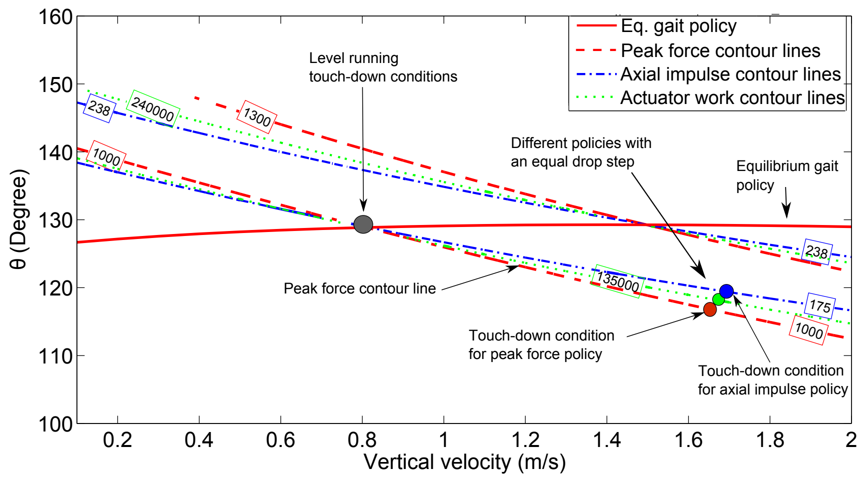

Figure 7.9: Contour lines for leg peak force (red), axial impulse(blue) and leg actuator electric work(green). The big gray circle shows the level running touch down condition and the small colored circles show the touch down angle at the drop step following each of the control policies. Since the contour lines are close to linear respect to vertical velocity (or time), a constant angular rate for the leg retraction would be a good approximation for the policies.

The shapes of the contour lines in figure 7.9 are nearly linear for small changes in vertical velocity. To study the shape of the contour lines further, we focus on only on the peak force contour lines, shown in figure 7.10. This figure shows the desired leg angle trajectory, which is a peak force contour line, and two fits (linear and quadratic function) for the desired leg angle trajectory. The linear fit of the desired leg angle trajectory drifts along the desired curve, and this drift gets smaller with increasing forward speed. The quadratic function, however, is an excellent fit for the leg angle trajectory.

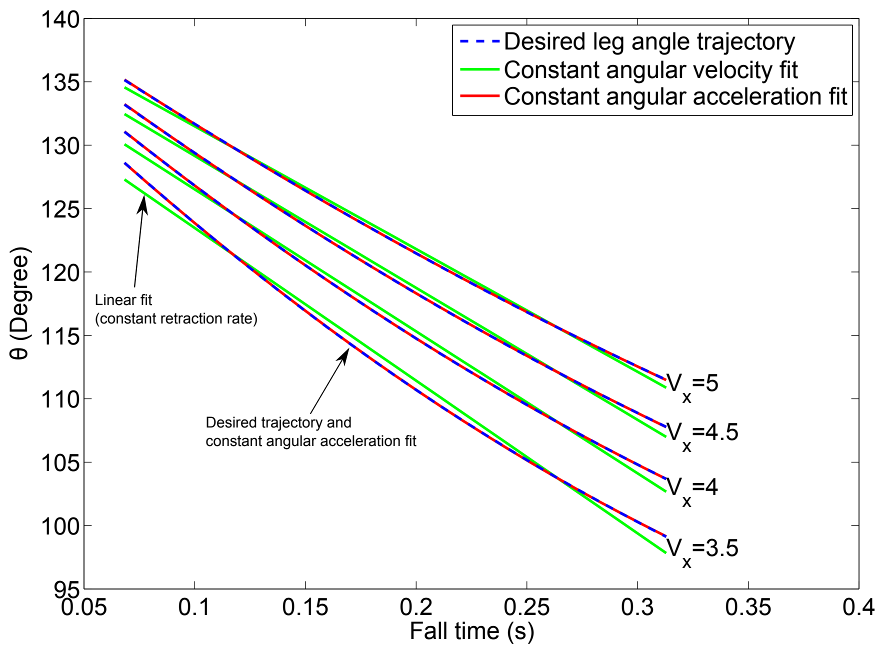

Figure 7.10: Desired and fit functions for the leg angle trajectory subjected to the constant peak force policy. The blue dashed lines are the desired leg angle trajectory and the green solid lines and red solid lines are linear and quadratic fit respectively. The constant angular acceleration fits the exact desired trajectory very well. As the forward speed increases, the constant retraction rate approaches the exact desired trajectory. The value for the retraction rate can be obtained from the slope of the contour lines.

7.5 Discussion

All three proposed control policies produce nearly identical leg angle trajectories, are clearly distinct from the equilibrium gait policy [98, 5], and successfully negotiate the drop step while achieving their specific objectives. The policies were hypothesized based on their relation to pragmatic locomotion goals such as safety and energy efficiency. They are mathematically related, and as such might be expected to generate similar behaviors; however, the spring-mass model can be sensitive to small policy changes, so it was unclear how they would relate to one another and the equilibrium gait when implemented. These results show that a single policy achieves both pragmatic locomotion goals of safety and efficiency at the same time.

Results show that the actuators require much more electrical energy in the drop step to maintain equilibrium gait than by using one of the proposed control policies. The 45% increase of the leg force may lead to serious structural damage to the leg, and even if the structure of the leg can sustain this new force, the motors and electronics may not be able to provide that much force and hence lead to falling. For the proposed control policies, on the other hand, the internal demands remain nearly the same as before. For example, the leg peak force increases only slightly (about $2 - 3\%$) for both constant impulse and constant work policy, and, of course, remains constant for the constant peak force policy. It should be noted that the electric energy that we consider here is to keep the leg motor locked and is due to the resistance of the electric motor. When there is need to do some mechanical work during the stance (which is not considered in this study), that work should be added to the resistance electric work.

The asymmetric shapes of the CoM trajectories resulting from the proposed control policies during the drop step imply that the robot accelerates horizontally in the drop step for all three proposed control policies. This is consistent with the behavior that animals show in the drop step [3]. However, with the equilibrium gait policy, the robot maintains the same forward speed during running. The increase of the horizontal velocity in the drop step for the proposed control policies is due to the conversion of potential energy (of the drop height) into kinetic energy. Since the velocity contributes quadratically to the kinetic energy, the resulting horizontal velocity does not increase significantly, especially for high forward speeds. For example, if the initial forward speed is $5m/s$, after redirecting the added potential energy from falling into a $20cm$ drop into horizontal velocity, the resultant forward speed will be $5.4m/s$. This means the forward speed increases only by 8% after falling from $20cm$ height.

In this study, we focused on the mechanical and electrical limitations of the actuators that facilitate the control policies. Other preferred requirements like the next stride apex height and apex horizontal velocity are of second priority for the control policies and can be determined similar to the dead-beat control strategies [84, 98], or the Raibert controller [108].

Since the contour lines in the leg angle (θ) - fall time (t) plane (figure 7.9) are nearly linear, retracting the leg with a constant angular velocity, determined by the average slope of the contour lines, would be a simple implementation. The value for the leg retraction rate agrees with Karssen et al. [99]. Further investigation of the contour lines reveals that leg retraction with a constant angular acceleration is a more accurate fit for the swing leg trajectory, but for high forward speeds ($> 6m/s$), the angular leg trajectory with constant angular velocity is close enough. To cover all speeds, however, the constant angular acceleration fit is the better choice.

The proposed control policies lead to retraction of the leg before the touch-down. This behavior is in general in agreement with the behavior of the ground speed matching control technique [97, 44] that requires the velocity of the toe perpendicular to the leg length remains zero at the time of touch-down. In figure 7.11 the comparison of the touch-down angle between the ground speed matching and the constant peak force control policy proposed in this study is presented. Since the ground speed matching policy determines the angular velocity of the leg ($\dot{\theta}$) at each time, to find the leg angle trajectory ($\theta(t)$) in this control policy, $\dot{\theta}$ should be integrated and hence a reference point is needed. It is assumed that the reference point for ground speed matching control policy corresponds to level ground running (equilibrium gait) which in this figure has falling time equal to $t = 0.1s$. As can be seen in figure 7.11, both policies require leg retraction for the swing leg, meaning that the constant peak force policy also helps in reducing the effect of the impact perpendicular to the leg length. Moreover, for the forward speed equal to $V_x = 3.5\frac{m}{s}$, the angular velocity of the constant peak force policy and the ground speed matching strategy are nearly the same which suggesting that implementing the constant peak force control policy matches the ground speed matching strategy for small ground drop steps, but as the forward velocity increases, the constant peak force policy deviates from the ground speed matching.

The objective functions that we chose for the policies are of great technical importance from a roboticist's point of view. We tried to find an exact map that regulates our objective functions, but surprisingly the map function happened to be simply a constant leg angular acceleration. For short flight times (falling from small drop

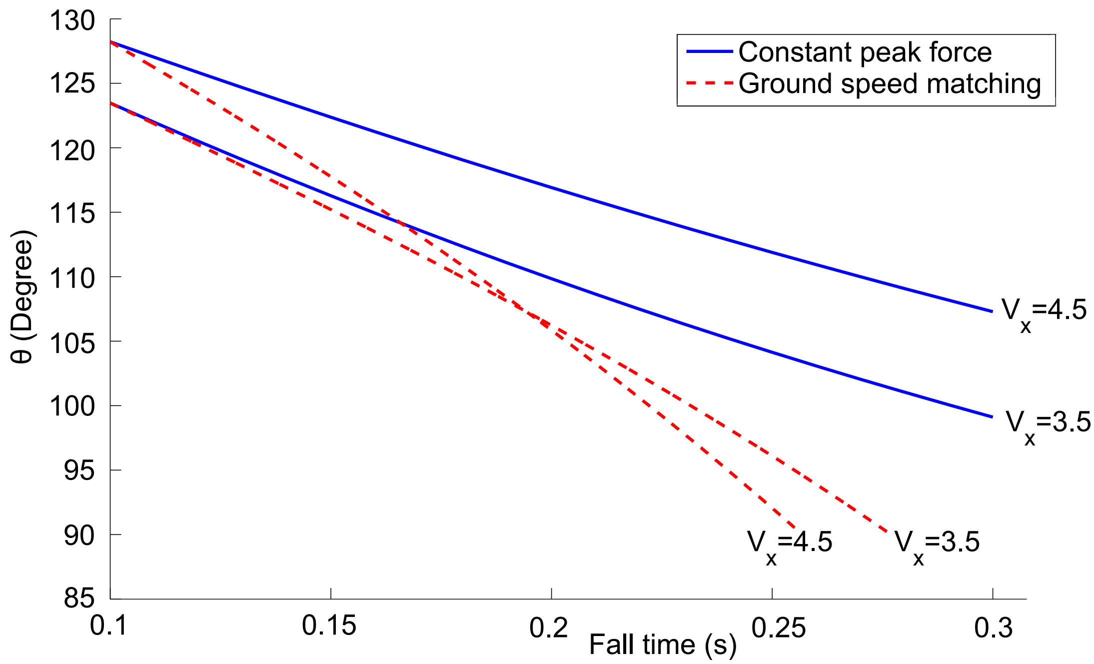

Figure 7.11: The comparison of the touch-down angle between the ground speed matching control policy and the constant peak force control policy. The discrepancy between the touch-down angles increase with falling time as the horizontal velocity of the system increases.

heights), constant leg angular velocity is a good approximation for this map. The outcomes agree with what Karssen et al. [99] found for the optimal swing leg retraction rate when the peak force is considered as the objective function. But contrary to their work, we did not limit our policy to a constant leg retraction rate.

The difference between the proposed control policies and the equilibrium gait policy increases as the forward speed increases. To provide steady state running for high forward speeds, using an equilibrium gait controller, the leg should protract in the falling half of the flight phase (see Appendix), but for all three proposed control policies the leg is retracted to reach the ground. The leg protraction in the equilibrium gait policy postpones the instant of touch-down and consequently increases the difference of the proposed control policies and the equilibrium gait policy. Karssen et al. [99] also reported that the difference between optimal swing leg retraction rate for disturbance rejection and other objective functions (including the leg peak force) increases with increasing forward speed.

The desired leg angle trajectory for each of the proposed control policies is different with the two-phase constant leg retraction rate in the clock-driven model that was proposed for robots like RHex [61] [62] [109]. In each of our proposed control policies, as well as in the clock-driven model, after the time of the expected touch-down, the leg trajectory follows a different trajectory function. However, in the policies proposed here, instead of a constant retraction rate, a constant angular acceleration is applied to the leg. More importantly, contrary to the clock-driven method, the leg control stops at the beginning of stance phase (the three proposed control policies are purely passive in stance phase). The clock-driven method is a simple bio-inspired technique, but it does not consider the structural or electrical capacity of the leg, and may therefore lead to failure during stance.

By using a new type of return map, the proposed control policies and their limitations can be depicted visually. In this new type of return map, contrary to return maps with constant mechanical energy [4, 5] (figure 7.12-a), the horizontal velocity is kept constant (figure 7.12-b). In a return map with constant energy, any change in the ground level alters the energy of the system and therefore, flight phase control policies with varying ground level can not be depicted on the map (figure 7.12-a). In the return map that we use here, instead of the mechanical energy, the horizontal velocity is kept constant (figure 7.12-b). The key difference of these two return maps is: the axes in the return map with constant mechanical energy represent the apex heights relative to the original ground level, but in the return map with constant forward speed, the two axes are the apex heights relative to the upcoming stance phase ground level. In figure (7.12-b), y_i represents the apex height relative to the upcoming stance phase. Therefore, any change in ground height is interpreted as the change in y_i (for example, if there is a 10cm drop step, the apex height increases by 10cm). The vertical axis of this graph (y_{i+1}) is the apex height relative to the upcoming stance ground level.

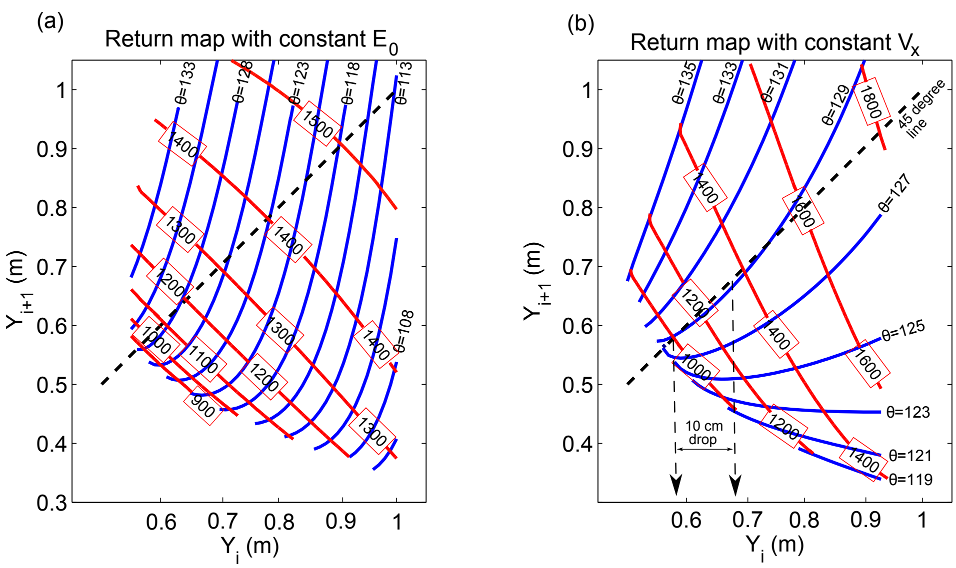

Figure 7.12: Return map with constant mechanical energy ([4, 5]) (a) and return map with constant horizontal velocity (b). There are two sets of contour lines: leg angle (θ) contour lines [Degree] are in blue and axial peak force contour lines [N] are in red.

When the constant peak force control policy is implemented, the leg angle is adjusted such that its return map is parallel to the axial peak force contour lines.

Using the constant forward speed for this map allows us to interpret the change of the ground level as a change in the apex height. Therefore, contrary to the conventional return map [4, 5], we do not need to change the graph. For example, if the apex height for steady state running is $57cm$ then the peak force would be $1000N$. Now, we assume the drop height is $10cm$; therefore, the apex height including the drop step would be $67cm$. To follow the constant peak force policy, the leg angle should be set to $\theta = 121°$ at the moment of touch-down, and the passive dynamics of the system will result in the same axial peak force as before ($1000N$). It should be noted that there is no need to know the ground level in advance, since the leg angle is continuously being updated expecting to reach the ground any moment. To achieve steady state running (equilibrium gait), the controller should follow the 45° line, which requires the touch down angle to be about $\theta = 129°$. Consequently, the peak force in the leg increases to about $1350N$ (35% increase). We also notice that although the constant peak force policy prevents the peak force from increasing, it has a limit for the maximum drop height that can be handled by this control policy. For example, to keep the peak force equal to $1000N$, the maximum drop height is $10cm$ (the end of the $1000N$ contour line). This implies that for deeper drops, the peak force has to increase to prevent the robot from falling or additional control inputs are required, such as a change in leg length.

Because of the negative slope of the force contour lines in the return map, the next apex height decreases with increasing drop height. This implies that the system gains horizontal velocity due to the transformation of potential energy into kinetic energy. This behavior is confirmed by simulations and can also be observed in animal experiments [3]. We know that for a successful running gait, the subsequent apex height is an important factor that also needs to be considered. The subsequent apex height after the drop step should be greater than a predefined threshold, and the flight phase should be long enough to allow the leg to be placed on the ground for the next stride. Therefore, based on the geometry of the leg, the negotiable drop height is limited by the controller. However, if the controller was allowed to change the leg length of the subsequent step, another option would be to continue running with a shorter leg length. For all these cases, the return map with constant horizontal velocity visualizes the limitations and can help designing an appropriate scenario for the control policy.

The findings of the return map that we presented for constant peak force policy, can be easily extended to axial impulse or leg work. In these cases, only the peak force contour lines in figure 7.12 would change to the impulse or leg work contour lines in the range of $175N.S$ to $300N.S$, and $135000N^2.S$ to $350000N^2.S$, respectively. The overall shape of the impulse/leg work contour lines are similar to the peak force contour lines in figure 7.12.

It should be remembered that all three proposed control policies adjust the leg angle during flight, and the system is assumed to be conservative. Therefore, to continue running on ground with a permanent drop step, the robot should dissipate the gained kinetic energy. In this case, a stance phase control would be required to bring the robot back to the preferred forward speed, or the robot would continue with a higher horizontal velocity. A simple and bio-inspired stance phase technique that was proposed by Schmitt et al. [54] and investigated more by [88] and [56] could be used to dissipate the gained energy. Since the energy that requires dissipation is only that due to the drop perturbation, the cost of dissipating this energy in subsequent steps is the same across all control policies compared. If the energy were dissipated within the perturbed step, this could lead to different energetics for different policies that require energy dissipation while meeting other mechanical objectives. The equilibrium gait policy requires high force, and the proposed control policies have relatively short stance periods, and these factors could influence the cost of dissipation depending on motor/muscle characteristics. By allowing the energy dissipation to occur in subsequent steps following the perturbation, the energy can be dissipated in the energetically optimal period of stance.

The simulations and the results presented in this work are designed for unexpected step-down disturbances in the ground level. For the case of step-up disturbances, since the touch-down occurs early, the vertical velocity of the CoM has not reachined its prior peak values, therefore an equilibrium gait can be obtained with lower values for the leg force or work (in section 7.5.1 it is explained more on the return map as well). The height of the step-up disturbance that can be handled depends on the length of the leg. To increase the control authority in handling the step-up disturbances (running over larger step-up disturbances), other scenarios (like shortening the leg length during the flight phase) can be used that are not in the scope of this study. As an example, during the first half of the flight phase (CoM going upward) the leg can be getting shortened (to provide enough space for the possible obstacles) and during the second half of the flight phase, as the leg length is being increased to its nominal length, the leg angle is adjusted accordingly to provide an equilibrium gait at the moment of contact with the leg length at that moment.

7.5.1 Stability analysis of the proposed control policies

In this section, we investigate the stability of the proposed control policies and compare them with the stability of the equilibrium gait policy. To give this comparison, we use the return map with constant energy level (figure 7.12) in more details for each case. More information about the return map with constant energy was presented earlier and can be found in [4, 42, 5]. For the conservative SLIP model, since the energy level is constant, the only variable of the system would be the apex height at each stride. Therefore, the perturbations in stability analysis are applied to the apex height while the whole energy of the system is kept constant. For more details about the stability analysis of the SLIP model running refer to [4, 43, 5, 41].

We first start with investigating the stability of the equilibrium gait policy. Figure 7.13 shows how the perturbation in the apex height changes the location of the states on the return map. The equilibrium gait policy controls the states to move along the 45 degree line to always have a symmetric trajectory. For example, if the level ground running is shown by point A in figure 7.13, after the perturbation, the system would be on state B along the 45 degree line. Since this policy always keeps the states on the 45 degree line, the next state has the same apex height as the perturbed state which implies neutral stability. Figure 7.14 shows the CoM trajectory of the perturbed and unperturbed systems with this control policy. Because of the neutral stability of the equilibrium gait policy, the perturbations do not vanish and the system continues running in the new symmetric trajectory.

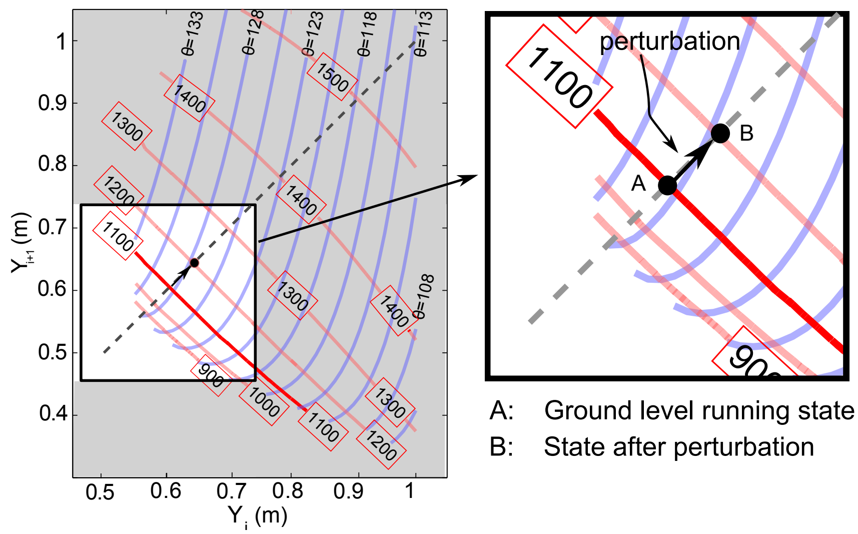

Figure 7.13: The return map with constant energy. After the perturbation, the location of the state changes from point A (ground level running) to the perturbed state on the 45 degree line (point B) and the system continue running in this state. It shows the neutral stability of the equilibrium gait policy. The red curves are leg peak force contour lines and the blue curves are touch-down angle contour lines.

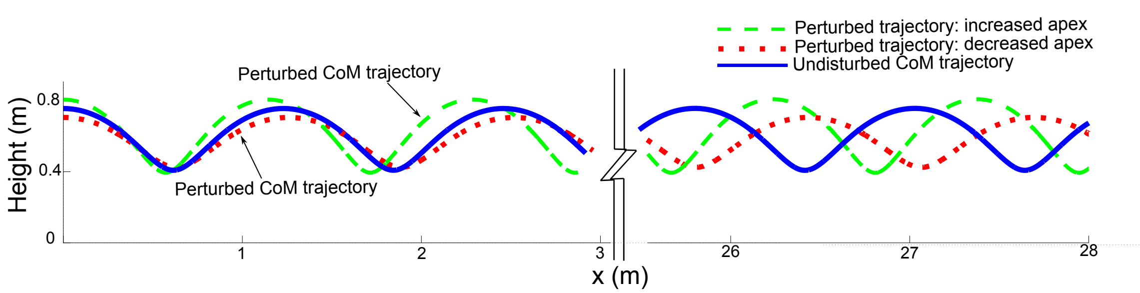

Figure 7.14: The CoM trajectory of the unperturbed and perturbed SLIP model with equilibrium gait policy. Because of the neutral stability of the equilibrium gait policy, the system remains in the perturbed state.

Figure 7.15 shows the stability of the proposed control policies (constant peak force policy for example). Like before, we assume the system is running on the level ground at state A. After the perturbation, the apex height goes to state B_1 which has the same leg peak force (it moves along the peak force contour lines). For the next step, the system goes to state B_2 to keep the leg peak force constant and then returns back to state B_1 and so on. The CoM trajectory of the system in this case is shown in figure 7.16. In this case, the CoM trajectory is periodic in two steps instead of one step in equilibrium gait policy and like equilibrium gait policy it has neutral stability.

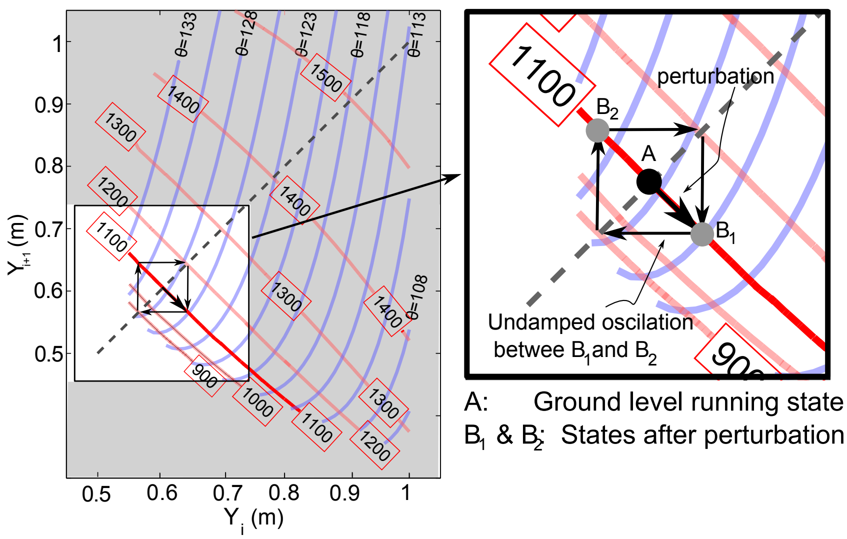

Figure 7.15: The return map for constant peak force policy. After the perturbation, the system oscillates between states B_1 and B_2.

Due to the negative slope of the leg peak force contour lines, the next apex height after the drop step is lower than the drop step apex height. It implies that after the drop step the system can continue in a new equilibrium gait with a lower leg peak force, impulse and leg work. The return map in this case is shown in figure 7.17. After the perturbation, the system goes from state A (ground level running) to

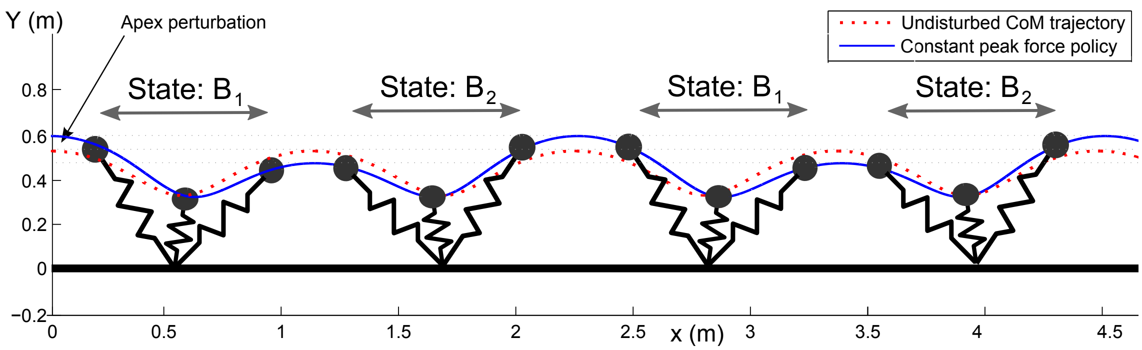

Figure 7.16: The CoM trajectory of the system going from state B_1 to state B_2 and return to B_1 and so on.

state B_1 along the contour lines to retain the leg peak force. For the next step, the system can converge to state B (on the 45 degree line) which is an equilibrium state with lower leg peak force. The CoM trajectory of the system in this case is more compatible with the animals data encountering drop step perturbation. The CoM trajectory of the system under drop step-like perturbation (increased apex height) is shown in figure 7.18.

When the perturbation is like a step-up obstacle, the perturbed apex height is smaller than the level running, thus the peak leg forces are lower, and the resulting new equilibrium gait will satisfy peak force limits.

In summary, the proposed control policies, like equilibrium gait policy, converge to new CoM trajectory after the disturbance. When they are used with equilibrium gait policy for after the drop step, the system will continue with a new symmetric CoM trajectory. Assuming the robot keeps the gained energy level, the robot will continue running with a higher forward speed.

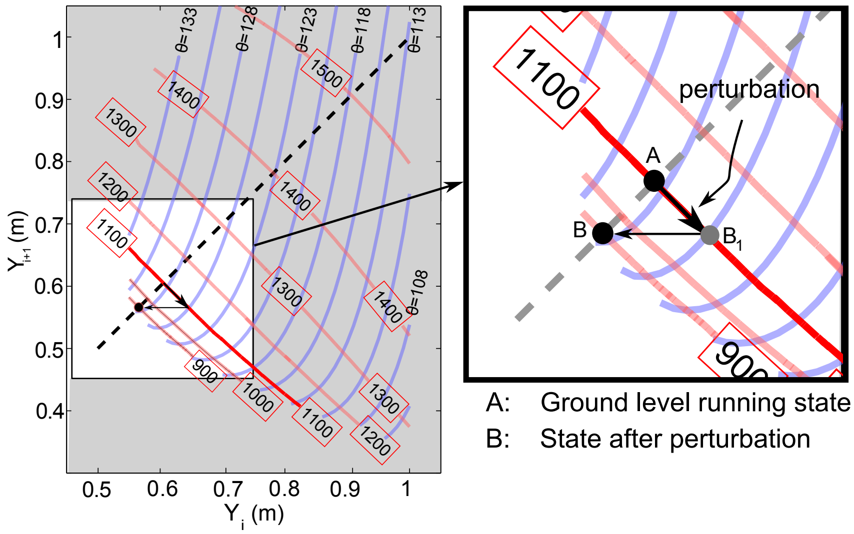

Figure 7.17: The return map with constant energy. After the perturbation, the system goes to state B_1 for one step and then using equilibrium gait policy, it stays at state B.

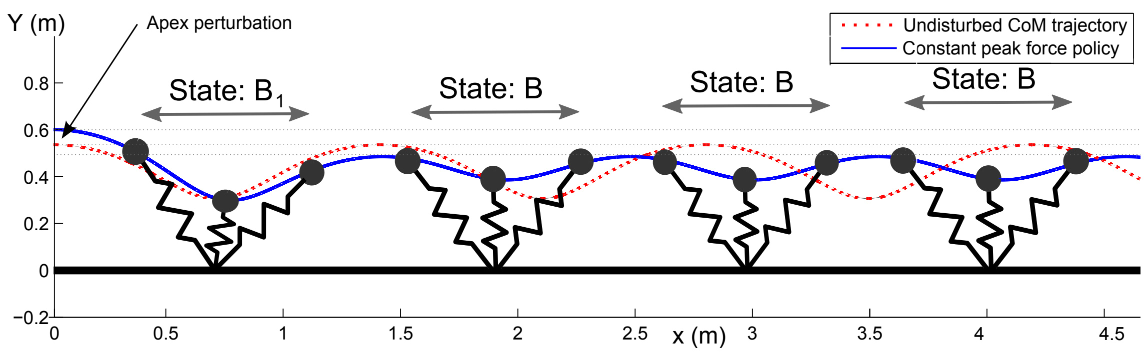

Figure 7.18: CoM trajectory of the perturbed and unperturbed system. After regulating the objective function (peak force here), the system goes through a transition state (B_1) and then stays at a state with lower peak force (B).

7.6 Conclusion and future work

Three flight phase control policies inspired by animal data, but suitable for machines, were proposed and implemented to the model of a spring-mass running robot. The control policies regulate their objective functions that target the mechanical/amperage limitation and electrical efficiency of the system. By using either of these bio-inspired control policies, the safety and efficiency of the robot during running is guaranteed, while their implementation is very easy with minimal sensing requirements.

All three proposed control policies (constant peak force, constant axial impulse and constant leg actuator electric work) successfully negotiated the drop step, and surprisingly resulted in similar behavior of the spring-mass robot. Therefore, by implementing either of these proposed control policies, both goals, damage avoidance and efficiency, would be satisfied.

We showed that a simple leg angular acceleration during the flight phase keeps running safe (avoiding the damage) and efficient. If the drop height is less than 10% of the leg length, a constant leg angular velocity (constant leg retraction rate) would lead to similar results. The value of the leg retraction rate (leg angular velocity) can be derived from the slopes of the leg peak force contour lines in the leg angle-falling time plane. It should be noted that implementing these policies is very easy because the constant angular acceleration for the leg can be provided by constant motor torque ($T = I \cdot \ddot{\theta}$) and since the relation between the motor torque and current is linear, therefore providing a constant current places the toe at the right location at each instant.

For future work we plan to implement these policies on our robot ATRIAS. We found that the amperage limitation is a big concern for electrically actuated spring-mass robots like ATRIAS, and therefore, we will start with the constant leg peak force policy.

7.7 Appendix: Equilibrium gait policy

The equilibrium gait policy ensures that the robot has symmetric CoM trajectories during stance with respect to the vertical axis defined by mid-stance (i.e. touch down and take off conditions are symmetrical). To result in symmetric gait for high forward speeds in the presence of a drop, the leg should protract as the CoM falls in the drop (figure 7.19). This protraction opens more room between the toe and the ground, and consequently leads to higher vertical velocity at the time of touch down. Figure 7.19 shows the leg angle trajectory with respect to falling time for different forward speeds that results in equilibrium gait. For low horizontal velocities, the leg angle function is monotonically decreasing, meaning that the leg should be retracted after apex. For high forward speeds (here $v_x > 3$) the robot should protract the leg in the beginning, and then (after gaining some downward velocity, and if it did not yet touch the ground) should start retracting the leg to provide the appropriate leg angle for equilibrium gait. For human-scale spring-mass running robots, high downward velocity (here more than about 2 m/s, which corresponds to a drop height of about 30% leg length) is not common to be rejected blindly. Therefore, for small to medium drops, the leg would have monotonic behavior. This is interpreted as retraction for low forward speeds, and protraction for high forward speeds as the robot falls.

Karssen et al. [99] also concluded that for high horizontal velocities, the trade-off between disturbance rejection, energy loss, and foot slipping increases. On the one hand side, the leg should be protracted the reject disturbances, but on the other hand, the leg should be retracted to reduce impacts and prevent foot slipping. Moreover, as the robot falls, the protraction increases the distance between the toe and the ground and postpones the contact moment, meantime the vertical velocity increases, and consequently the leg peak force and axial impulse increase even more.

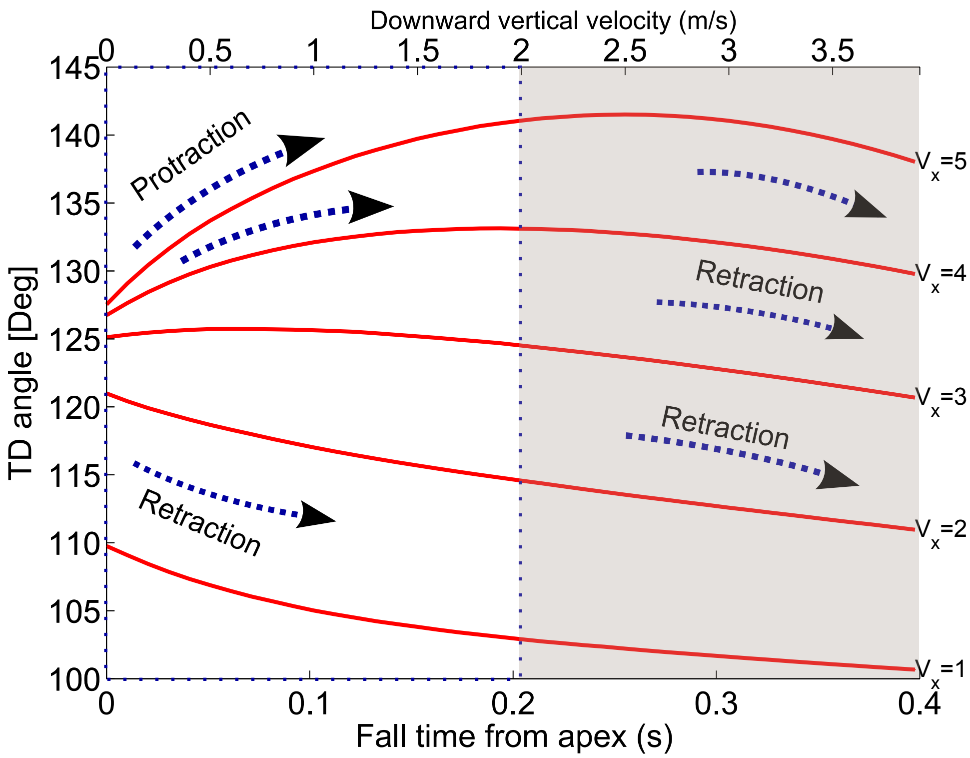

Figure 7.19: The required leg angle trajectory for equilibrium gait policy. For low horizontal velocities, the leg should be retracted as it falls. For high forward speeds (here about $v_x > 3m/s$) the robot should protract the leg in the beginning and then it should start retracting the leg. The shaded area corresponds to deep drops (disturbances more than about 30% of the leg length that is not very common for legged robots to reject blindly.

Chapter 8 – Conclusion

In this thesis, after analyzing the dynamics of the spring-mass model for walking, six control policies have been proposed to stabilize the spring-mass walking robots and one flight phase control strategy has been proposed for spring-mass running robots. The proposed control policies were derived from template, if possible, they were confirmed through anchor and finally stabilized the real robot. The emphasis on the control policies are on the passive dynamics of the system. Stability, robustness, efficiency and damage avoidance are the main goals for the control policies to fulfill. The following general conclusions can be obtained from this research:

- The various types of the equilibrium gaits for walking are like a continuum and can continuously transform to each other.
- Even though deadbeat control policy mathematically exists for spring-mass walking model, the sensitivity of that makes it impractical for real robots. Therefore, before moving on to implement the policy on the full order model, the sensitivity analysis at the level of reduced order model should be checked.
- The idea of self-stability was expanded for spring-mass walking model. Instead of touch-down angle, other possible parameters were targeted and showed that they can stabilize the gait very robustly with low sensitivity to the errors and noises.

- For the control policies that come from template, self-stability characteristic helps the system against the errors due to the difference between the template and the anchor.
- Inspired by feed-forward control policy for running [54], the idea of having stance phase as a feed-forward function to add and remove energy for walking was successfully shown on template and worked well on anchor.
- Inspired from animals' running pattern, it was shown that retaining steady state running is clearly not what animals do during running. Instead, other meaningful objective functions like avoiding damage and/or efficiency seem to be the answer. Surprisingly, both damage avoidance and energy efficiency can be fulfilled with simple implementation strategy (constant angular acceleration for swing leg).

In more detail, the conclusions for each chapter are as follows: In chapter 3, the dynamics of the bipedal spring-mass model was analyzed for walking and the touch-down angle of the swing leg was assumed as the only control input to the system. Three regions in the state space were found: i) the states that can start successful walking gaits, ii) the states that can be reached at the end of walking gaits and iii) the intersection of the two previous sets which is called workspace of the system. The equilibrium points in a constant energy level were found and the relation between them can be visualized by projecting them on the workspace of the system. It was found that the equilibrium gaits are like a continuum evolving as the height of the CoM changes at the Poincare section. The following conclusions can be obtained from the analysis of this chapter:

- The dimension of the workspace in y direction is about $2\Delta_s$ where $\Delta_s = \frac{mg}{k}$ is the static deflection of the spring under the weight of the system.
- The velocity of the system at the Poincare section is maximized for the middle of the workspace where the deflection of the spring is equal to the static deflection (Δ_s).
- The symmetric equilibrium gaits are continuously changing on the $\psi = 0$ axis and forming different types of symmetric equilibrium points.
- Asymmetric equilibrium points are branched from the symmetric axis $\psi = 0$.
- Each equilibrium point can correspond to one or more touch-down angles, but even though two touch-down angles can repeat one equilibrium point at the Poincare section, the gait history is different and only the states at the Poincare section is the same.
- By changing the height of the CoM at the Poincare section, the type of the equilibrium point varies. Bouncier gaits correspond to large height at the right of the workspace and as the height at the Poincare section decreases to static deflection (Δ_s), the trajectory of the CoM becomes flat during the gait and the grounded running gaits are obtained.

In chapter 4, a deadbeat control strategy for the bipedal spring-mass model was presented. Since the system has one control input (touch-down angle of the swing leg) and two outputs (height of the CoM and the orientation of the velocity vector), any arbitrary state can not be achieved in one step. The deadbeat control policy in this chapter shows that two steps are necessary and sufficient to guarantee the stability of an equilibrium point with this control policy. The applicability problem of this strategy for real robots is the sensitivity of the system to the touch-down angles. Since the deadbeat control policy requires the system to go to a transition state before settling down to the desired state, and because of the sensitivity of the behavior to the touch-down angle, the system can not converge to the desired state because it can not be exactly at the right transition state. The following conclusions can be gained from this chapter as well:

- Two steps are necessary and sufficient for deadbeat control of the bipedal spring-mass model.
- The basins of attraction are different for different equilibrium points.
- The deadbeat control policy sometimes is very sensitive to the touch-down angle and this sensitivity makes the transition to the desired state practically very difficult and unlikely.

In chapter 5, four new control policies for the swing leg of the bipedal spring-mass model were proposed and compared with current strategies. The stability analysis of the control policies showed the stability of the proposed policies. The basins of attraction showed that the control policies are highly robust against external perturbations. The applicability of the proposed control policies was shown by implementing one of them on the full order model of the robot as well as our spring-mass robot ATRIAS itself which the control policy could successfully stabilize the robot for walking. Following conclusions can be obtained from the outcome of this chapter:

- All four proposed swing leg control policies i) regulating the touch-down time, ii) regulating the stance leg angle, iii) regulating the CoM horizontal displacement and iv) regulating the step length, outperform the current constant angle of attack control policy and the constant aperture angle control policy that exist for the bipedal spring-mass model.
- State-based control policies stabilize more gaits than time-based control policy.
- The constant stance leg angle and the constant CoM horizontal displacement are similar in stability and behavior. They also show the best performance for the stability and robustness.
- Both the constant aperture angle control policy and the constant step length policy have marginal stability. The constant step length policy can provide larger basin of attraction for the system compared to the constant aperture angle control policy.
- The implementation on the real platform (ATRIAS) confirmed that the proof of concept for the proposed switching policies, is valid on the robot and stabilize the gait.

In chapter 6, a time based feed-forward function was assumed for the stance phase of the bipedal spring-mass model combined with the time-based swing leg control strategy. The feed-forward function varies the zero force leg length of the system during the stance phase and therefore changes the energy in the system. The analysis was performed on the system with and without physical damping in parallel to the spring. The implementation of the feed-forward control strategy on the full order model of the robot showed that this policy can stabilize the full order model with the expected behavior. Following conclusions can be obtained from the results of this chapter:

- The behavior of the systems with damping is faster to converge to the limit cycles than undamped spring-mass systems.
- The bipedal spring-mass model with damping converges to asymmetric equilibrium gaits.
- Both symmetric and asymmetric equilibrium gaits can be achieved for the bipedal spring-mass model without damping.
- Simulation on the full order model showed the validity of the concept for stability and robustness on the model with full details and in the presence of significant noise.

In chapter 7 we considered the leg angle as the only control parameter during the flight phase to control spring-mass running robots. In the proposed control policies we investigated in this chapter, the leg peak force, axial impulse and leg actuator work during stance phase were considered as the objective functions to be regulated by adjusting the leg angle during the flight phase. We found out that by regulating any of these three objective functions, both goals of damage avoidance and energy efficiency would be fulfilled at once. Results showed that implementing these policies in real robots are as easy as implementing a constant angular acceleration for the leg retraction during the flight phase. Furthermore, we proposed a new graph that depicts the behavior of the flight phase control policies in the presence of ground level changes. By the help of this graph, the limitations of the flight phase control policies (like the maximum drop height that can be rejected to have a successful stance phase) can be found. The general conclusions for this chapter are:

- Considering damage avoidance and/or energy efficiency as the primary goals during running is crucial for economically designed running robots and leads to the same behavior that is observed from animals' running.
- When regulating any of the three proposed objective functions (peak force, axial impulse or leg actuator work) during running, both goals of damage avoidance and energy efficiency are fulfilled at once.
- Implementing a constant leg angular acceleration is enough to regulate either of the proposed objective functions (leg peak force, axial impulse or leg actuator work).
- The control policies are feed-forward and there is no need for any external sensing.
- By implementing a very simple constant angular acceleration trajectory for the swing leg, both goals of safety and efficiency are fulfilled.

By the results of this work, roboticists have a better understanding of the behavior of the spring-mass walking and running robots to achieve stable, robust and safe locomotion. It was found that even though deadbeat control is possible for walking in two steps, but the applicability of deadbeat control is questionable due to the sensitivity of that to touch-down angle errors. By the new proposed control strategies in this study for swing leg, stable and robust walking for spring-mass robots are possible with large basins of attraction. For energy management, a simple feed-forward strategy that was proposed in this work can be used to take care of the energy changes that the system experiences during walking on rough ground. For spring-mass running robots the focus of the proposed control policies is damage avoidance in uneven terrain which can be implemented by providing the constant angular acceleration for the swing leg trajectory.

Bibliography

[1] C. M. Hubicki, J. A. Grimes, M. S. Jones, D. Renjewski, A. Sprowitz, and J. Hurst, “Atrias 2.1: Enabling agile biped locomotion with a template-driven approach to robot design,” *International Journal Robotic Research*, vol. to be submitted, 2014.

[2] J. A. Grimes and J. Hurst, “The design of atrias 1.0 a unique monopod, hopping robot,” in *Proc 15th Int Conf on Climbing and Walking Robots (CLAWAR)*, 2012.

[3] Y. Blum, H. R. Vejdani, A. V. Burn-Jeffery, C. M. Hubicki, J. W. Hurst, and M. A. Daley, “Swing-leg trajectory of running guinea fowl suggests task-level priority of force regulation rather than disturbance rejection,” *PLoS ONE*, 2014.

[4] A. Seyfarth, H. Geyer, M. Guenther, and R. Blickhan, “A movement criterion for running,” *Journal of Biomechanics*, vol. 35, pp. 649–655, 2002.

[5] M. Ernst, H. Geyer, and R. Blickhan, “Extension and customization of self-stability control in compliant legged systems,” *Bioinspiration & Biomimetics*, vol. 7, no. 4, p. 046002, 2012.

[6] H. Geyer, A. Seyfarth, and R. Blickhan, “Compliant leg behaviour explains basic dynamics of walking and running,” *Proceedings of the Royal Society B*, vol. 273, pp. 2861–2867, 2006.

[7] H. Geyer, *Simple models of legged locomotion based on compliant limb behavior*. PhD thesis, University of Jena, 2005.

[8] J. Rummel, Y. Blum, and A. Seyfarth, “Robust and efficient walking with spring-like legs,” *Bioinspiration & Biomimetics*, vol. 5, no. 4, p. 046004, 2010.

[9] T. McGeer, “Passive dynamic walking,” *the international journal of robotics research*, vol. 9, no. 2, pp. 62–82, 1990.

[10] D. Koepl and J. Hurst, “Force control for planar spring-mass running,” in *International Conference on Intelligent Robots and Systems*, (San Francisco, USA), 2011.

[11] M. Garcia, C. A., R. A., and C. M., "The simplest walking model: Stability, complexity, and scaling," *J Biomech Eng.*, vol. 120, pp. 281–288, 1998.

[12] M. J. Coleman and A. Ruina, "An uncontrolled walking toy that cannot stand still," *Physical Review Letters*, vol. 80, pp. 3658 – 3661, 1998.

[13] M. J. Coleman, M. Garcia, K. Mombaur, and A. Ruina, "Prediction of stable walking for a toy that cannot stand," *Physical Review E*, vol. 64, p. 022901, 2001.

[14] S. Collins, A. Ruina, R. Tedrake, and M. Wisse, "Efficient bipedal robots based on passive dynamic walkers," *Science Magazine*, vol. 307, pp. 1082–1085, 2005.

[15] M. Wisse, *Essentials of dynamic walking; analysis and design of two-legged robots*. PhD thesis, Technische Universiteit Delft, 2004.

[16] D. G. E. Hobbelen and M. Wisse, "Swing-leg retraction for limit cycle walkers improves disturbance rejection," *Robotics, IEEE Transactions on*, vol. 24, no. 2, pp. 377–389, 2008.

[17] M. Gomes and A. Ruina, "Walking model with no energy cost," *Phys. Rev. E*, vol. 83, p. 032901, Mar 2011.

[18] P. A. Bhounsule, J. Cortell, and A. Ruina, "Design and control of Ranger: an energy-efficient, dynamic walking robot," in *Proceedings of the Fifteenth International Conference on Climbing and Walking Robots and the Support Technologies for Mobile Machines (CLAWAR)*, pp. 441–448, 2012.

[19] A. Goswami, B. Thuilot, and B. Espiau, "A study of the passive gait of a compass-like biped robot: Symmetry and chaos," *The International Journal of Robotics Research*, vol. 17, no. 12, pp. 1282–1301, 1998.

[20] A. Goswami, "Postural stability of biped robots and the foot-rotation indicator (fri) point," *The International Journal of Robotics Research*, vol. 18, no. 6, pp. 523–533, 1999.

[21] Z. Liu, Y. Tian, P. Zhang, and C. Zhou, "The analysis on bifurcation and chaos in the compass-gait biped," in *Robotics and Biomimetics, 2007. ROBIO 2007. IEEE International Conference on*, pp. 972–977, 2007.

[22] J.-S. Moon and M. Spong, "Bifurcations and chaos in passive walking of a compass-gait biped with asymmetries," in *Robotics and Automation (ICRA), 2010 IEEE International Conference on*, pp. 1721–1726, 2010.

[23] B. Thuilot, A. Goswami, and B. Espiau, "Bifurcation and chaos in a simple passive bipedal gait," in *Robotics and Automation, 1997. Proceedings., 1997 IEEE International Conference on*, vol. 1, pp. 792–798 vol.1, 1997.

[24] H. Gritli, N. Khraief, and S. Belghith, "Period-three route to chaos induced by a cyclic-fold bifurcation in passive dynamic walking of a compass-gait biped robot," *Communications in Nonlinear Science and Numerical Simulation*, vol. 17, no. 11, pp. 4356 – 4372, 2012.

[25] S. Anderson, M. Wisse, C. Atkeson, J. Hodgins, G. Zeglin, and B. Moyer, "Powered bipeds based on passive dynamic principles," in *Humanoid Robots, 2005 5th IEEE-RAS International Conference on*, pp. 110–116, 2005.

[26] P. A. Bhounsule, *A controller design framework for bipedal robots: trajectory optimization and event-based stabilization.* PhD thesis, Cornell University, 2012.

[27] F. Iida and R. Tedrake, "Minimalistic control of a compass gait robot in rough terrain," in *Robotics and Automation, 2009. ICRA '09. IEEE International Conference on*, pp. 1985–1990, 2009.

[28] F. Iida and R. Tedrake, "Minimalistic control of biped walking in rough terrain," *Autonomous Robots*, vol. 28, no. 3, pp. 355–368, 2010.

[29] K. Byl and R. Tedrake, "Approximate optimal control of the compass gait on rough terrain," in *Robotics and Automation, 2008. ICRA 2008. IEEE International Conference on*, pp. 1258–1263, 2008.

[30] Y. Jeon, Y. Park, and Y. Park, "A study on stability of limit cycle walking model with feet: Parameter study," *International Journal of Advanced Robotic Systems*, 2013.

[31] M. Kwan and M. Hubbard, "Optimal foot shape for a passive dynamic biped," *Journal of Theoretical Biology*, vol. 248, no. 2, pp. 331 – 339, 2007.

[32] M. Wisse, A. L. Schwab, and F. C. T. van der Helm, "Passive dynamic walking model with upper body," *Robotica*, vol. 22, pp. 681–688, 11 2004.

[33] M.-Y. Chen and K. Byl, "Analysis and control techniques for the compass gait with a torso walking on stochastically rough terrain," in *American Control Conference (ACC), 2012*, pp. 3451–3458, 2012.

[34] H. Gritfl, N. Khraeif, and S. Beighith, “Semi-passive control of a torso-driven compass-gait biped robot: bifurcation and chaos,” in *Systems, Signals and Devices (SSD), 2011 8th International Multi-Conference on*, pp. 1–6, 2011.

[35] E. Borzova and Y. Hurmuzlu, “Passively walking five-link robot,” *Automatica*, vol. 40, no. 4, pp. 621 – 629, 2004.

[36] A. P. Krishchenko, S. B. Tkachev, and D. A. Fetisov, “Planar walking control for a five-link biped robot,” *Computational Mathematics and Modeling*, vol. 18, 2007.

[37] D. G. E. Hobbelen and M. Wisse, “A disturbance rejection measure for limit cycle walkers: The gait sensitivity norm,” *IEEE Transactions on Robotics*, vol. 23, no. 6, 2007.

[38] T. Chyou, G. Liddell, and M. Paulin, “An upper-body can improve the stability and efficiency of passive dynamic walking,” *Journal of Theoretical Biology*, vol. 285, no. 1, pp. 126 – 135, 2011.

[39] R. Blickhan, “The spring-mass model for running and hopping,” *Journal of Biomechanics*, vol. 22, pp. 1217–1227., 1989.

[40] R. J. Full and D. E. Koditschek, “Templates and anchors: Neuromechanical hypotheses of legged locomotion on land,” *Journal of Experimental Biology*, vol. 202, pp. 3325–3332., 1999.

[41] H. Geyer, A. Seyfarth, and R. Blickhan, “Spring-mass running: Simple approximate solution and application to gait stability,” *Journal of Theoretical Biology*, vol. 232, pp. 315–328, 2005.

[42] A. Seyfarth, H. Geyer, and H. Herr, “Swing-leg retraction: A simple control model for stable running,” *Journal of Experimental Biology*, vol. 206, pp. 2547–2555., 2003.

[43] Y. Blum, S. W. Lipfert, J. Rummel, and A. Seyfarth, “Swing leg control in human running,” *Bioinspiration & Biomimetics*, vol. 5, p. 026006, 2010.

[44] Y. Blum, A. Birn-Jeffery, M. A. Daley, and A. Seyfarth, “Does a crouched leg posture enhance running stability and robustness?,” *Journal of Theoretical Biology*, vol. 281, pp. 97–106, 2011.

[45] R. M. Ghigliazza, R. Altendorfer, P. Holmes, and D. Koditschek, "A simply stabilized running model," *SIAM Journal on Applied Dynamical Systems*, vol. 2, pp. 187–218, 2003.

[46] A. Wu and H. Geyer, "The 3-d spring–mass model reveals a time-based deadbeat control for highly robust running and steering in uncertain environments," *IEEE Transactions on Robotics*, no. 99, pp. 1–11, 2013.

[47] H. R. Vejdani, Y. Blum, M. A. Daley, and J. Hurst, "Bio-inspired swing leg control for spring-mass running robots," *Bioinspiration & Biomimetics*, vol. 8, p. 046006, 2013.

[48] M. Srinivasan and A. Ruina, "Computer optimization of a minimal biped model discovers walking and running," *Nature*, vol. 439, pp. 72–75, Jan. 2006.

[49] M. Srinivasan, "Fifteen observations on the structure of energy-minimizing gaits in many simple biped models," *Journal of the Royal Society Interface*, 2010. doi: 10.1098/rsif.2009.0544.

[50] M. G. Pandy, "Simple and complex models for studying muscle function in walking," *Philos Trans R Soc Lond B Biol Sci.*, vol. 358, p. 15011509, 2003.

[51] C. Lee and F. C., "Determinants of the center of mass trajectory in human walking and running," *J. Exp. Biol.*, vol. 201, p. 29352944, 1998.

[52] S. Gard, S. Miff, and A. Kuo, "Comparison of kinematic and kinetic methods for computing the vertical motion of the body center of mass during walking," *Hum Mov Sci.*, vol. 22, pp. 597–610, 2004.

[53] H. Martinez Salazar and J. Carbajal, "Exploiting the passive dynamics of a compliant leg to develop gait transitions," *PHYSICAL REVIEW E*, vol. 83, p. 066707, 2011.

[54] J. Schmitt and J. Clark, "Modeling posture-dependent leg actuation in sagittal plane locomotion," *Bioinspiration & Biomimetics*, vol. 4, pp. 17–33, 2009.

[55] J. Schmitt, M. Garcia, R. C. Razo, P. Holmes, and R. J. Full, "Dynamics and stability of legged locomotion in the horizontal plane: A test case using insects," *Biological Cybernetics*, vol. 86, pp. 343–353, 2002.

[56] B. Andrews, B. Miller, J. Schmitt, and J. E. Clark, "Running over unknown rough terrain with a one-legged planar robot," *Bioinspiration & Biomimetics*, vol. 6, no. 2, p. 026009, 2011.

[57] M. Srinivasan and P. Holmes, “How well can spring-mass-like telescoping leg models fit multi-pedal sagittal-plane locomotion data?,” *Journal of Theoretical Biology*, vol. 255, no. 1, pp. 1 – 7, 2008.

[58] I. Poulakakis and J. Grizzle, “The spring loaded inverted pendulum as the hybrid zero dynamics of an asymmetric hopper,” *Automatic Control, IEEE Transactions on*, vol. 54, no. 8, pp. 1779–1793, 2009.

[59] N. F. Lepora, P. Verschure, and T. J. Prescott, “The state of the art in biomimetics.,” *Bioinspiration & biomimetics*, vol. 8, p. 013001, Mar. 2013.

[60] M. Raibert, M. Chepponis, and H. B. Brown, “Experiments in balance with a 3d one-legged hopping machine,” *International Journal of Robotics Research*, vol. 3, pp. 75–92, 1984.

[61] U. Saranli, M. Buehler, and D. E. Koditschek, “RHex: A simple and highly mobile hexapod robot,” *International Journal of Robotics Research*, vol. 20, pp. 616–631, 2001.

[62] A. Altendorfer, N. Moore, H. Komsuoglu, M. Buehler, H. B. Brown Jr., D. McMordie, U. Saranli, R. J. Full, and D. E. Koditschek, “Rhex: A biologically inspired hexapod runner,” *Autonomous Robots*, vol. 11, no. 3, pp. 207–213, 2001.

[63] J. A. Grimes, H. R. Vejdani, and J. W. Hurst, “Atrias 1.0: Design and demonstration of a spring-mass prototype robot in human scale,” *Mechanism and Machine Theory*, vol. Submitted, 2013.

[64] I. Poulakakis and J. Grizzle, “Monopedal running control: Slip embedding and virtual constraint controllers,” in *Intelligent Robots and Systems, 2007. IROS 2007. IEEE/RSJ International Conference on*, pp. 323–330, 2007.

[65] H. Park, K. Sreenath, J. Hurst, and J. Grizzle, “Identification of a bipedal robot with a compliant drivetrain,” *Control Systems Magazine*, vol. 31, April 2011.

[66] J. Rummel and A. Seyfarth, “Passive stabilization of the trunk in walking,” in *SIMPAR 2010 Workshops - Intl. Conf. on SIMULATION, MODELING and PROGRAMMING for AUTONOMOUS ROBOTS*, pp. 127–136, 2010.

[67] H.-M. Maus, S. W. Lipfert, M. Gross, J. Rummel, and A. Seyfarth, "Upright human gait did not provide a major mechanical challenge for our ancestors," *Nature Communications*, vol. 1, p. 70, 2010.

[68] H. K. Khalil, *Nonlinear Systems.* Prentice Hall, 2002.

[69] E. R. Westervelt, J. W. Grizzle, C. Chevallereau, J. H. Choi, and B. Morris, *Feedback control of dynamic bipedal robot locomotion.* CRC press, Boca Raton, Florida., 2007.

[70] J. Grizzle, G. Abba, and F. Plestan, "Asymptotically stable walking for biped robots: analysis via systems with impulse effects," *Automatic Control, IEEE Transactions on*, vol. 46, no. 1, pp. 51–64, 2001.

[71] J. Rummel, Y. Blum, H. Maus, C. Rode, and A. Seyfarth, "Stable and robust walking with compliant legs," in *Robotics and Automation (ICRA), 2010 IEEE International Conference on*, pp. 5250–5255, 2010.

[72] H. Martinez Salazar, *Exploiting Embodiment in the Design of Bipedal Robots.* PhD thesis, University of Zurich, 2013.

[73] A. Merker, J. Rummel, and A. Seyfarth, "Stable walking with asymmetric legs," vol. 6, 2011.

[74] H. Maus and A. Seyfarth, "Walking in circles: a modelling approach," *Journal of The Royal Society Interface*, vol. 11, no. 99, 2014.

[75] E. Andrada, C. Rode, and R. Blickhan, "Grounded runningin quails: Simulations indicate benefits of observed fixed aperture angle between legs before touch-down," *Journal of Theoretical Biology*, vol. 335, pp. 97–107, 2013.

[76] P. Holmes, R. J. Full, D. Koditschek, and J. Guckenheimer, "The dynamics of legged locomotion: Models, analyses, and challenges," *SIAM REVIEW*, vol. 48, pp. 207–304, 2006.

[77] G. Garofalo, C. Ott, and A. Albu-Schaffer, "Walking control of fully actuated robots based on the bipedal slip model," in *Robotics and Automation (ICRA), 2012 IEEE International Conference on*, pp. 1456–1463, 2012.

[78] K. Sreenath, H. Park, I. Poulakakis, and J. Grizzle, "Compliant hybrid zero dynamics controller for achieving stable, efficient and fast bipedal walking on mabel," *The International Journal of Robotics Research*, vol. 30, pp. 1170–1193, 2011.

[79] R. Gregg, A. Tilton, S. Candido, T. Bretl, and M. Spong, "Control and planning of 3-d dynamic walking with asymptotically stable gait primitives," *Robotics, IEEE Transactions on*, vol. 28, no. 6, pp. 1415–1423, 2012.

[80] D. Schmitt, "Insights into the evolution of human bipedalism from experimental studies of humans and other primates," *Journal of Experimental Biology*, vol. 206, pp. 1437–1448, 2003.

[81] S. Carver, N. Cowan, and J. Guckenheimer, "Lateral stability of the spring-mass hopper suggests a two-step control strategy for running," *Chaos*, vol. 19, p. 026106, 2009.

[82] R. Altendorfer, D. E. Koditschek, and P. Holmes, "Stability analysis of a clock-driven rigid-body slip model for rhex.," *International Journal Robotic Research*, vol. 23, no. 10-11, pp. 1001–1012, 2004.

[83] R. R. Burridge, A. A. Rizzi, and D. E. Koditschek, "Sequential composition of dynamically dexterous robot behaviors," *The International Journal of Robotics Research*, vol. 18, no. 6, pp. 534–555, 1999.

[84] A. Seyfarth and H. Geyer, "Natural control of spring-like running: optimized self-stabilization," in *International Conference on Climbing and Walking Robots*, (London, UK), 2002.

[85] H. Geyer, A. Seyfarth, and R. Blickhan, "Natural dynamics of spring-like running: emergence of self-stability," in *International Conference on Climbing and Walking Robots*, (London, UK), 2002.

[86] R. J. Full, K. Autumn, J. I. Chung, and A. Ahn, "Rapid negotiation of rough terrain by the death-head cockroach," *American Zoologist*, vol. 38, p. 81A, 1998.

[87] M. A. Daley and A. A. Biewener, "Running over rough terrain reveals limb control for intrinsic stability," *Proceedings of the National Academy of Sciences of the USA*, vol. 103, pp. 15681–15686, 2006.

[88] B. Miller, J. Schmitt, and J. E. Clark, "Quantifying disturbance rejection of slip-like running systems," *The International Journal of Robotics Research*, vol. 31, no. 5, p. 573587, 2012.

[89] M. Raibert, K. Blankespoor, G. Nelson, R. Playter, and t. B. Team, "Bigdog, the rough-terrain quadruped robot," in *World Congress of the International Federation of Automatic Control*, (Seoul, Korea), 2008.

[90] J. W. Grizzle, J. Hurst, B. Morris, H.-W. Park, and K. Sreenath, "MABEL, a new robotic bipedal walker and runner," in *Conference on American Control Conference*, (St. Louis, USA), 2009.

[91] A. D. Kuo, "Choosing your steps carefully," *IEEE Robotics & Automation Magazine*, vol. 14, pp. 18–29, 2007.

[92] C. T. Moritz and C. T. Farley, "Passive dynamics change leg mechanics for an unexpected surface during human hopping," *Journal of Applied Physiology*, vol. 97, pp. 1313–1322, 2004.

[93] M. A. Daley, A. Voloshina, and A. A. Biewener, "The role of intrinsic muscle mechanics in the neuromuscular control of stable running in the guinea fowl," *Journal of Physiology*, vol. 587, p. 26932707, 2009.

[94] M. A. Daley and A. A. Biewener, "Leg muscles that mediate stability: mechanics and control of two distal extensor muscles during obstacle negotiation in the guinea fowl," *Philosophical Transactions of the Royal Society B*, vol. 366, pp. 1580–1591, 2011.

[95] A. Birn-Jeffery and M. A. Daley, "Birds achieve high robustness in uneven terrain through active control of landing conditions," *Journal of Experimental Biology*, vol. 215, pp. 2117–2127, 2012.

[96] H. M. Herr and T. A. McMahon, "A galloping horse model," *International Journal of Robotics Research*, vol. 20, pp. 26–37, 2001.

[97] M. A. Daley and J. R. Usherwood, "Two explanations for the compliant running paradox: Reduced work of bouncing viscera and increased stability in uneven terrain," *Biology Letters*, vol. 6, pp. 418–421, 2010.

[98] M. Ernst, H. Geyer, and R. Blickhan, "Spring-legged locomotion on uneven ground: a control approach to keep the running speed constant," in *International Conference on Climbing and Walking Robots*, (Istanbul, Turkey), 2009.

[99] J. Karssen, M. Haberland, M. Wisse, and S. Kim, "The optimal swing-leg retraction rate for running," in *Robotics and Automation (ICRA), 2011 IEEE International Conference on*, pp. 4000 –4006, may 2011.

[100] T. A. McMahon and G. C. Cheng, "The mechanics of running: How does stiffness couple with speed?," *Journal of Biomechanics*, vol. 23, pp. 65–78, 1990.

[101] C. T. Farley and O. Gonzalez, "Leg stiffness and stride frequency in human running," *Journal of Biomechanics*, vol. 29, pp. 181–186, 1996.

[102] D. P. Ferris, M. Louie, and C. T. Farley, "Running in the real world: Adjusting leg stiffness for different surfaces," *Proceedings of the Royal Society B*, vol. 265, pp. 989–994., 1998.

[103] S. Grimmer, M. Ernst, M. Günther, and R. Blickhan, "Running on uneven ground: Leg adjustment to vertical steps and self-stability.," *Journal of Experimental Biology*, vol. 211, pp. 2989–3000, 2008.

[104] R. Blickhan, A. Seyfarth, H. Geyer, S. Grimmer, H. Wagner, and M. Gunther, "Intelligence by mechanics," *Philosophical Transactions of the Royal Society A*, vol. 365, pp. 199–220, 2007.

[105] M. Srinivasan, "Fifteen observations on the structure of energy-minimizing gaits in many simple biped models," *Journal of The Royal Society Interface*, vol. 8, no. 54, pp. 74–98, 2011.

[106] E. R. Westervelt, J. W. Grizzle, C. Chevallereau, J. H. Choi, and B. Morris, *Feedback Control of Dynamic Bipedal Robot Locomotion.* CRC Press, Boca Raton, 2007.

[107] C. Remy, K. Buffinton, and R. Siegwart, "Comparison of cost functions for electrically driven running robots," in *Robotics and Automation (ICRA), 2012 IEEE International Conference on*, pp. 2343–2350, 2012.

[108] M. H. Raibert, *Legged Robots That Balance.* Cambridge: The MIT Press, 1986.

[109] A. Altendorfer, D. E. Koditschek, and P. Holmes, "Stability analysis of a clock-driven rigid-body slip model for rhex," *The International Journal of Robotics Research*, vol. 23, no. 10-11, pp. 1001–1012, 2004.